LBL-35769
UC-401

CHEMICAL SCIENCES

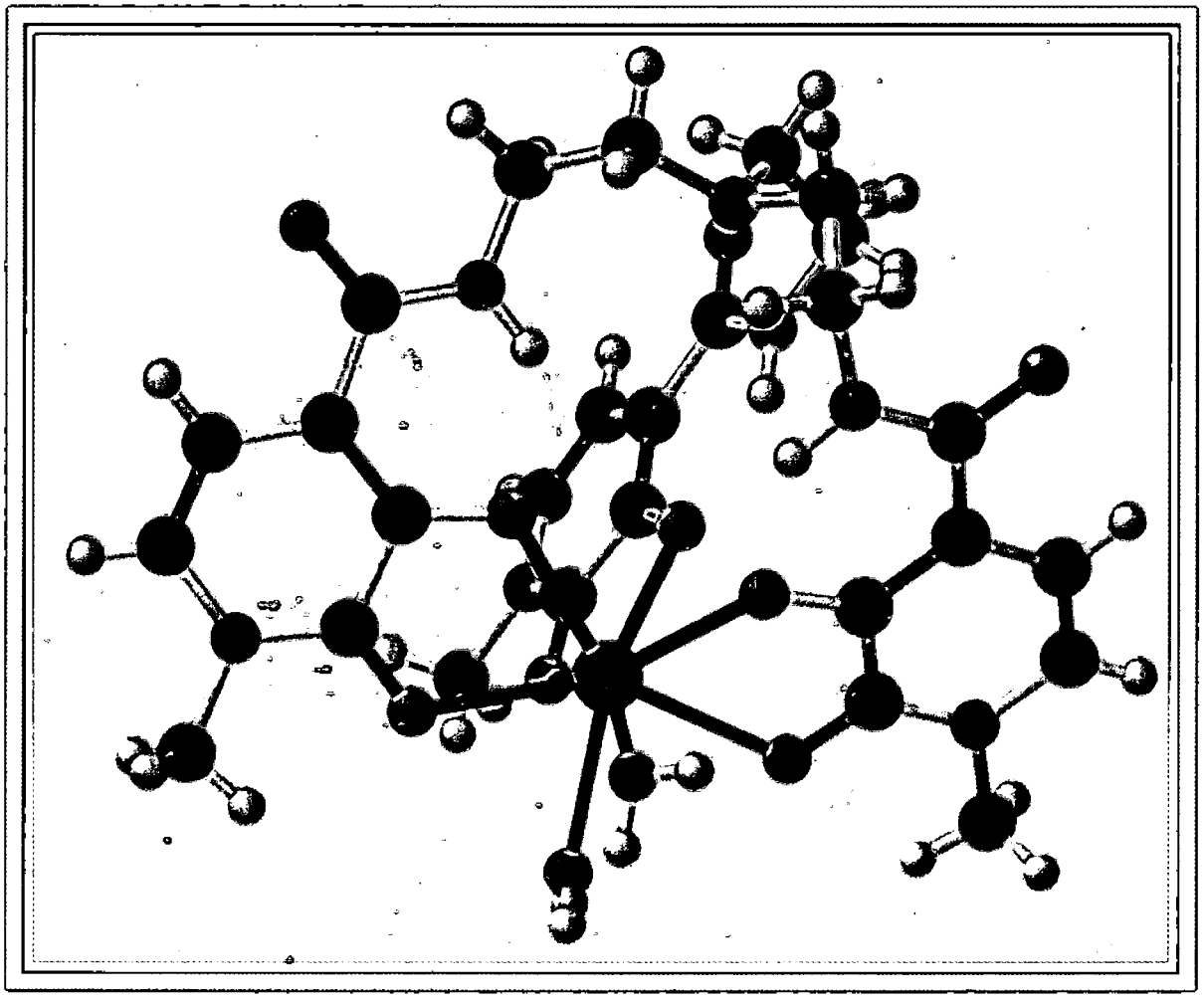

Annual Report 1993

October 1994

Lawrence Berkeley Laboratory
University of California
Berkeley, California 94720

Prepared for the U.S. Department of Energy under Contract DE-AC03-76SF00098

DISCLAIMER

LBL-35769
UC-401

CHEMICAL SCIENCES DIVISION

Annual Report 1993

September 1994

Lawrence Berkeley Laboratory
University of California
Berkeley, California 94720

Prepared for the U.S. Department of Energy under Contract No. DE-AC03-76SF00098

Contents

REMARKS BY THE DIVISION DIRECTOR

The Chemical Sciences Division (CSD) is one of eleven research Divisions of the Lawrence Berkeley Laboratory, a Department of Energy National Laboratory. The CSD is comprised of individual groups and research programs that are organized into five scientific areas: Chemical Physics, Inorganic/Organometallic Chemistry, Actinide Chemistry, Atomic Physics, and Physical Chemistry. The CSD is unique in that a good deal of our Division's research activity occurs in laboratories located on the campus of the University of California at Berkeley, involving students and faculty in the Department of Chemistry. Several large programs, notably the Actinide Chemistry Program and the Atomic Physics Program, are based at the Lawrence Berkeley Laboratory (LBL) site just east of and above the University campus. The two sites, the campus and the Laboratory, are linked by an efficient minibus system that transports students, faculty, staff, and visitors between the two institutions.

The benefits of close ties with the campus are broad and numerous. One of the most important of these is the vigor, dedication, and high productivity that graduate student research assistants bring to our various research projects. In addition, the Laboratory has a staff of highly skilled engineers and crafts technicians who support the scientific mission, and it is the site of several major, world-class user facilities such as the Advanced Light Source (ALS). Combined, the two institutions represent a highly enriched research environment, attracting a large number of eminent scientists and leaders from all over the world—many of whom have close associations with the Chemical Sciences Division's research programs.

In FY 1993, the Division made considerable progress on developing two end-stations and a beamline to advance combustion dynamics research at the ALS. In support of DOE's national role in combustion research and chemical science, the beamline effort will enable researchers from around the world to make fundamental advances in understanding the structure and reactivity of critical reaction intermediates and transients, and in understanding the dynamics of elementary chemical reactions. The Combustion Dynamics Beamline Initiative at the ALS envisions both experimental and theoretical efforts that would lead to accurate and reliable models for predicting combustion properties to improve the design of engines, burners, and other combustion devices.

The Division has continued to place a strong emphasis on full compliance with environmental health and safety guidelines and regulations and has made progress in technology transfer to industry. A seminar series in environmental remediation was launched in FY 1993 and in the coming years we will be focusing the Chemical Sciences Division's research efforts on this important area. Finally, the Division has begun a new program in advanced battery research and development that should help strengthen industrial competitiveness both at home and abroad. This new battery research program began its operations effective August 1993. We look forward to continued progress in both environmental remediation and technology transfer.

Awards and honors received by CSD investigators in FY 1993 include:

- Neil Bartlett received the Bonner Chemiepreis from Friedrich Wilhelms Universität, Bonn Germany; and an Honorary Doctor of Laws degree from Simon Fraser University, British Columbia.
- Y.T. Lee was Honorary Professor at Bilkent University in Ankara, Turkey; he was a Merck Lecturer at Hope College, a J.T. Baker Lecturer at Columbia, an Eyring Lecturer at Arizona State University, and an E.K.C. Lecturer at the University of California, Irvine; and he received an Honorary Doctorate of Science from the University of Southern California, Los Angeles, and a Fellowship Certificate from The Photonics Society of Chinese-Americans.
- William Lester, Jr. selected and appeared in the nationally-aired PBS special, "Your Toxic Trash"; and he was a member of the national board of AAAS, the Federal Networking Counsel Advisory Committee, and the National Science Foundation's Blue Ribbon Panel on High Performance Computing.
- Kenneth Raymond received the Humboldt Senior Scientist Award in 1992, and the Bader Award in Bioinorganic and Bioorganic Chemistry.

Charles B. Harris
Division Director
Chemical Sciences Division

Chemical Sciences

FUNDAMENTAL INTERACTIONS

PHOTOCHEMICAL AND RADIATION SCIENCES

Photochemistry of Materials in the Stratosphere*

Harold S. Johnston, Investigator

INTRODUCTION

This research is concerned with global change in the chemistry of the atmosphere, including theoretical and interpretative gas-phase and heterogeneous photochemistry. Work continues on writing former graduate student theses for publication.

The principal investigator is (1) an advisor to the Upper Atmosphere Research Program, Atmospheric Effects of Stratospheric Aircraft, of the National Aeronautics and Space Administration (NASA); (2) Trustee for the National Institute for Global Environmental Change, administered by the University of California; and (3) Member of the National Needs Task Force of the Lawrence Berkeley Laboratory.

1. New Method of Obtaining the Internal Energy Distribution of Highly Excited Nitrogen Dioxide Molecules (Publications 3 and 6)

Publication 3 is a derivation of the new spectroscopic method and a test of its statistical significance. For synthetic distributions of extreme shapes (squares or triangles) with very large added random noise, the method recovers the first moment of the internal energy to better than 1%, the second moment to 10 to 20%, and the third moment as to sign in all cases and within 50% as to magnitude, except for the most extreme tests. Publication 4 gives the *first* published example of the experimental determination of the first, second, and third moments of a highly excited polyatomic molecule as it undergoes a series of deactivating collisions. These experiments were carried out over a wide range of collision numbers for NO_2 at four wavelengths and with 12 inert gases. Already this work has stimulated other physical chemists to develop other new experimental methods of obtaining second moments of internally excited molecules. Publications 5 and 6 measure the approximate internal energy populations of photolysis-produced NO_2 fluorescence ($RNO_2 + h\nu \rightarrow R + NO_2^*$), and the interpretation of such data gives information supplementary to results by other methods.

Publication 2 involves collaboration between this project and that of Professor Yuan T. Lee. The thresholds for three different product channels from electronically excited NO_3 molecules were obtained from translational spectroscopy in Lee's molecular beam system. The enthalpy of formation of NO_3 was obtained as 17.9 ± 0.8 kcal/mol (298 K), whereas the previous best value was 17 kcal/mol, uncertain to ±5 kcal/mol. From these observed thresholds, the quantum yields of NO_3 in the atmosphere can be found.

*This work was supported by the Director, Office of Energy Research, Office of Basic Energy Sciences, Chemical Sciences Division, of the U.S. Department of Energy under Contract No. DE-AC03-76SF00098.

FY 1993 PUBLICATIONS AND REPORTS

Refereed Journals

1. J.D. Burley, C.E. Miller, and H.S. Johnston, "Spectroscopy and Photoabsorption Cross Sections of FNO," J. Mol. Spectrosc. **158**, 377 (1993); LBL-31548.
2. H.F. Davis, B. Kim, H.S. Johnston, and Y.T. Lee, "Dissociation Energy and Photochemistry of NO_3," J. Phys. Chem. **97**, 2172 (1993); LBL-33113.
3. H.S. Johnston, C.E. Miller, B.Y. Oh, K.O. Patten, Jr., and W.N. Sisk, "Internal Energy Distributions from Nitrogen Dioxide Fluorescence. 1. Cumulative Sum Method," J. Phys. Chem. **97**, 9890 (1993); LBL-31549.
4. K.O. Patten, Jr., and H.S. Johnston, "Internal Energy Distributions from Nitrogen Dioxide Fluorescence. 2. Collisional Energy Transfer from Excited Nitrogen Dioxide," J. Phys. Chem. **97**, 9904 (1993); LBL-31550.
5. W.N. Sisk, C.E. Miller, and H.S. Johnston, "Internal Energy Distributions from Nitrogen Dioxide Fluorescence. 3. Photolysis of Jet-Cooled N_2O_4," J. Phys. Chem. **97**, 9916 (1993); LBL-31551.
6. C.E. Miller and H.S. Johnston, "Internal Energy Distributions from Nitrogen Dioxide Fluorescence. 4. Variable Wavelength Photodissociation of $ClNO_2$ and $HONO_2$," J. Phys. Chem. **97**, 9924 (1993); LBL-31552.

Invited Talk

7. H.S. Johnston, "Stratospheric NO_x Chemistry," symposium, Challenges in Atmospheric Chemistry and Global Change: Yesterday, Today, and Tomorrow, University of Colorado, Boulder, CO, December 1993.

CHEMICAL PHYSICS

Energy Transfer and Structural Studies of Molecules on Surfaces*

Charles B. Harris, Investigator

INTRODUCTION

The goal of this research is to understand the dynamics of excited electronic states on surfaces, at interfaces, and in condensed phases. The research program is both theoretical and experimental in character. It includes nonlinear optical and ultrafast laser techniques in the picosecond to femtosecond regime, in addition to more conventional surface science instruments for characterizing surfaces and adsorbate-surface interactions. Recent work has focused on the application of the new techniques that we have developed to probe the dynamics of electrons at interfaces and carrier diffusion in semiconductors. The results of this program have a direct bearing on the properties of nanoscale and quantum electronic devices, optoelectronic materials, and on other problems of general interest such as the dynamics of electrical transmission in conductors on ultrafast timescales and the optical properties of thin films.

1. Electronic Dynamics at Metal-Insulator Interfaces (Publications 1, 2)

C.B. Harris, R.E. Jordan, R.L. Lingle, Jr., W.R. Merry, J.D. McNeill, and D.F. Padowitz

New results for electron dynamics at interfaces and in thin films are emerging from a combination of ultrafast lasers and electron spectroscopy. Time- and angle-resolved two-photon photoemission spectroscopy probes the band structure and femtosecond dynamics of excited electronic states at surfaces and interfaces. Electrons excited just below the photoemission threshold of a metal may remain bound at the metal surface by the image potential. We have found that these image potential states persist in the presence of adsorbed molecules. Electrons in the image potential states, localized in the microscopic region just outside the surface and interacting strongly with adsorbed molecules, provide a unique probe of the potential at the metal-insulator interface and of the dynamics of the electron in atomically thin films.

We are extensively studying the electronic structure of rare-gas films on metal substrates. The metallic image potential state persists in the case of a rare-gas monolayer; the primary effect of the monolayer is to decouple the in-plane motion of the electron from the metal band structure (Publication 1). However, dramatically different results are obtained for multilayers as compared to the monolayer, since energy levels associated with the xenon slab itself become important. These results track the development of the band structure of the interface in a layer-by-layer fashion. Xenon layers on a metal surface form a model system for investigating the transition from a 2-D to a 3-D electronic structure. These interfaces show a rich spectrum. From these data and from the alkane studies, we conclude that most physisorbed monolayers behave similarly, excluding the image electron from the adlayer and decoupling its surface-parallel motion from the influence of the metal band structure. Binding energy and dispersion effects unique to a particular adsorbate species appear for two or more layers.

Alkali layers on noble metals have been investigated both experimentally and theoretically. A TPPE study of K/Ag(111) found that the effective mass of the image potential electron is in relatively good agreement with predictions of a density functional calculation. We have successfully modeled the binding energy of image potential electrons on alkali layers using multiple reflection theory. We conclude that multiple reflection theory is more robust than previously believed (Publication 2).

A very significant discovery within the past year has been the observation of 2-D localization of electrons at metal-alkane interfaces as a nondispersive feature in angle-resolved TPPE. This finding represents the development of a new tool to study the spatial extent of interfacial electronic states. Our method is a unique and important tool for the study of localization because it measures the energy spectrum of the localized states and can be applied to atomically thin samples. Generally, we find that all aspherical alkanes support localized electronic states at the interface, while the spherical neopentane does not. Figure 1-1 shows the dispersion data as a function of angle for bilayers of n-pentane and neopentane. We may predict that similar localized states exist at metal-polymer interfaces and contribute to their electronic properties.

* This work was supported by the Director, Office of Energy Research, Office of Basic Energy Sciences, Chemical Sciences Division, of the U.S. Department of Energy under Contract No. DE-AC03-76SF00098.

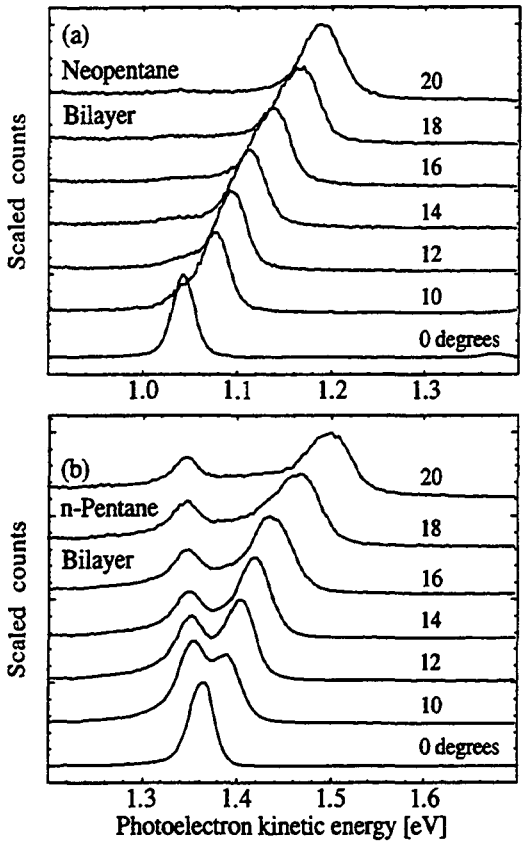

Figure 1-1. Bilayer dispersion. A nondispersive feature (interpreted as a localized electron state) is prominent in Figure 1-1(b) for the n-pentane bilayer, while the parabolically dispersing band (extended electron state) dominates the bilayer spectrum of neopentane. Curve heights have been scaled. (XBL 947-4212)

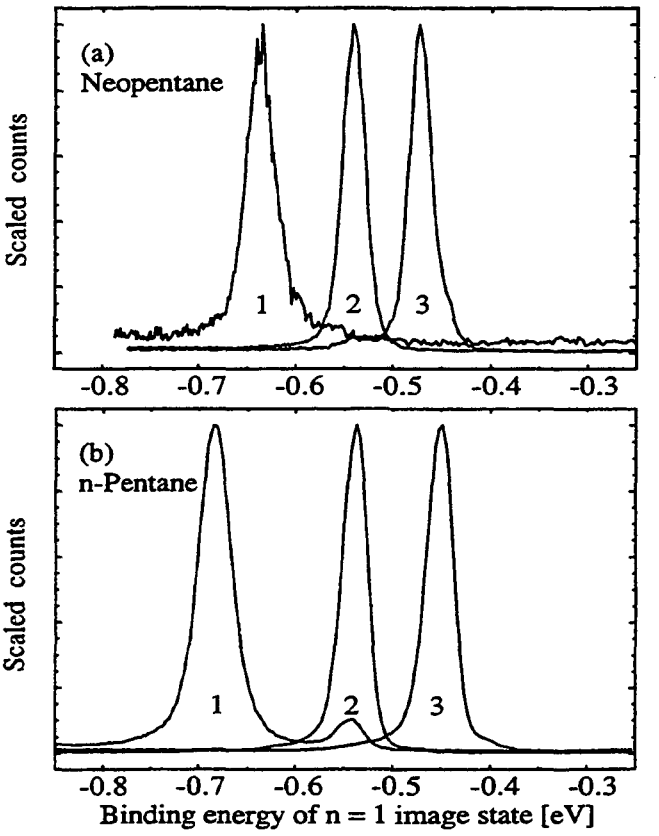

Figure 1-2. The $n = 1$ image potential peak in the TPPE spectrum shifts to smaller binding energy (higher photoelectron kinetic energy) as successive layers of dielectric material are adsorbed. The image potential states form a Rydberg series of hydrogenic levels and persist on many adsorbate-covered metal surfaces. The binding energy of the $n = 1$ image state on bare Ag(111) is –0.77 eV. The monolayer peak in Figure 1-2(b) is accompanied by a small bilayer peak, illustrating the *in situ* monitoring of layer growth. (XBL 947-4211)

We have completed a systematic study of physisorbed metal-alkane interfaces. First, we have extensively investigated the sensitivity of two-photon photoemission (TPPE) to various adsorption phenomena. We have shown that TPPE is extremely sensitive to layer thickness at the level of a few percent of a monolayer. TPPE data for the image potential state in the presence of layers of n-pentane and neopentane are shown in Figure 1-2. We are able to distinguish between adlayer growth modes and map out surface phase diagrams. We have catalogued the distinct surface spectra characteristic of a 2-D gas layer, a 2-D solid layer, island formation, and clustering of a nonwetting adsorbate. Secondly, we have studied the dielectric properties of atomically thin slabs by measuring the effect of layer thickness on image potential electron binding energy. These layer-by-layer shifts are due to dielectric screening of the image potential and show how the atomic polarizability develops into the bulk dielectric constant. Thirdly, dispersion measurements of the image electron band structure have shown that the effect of the monolayer is to decouple the in-plane motion of the image potential electron from the metal bulk band structure, leaving it as a free electron in 2-D. However, the image electron effective mass increases for alkane multilayers.

2. Ultrafast Dynamics in Solution† (Publication 3)

C.B. Harris, M.C. Asplund, S.E. Bromberg, J.C. King, B.J. Schwartz, C.P. Vala, J.Z. Zhang

One of the unique aspects of liquid-phase chemical reactivity is the ability of reacting species to become trapped in a "cage" of solvent molecules. This caging can qualitatively change the chemistry of a system by confining the reactive species and allowing them to interact over an extended period of time. The time scale of this process has not been well characterized and remains a central problem in liquid-phase reaction dynamics. To study this process we have examined the primary geminate recombination, the

nondiffusive recombination of fragments following photodissociation. We use transient absorption spectroscopy to directly follow the production and disappearance of CH_2I radical fragments produced after the photodissociation of methylene iodide (CH_2I_2) with femtosecond time resolution. These results provide the first direct observation of primary geminate recombination.

Our results show that primary geminate recombination is dominated by recombination after a single collision with the solvent. The data indicate that a portion of the CH_2I fragments recombine with the dissociated iodine atom in 350 fs. This time scale allows for only a single collision of the photofragments with the surrounding solvent cage.

In other work, the vibrational relaxation dynamics of large molecules undergoing photodissociation have been investigated. The vibrational relaxation dynamics following the dissociation of C≡O from $M(CO)_6$ (M = Cr, Mo, W) were studied with picosecond transient absorption spectroscopy (Publication 3). After dissociation of the C≡O, the pentacarbonyl species forms a complex with a solvent molecule. The cooling of this solvated pentacarbonyl complex was monitored from 1 ps to 1 ns in this study. The vibrational relaxation of each of these three compounds was different. The $W(CO)_5$·S (S = cyclohexane) vibrationally relaxed in 35 ps; whereas, $Mo(CO)_5$·S relaxed twice as quickly (18 ps). This is surprising because the higher density of states in $W(CO)_5$·S would be expected to lead to faster cooling of the hot solvated complex. The primary cooling of $Cr(CO)_5$·S is completed in 18 ps just as in $Mo(CO)_5$·S, but a slower component in the relaxation, approximately 150 ps, is also present. This component is assigned to vibrational relaxation of the C≡O stretching mode. From comparisons with other studies, it appears that the existence of this slower cooling component is only present in first row transition metal carbonyls.

Much of our current work is centered on development of a new ultrafast spectrometer with increased wavelength tunability. When completed, this system will be able to probe molecules in the ultraviolet, visible, and mid-infrared regions of the spectrum. Continuous tuning over these regions will allow studies of nearly any molecular species. The information provided by the infrared probing is much more diagnostic of the structure of the species being studied. We expect the resulting studies will provide new insight into both the physics of chemical reactions in solution and an in-depth understanding of the mechanisms of these reactions.

3. Work in Progress

Local potential fluctuations in alloy semiconductors, specifically CdS_xSe_{1-x}, are being probed by their effects on the carrier dynamics as revealed by ultrafast fluorescence upconversion. Such substitutional alloys occupy an important position between well-characterized, highly ordered pure crystals and highly disordered glassy semiconductors. Our research focuses on how the disorder in these alloys affects the carrier dynamics via local potential fluctuations resulting from the random occupation of the sulfur-selenium sites. Fast fluorescence decay components in the range of 50–150 ps have been observed, the exact values being dependent on both the specific alloy composition as well as the wavelength of the emitted light within a given sample. Decays also exhibit longer tails of several hundreds of picoseconds.

The 1-ps resolution of the current fluorescence upconversion spectrometer, employing a synchronously pumped dye laser and single-photon counting detection, allows precise probing of not only the fluorescence decays but also of the fast rise times. This information is important both because of its direct revelation of effects on intraband relaxation and because of its ability to probe the diffusion of carriers through alloys with graded composition. These samples, in which the percentage of the sulfur (and hence selenium) is varied in a well-characterized manner with depth, exhibit a linear dependence of the average band-gap with position. The diffusion of the carriers can then be probed by analyzing the temporal characteristics of the emitted light as a function of wavelength.

The work on electron dynamics at surfaces and interfaces continues in several directions. Experiments to further explore the mechanism of electron localization at metal-insulators are in progress. Chemisorbed methyl thiolate and sulfur on Ag(111) have been preliminarily studied; features are observed that are apparently not derived from the image potential state. These features are probably due to localized unoccupied electronic states associated with the chemisorption bond. Laser modifications are being made to enable the study of these very interesting and technologically relevant interfaces. One of the most important applications of our high-resolution femtosecond two-photon photoemission technique will be the study of metal-semiconductor junctions and quantum wells.

†National Science Foundation Program using DOE equipment.

FY 1993 PUBLICATIONS AND REPORTS

Refereed Journals

1. W.R. Merry, D.F. Padowitz, R.E. Jordan, and C.B. Harris, "Electrons at Metal-Insulator Interfaces I. The Effect of Xe Monolayers on the Image Potential States of Ag(111)," Surf. Sci. **295**, 393 (1993).
2. J.D. McNeill and C.B. Harris, "An Exact Phase Shift Model for Image States on Metal Surfaces with Alkali Metal Overlayers," S.S. Comm. **87**, 1089 (1993).
3. J.C. King, J.Z. Zhang, B.J. Schwartz, and C.B. Harris, "Vibrational Relaxation of $M(CO)_6$ (M = Cr, Mo,W): Effect of Metal Mass on Vibrational Cooling Dynamics and NonBoltzmann Internal Energy Distribution," J. Chem. Phys. **99**, 7595 (1993).

Other Publications

4. R.L. Lingle, Jr., D.F. Padowitz, R.E. Jordan, J.D. McNeill, and C.B. Harris, "Localization of Electrons at Interfaces," in *Reaction Dynamics in Clusters and Condensed Phases*, edited by J. Jortner *et al.* (Kluwer Academic Publishers, The Netherlands, 1994), pp. 169–178.
5. D.F. Padowitz, C.B. Harris, R.E. Jordan, R.L. Lingle, Jr., J.D. McNeill, and W.R. Merry, "Two-Photon Phototemission and the Dynamics of Electrons at Interfaces," *SPIE Proceedings: Laser Techniques for Surface Science*, Vol. 2125, 1994 (in press); LBL-35194.
6. R.L. Lingle, Jr., D.F. Padowitz, R.E. Jordan, J.D. McNeill, and C.B. Harris, "Two-Dimensional Localization of Electrons at Interfaces," Phys. Rev. Lett. (submitted) (1993); LBL-34430.

Invited Talks

7. C.B. Harris, "Electrons at Metal-Insulator Interfaces," Twelfth International Vacuum Congress, Eighth International Conference on Solid Surface, The Hague, The Netherlands, October 12–16, 1992.
8. C.B. Harris, "Dynamics of Electrons at Interfaces," Department of Chemistry, University of Alexandria, Egypt, January 21, 1993.
9. C.B. Harris, "Dynamics and Properties of Electrons at Interfaces," Department of Chemistry, University of California, Santa Barbara, CA, February 15, 1993.
10. C.B. Harris, "Dynamics of Electrons at Interfaces," Department of Chemistry, University of Minnesota, February 15, 1993.
11. C.B. Harris, "Dynamics and Properties of Electrons at Metal Interfaces," Department of Chemistry, University of California, Santa Cruz, CA, March 17, 1993.
12. C.B. Harris, "Dynamics of Electrons at Interfaces," ACS Symposium on Physical Chemistry in Restricted Geometries, Denver, CO, March 28–April 2, 1993.
13. C.B. Harris, "Dynamics and Properties of Electrons at Metal Interfaces," Department of Chemistry, University of North Carolina, NC, April 15, 1993.
14. C.B. Harris, "Dynamics and Properties of Electrons at Metal Interfaces," Department of Chemistry, Duke University, NC, April 16, 1993.
15. C.B. Harris, "Dynamics and Properties of Electrons Interacting with Clusters and Thin Films on Metal Surfaces," 26th Jerusalem Symposium on Reaction Dynamics in Clusters and Condensed Phases, Jerusalem, Israel, May 17–20, 1993.
16. C.B. Harris, "The Dynamics of Electrons at Interfaces," Fourth International Conference on the Structure of Surfaces, Shanghai, China, August 16-19, 1993.
17. C.B. Harris, "Dynamics and Properties of Electrons Interacting with Clusters and Thin Films on Metal Surfaces," Department of Chemistry, University of Illinois, IL, September 29, 1993.

Laser Sources and Techniques*

Andrew H. Kung, Investigator

INTRODUCTION

This program focuses on the development of novel laser and spectroscopic techniques in the IR, UV, and VUV regions for studying combustion-related molecular dynamics at the microscopic level. Laser spectroscopic techniques have proven to be extremely powerful in the investigation of molecular processes that require very high sensitivity and selectivity. Our approach is to use quantum electronic and nonlinear optical techniques to extend the spectral coverage and to enhance the optical power of ultra-high-resolution laser sources to obtain photoionization, fluorescence, and photoelectron spectra of jet-cooled free radicals and to analyze reaction products resulting from unimolecular and bimolecular dissociations. New spectroscopic techniques are developed with these sources for the detection of optically thin and often short-lived species. Recent activities center on regenerative amplification of high-resolution solid-state lasers, development of tunable high-power mid-IR lasers and short-pulse UV/VUV tunable lasers, and construction of an oil-free rotating source beam machine for spectroscopy and dynamics studies of free radicals. In conjunction with these developments, this program provides for scientific and technical management of the construction of a chemical dynamics beamline at the Advanced Light Source.

1. Regenerative Amplification of Single-Frequency Optical Parametric Oscillators (Publication 1)

A.H. Kung

Near-diffraction-limited and very narrow-band pulses are obtained by regenerative amplification in Ti:sapphire of a pulsed single-frequency optical parametric oscillator (OPO). The technique combines the virtues of high-power tunable solid-state lasers and broadly tunable low-jitter parametric oscillators to yield ~2-ns pulses that can be tuned through the entire gain range of the Ti:sapphire crystal. The measured output power is 20 MW at 850 nm. Addition of a four-pass Ti:sapphire amplifier boosts single-pulse energies to >100 mJ. When operating in the pulse-train mode, energies of 200 mJ per pulse train are obtained.

*This work was supported by the Director, Office of Energy Research, Office of Basic Energy Sciences, Chemical Sciences Division, of the U.S. Department of Energy under Contract No. DE-AC03-76SF00098.

2. High-Resolution High-Power Tunable Infrared Laser (Publication 5)

J. Xie and A.H. Kung

A tunable mid-infrared laser with high resolution and high power is a very powerful tool for studying the structure and reaction dynamics of hydrocarbon radicals, which play a crucial role in the combustion of fossil fuels. For instance, multiple infrared photon excitation photodissociation can best imitate the combustion process, and resonant IR excitation followed by UV dissociation can selectively break a defined chemical bond. We have chosen high-order Raman shifting of the Ti:sapphire laser in hydrogen to generate IR. The pump laser is the OPO-regenerative amplifier system described in the previous section. As a first test of the Raman shifting process, we constructed a 5-pass hydrogen cell to produce IR in the region of 2–4 μm using second-order Stokes. With the laser optimized to operate with a 6-pulse train at a total of 130 mJ and hydrogen pressure at 180 psi, we have obtained 11 mJ of IR radiation at 3 μm, and 5 mJ at 4 μm. These results correspond to ~30% photon conversion efficiency. Also, we have obtained 40 mJ of 1.6-μm IR light from first-order Stokes shifting after one pass, for a photon efficiency of ~60%. A 0.027 cm^{-1} of linewidth was measured.

3. Construction of an Oil-Free Rotating-Source Photodissociation Apparatus

J. Xie, A. Soliva, and Y.T. Lee

An oil-free rotating-source molecular beam machine similar to one in Y.T. Lee's group has been designed for studying photodissociation of free radicals. The oil-free chamber will permit studies of hydrocarbon radicals and will have a low background in the mass spectrometer detection. We have finished construction of the main chamber and source chamber, and we are putting together the detector chamber. With completion of this apparatus, we will use the tunable IR laser source to study the photodissociation of C_3H_7,

$$n\text{-}C_3H_7 \rightarrow C_3H_6 + H, \qquad \Delta H = 37 \text{ kcal/mol}$$

and $$n\text{-}C_3H_7 \rightarrow C_2H_4 + CH_3, \qquad \Delta H = 31 \text{ kcal/mol}$$

by selectively pumping the CH stretch and C–C stretch individually. A UV laser will be used to dissociate the vibrationally excited n-C_3H_7. We will search for Franck–

Condon overlap and UV photon energies that will induce dissociation according to the initial vibrational selection. We will also study IR multiple-photon dissociation of radicals.

4. VUV High-Resolution and High-Flux Beamline for Chemical Dynamics Studies at the Advanced Light Source (Publication 4)

M. Koike, P.A. Heimann, A.H. Kung, T. Namioka, R. DiGennaro, B. Gee, and N. Yu

An undulator beamline devoted to chemical dynamics experiments and consisting of VUV high-resolution and high-flux branch lines has been designed at the Advanced Light Source. The radiation source is an undulator having a 10-cm period, and the fundamental in the energy range from 6 to 30 eV is utilized by the experiments. The higher harmonics of the undulator due to operation at high K values is suppressed by a novel gas filter. In the first branch, high-flux 2%-bandwidth radiation is directed toward an end station for photodissociation. A photon flux calculation predicts 10^{16} photons/s at this end station. In the second branch, highly monochromatized radiation is sent to an end station for photoelectron spectroscopy and photoionization studies. For this purpose, a vertical-dispersion 6.65-m off-plane Eagle mounting is chosen for the monochromator, expecting to achieve a resolving power of $\sim 5 \times 10^4$ with a 1,200-grooves/mm grating, and 1×10^5 to 2×10^5 with a 4,800-grooves/mm grating.

5. Work in Progress

To obtain longer wavelength in the IR (4–10 μm), we need more passes to give higher gain for third-order Stokes Raman shift. We have constructed a multiple-pass cell able to accommodate more than 50 passes of the laser beam by using two 3.5-in.-diameter concave mirrors. The multiple-pass cell is designed with the following characteristics: First, two mirrors are placed inside the pressure cell to eliminate window losses; these mirrors can be tilted in the X-Y directions by external control. Second, the input mirror can be translated to change the cavity length for mode-matching of the input laser beam. Third, after the mirrors are aligned, we use a rotating periscope to intercept the beam after a desired number of passes for output. Finally, two small mirrors are placed in the middle of the tube but far off-axis to avoid touching the laser beams. These mirrors allow direct observation of the inside of the pressure cell and will greatly enhance our ability to align the laser to the cell. With >50 passes we expect to extend the generated IR wavelength to beyond 10 μm.

Infrared spectroscopy of gas-phase free radicals with more than two carbons, such as C_3H_7, has not been studied in detail for lack of means to produce high-density free radicals and because of low detection sensitivities of conventional IR absorption spectroscopy. We are testing a time-of-flight mass spectrometer for studying the IR spectroscopy of free radicals via photoionization detection. The free radicals will be produced in a supersonic expansion. IR-VUV double resonance will be used to obtain IR spectra. The low I.P.s, 8.1 eV for *n*-C_3H_7 and 7.5 eV for *iso*-C_3H_7, require only low-energy VUV photons and should discriminate any stable molecules from being ionized in the beam. Infrared spectroscopy of C_3H_7 will open the door for photodissociation dynamics studies by IR pumping.

FY 1993 PUBLICATIONS AND REPORTS

Refereed Journals

1. A.H. Kung, "Regenerative Amplification of a Single-Frequency Optical Parametric Oscillator," Opt. Lett. **18**, 2017 (1993).

Other Publications

2. A.H. Kung and Y.T. Lee, "Application of VUV Undulator Beam Line to Chemical Dynamics at ALS," *Proceedings of the 46th Okazaki Conference on Application of Synchrotron Radiation to Molecular Science: Present Status and Future Prospects, January 1993*; LBL-34283A.
3. A.H. Kung, "Regenerative Amplification of Single-Frequency Optical Parametric Oscillators," *Proceedings of the Conference on Lasers and Electro-Optics, Baltimore, MD, May 1993*; LBL-34284A.
4. M. Koike, P.A. Heimann, A.H. Kung, T. Namioka, R. DiGennaro, B. Gee, and N. Yu, "VUV High-Resolution and High-Flux Beamline for Chemical Dynamics Studies at the Advanced Light Source," Nuclear Inst. and Methods (in press).
5. J. Xie and A.H. Kung, "High-Resolution High-Power Mid-IR Generation by Second-Order Stokes Shift in Hydrogen," *Proceedings of the Annual Meeting of the IEEE Laser and Electro-Optics Society, San Jose, CA*, November 1993; LBL-34285A.

LBL Reports

6. P. Heimann, M. Koike, A.H. Kung, C.Y. Ng, M.G. White, and A. Wodtke, "Application of Synchrotron Radiation in Chemical Dynamics," Workshop Report; LBL-34131.

Crossed Molecular Beams*

Yuan T. Lee, Investigator

INTRODUCTION

The major thrust of this research project is to elucidate detailed dynamics of simple elementary reactions that are theoretically important and to unravel the mechanism of complex chemical reactions or photochemical processes that play important roles in many macroscopic processes. Molecular beams of reactants are used to study individual reactive encounters between molecules or to monitor photodissociation events in a collision-free environment. Most of the information is derived from measurement of the product fragment energy and angular and state distributions. Recent activities are centered on the mechanisms of elementary chemical reaction dynamics in divalent systems, nonadiabatic collision dynamics, the dependence of the chemical reactivity of electronically excited atoms on the alignment of excited orbitals, the primary photochemical processes of polyatomic molecules, intramolecular energy transfer of chemically activated and locally excited molecules, the energetics of free radicals that are important to combustion processes, the infrared-absorption spectra of carbonium ions, and bond-selective photodissociation through electronic excitation.

1. State-Specific Reactions of $Ba(^1S_0)$ and $Ba(^1D_2)$ with Water and Methanol (Publication 6)

H.F. Davis, A.G. Suits, Y.T. Lee, C. Alcaraz, and J.-M. Mestdagh

The reactions of $Ba(6s^2\ ^1S_0)$ and $Ba(6s5d\ ^1D_2)$ with water and methanol were studied under single collision conditions using crossed molecular beams. Reaction of ground-state $Ba(^1S) + H_2O$ led to dominant formation of $BaO + H_2$ at all collision energies studied (12–30 kcal/mol). Although the reaction $Ba(^1S) + H_2O \rightarrow BaOH + H$ could also be observed at collision energies above the endoergicity of the reaction (13 kcal/mol), it remained a minor channel even at the highest collision energy. Electronic excitation of the Ba atom reactant to the metastable $^1D_2$ state led to a large enhancement in reactivity, but the products were BaOH + H rather than $BaO + H_2$. The dominance of $BaO + H_2$ from ground-state $Ba(^1S)$ even at collision energies nearly equal to the $Ba(^1D)$ excitation energy of 11,395 cm^{-1} (~32 kcal/mol) indicates that the observed reaction state specificity results from participation of different potential energy surfaces for reactions of ground- and excited-state atoms. Collisions of $Ba(^1S)$ and $Ba(^1D)$ with methanol led only to formation of $BaOCH_3 + H$. We observed no $BaOH + CH_3$ or $BaO + CH_4$, even though they are the more thermodynamically favorable channels. Although reactivity with methanol was strongly enhanced by electronic excitation of the incident Ba atom, no reaction was observed from $Ba(^1S)$ or $Ba(^1D)$ + dimethyl ether (CH_3OCH_3). These observations strongly suggest that the reactions leading to radical formation involve H-atom migration.

2. Infrared Spectra of CH_5^+ Core in $CH_5^+(H_2)$ (Publication 8)

D.W. Boo and Y.T. Lee

The infrared spectra of the CH_5^+ core in $CH_5^+(H_2)$ are presented. These spectra are the first spectroscopic results for the CH_5^+-related systems. The C–H stretching bands of the CH_5^+ core were observed as one broad feature with shoulders, centered at 2,966 cm^{-1}. The predicted C–H stretching frequencies for the minimum energy structure containing CH_5^+ with eclipsed C_s symmetry match quite well those of the observed features after appropriate scaling. Possible reasons for the band broadening are also discussed.

3. Crossed Molecular Beam Study of the Reaction of $O(^3P)$ + Allene (Publication 7)

A.M. Schmoltner, S.Y. Huang, R.J. Brudzynski, P.M. Chu, and Y.T. Lee

The reaction between ground-state (^3P) oxygen atoms and allene was studied under single collision conditions using the crossed molecular beams method. Product angular distributions and the translational energy distribution were determined for each channel. Two major reaction channels could be identified unambiguously: the formation of carbon monoxide and ethylene following oxygen atom attack on the central carbon atom, and the formation of allenyloxy (formyl-vinyl) radical and hydrogen atom following oxygen atom attack on the terminal carbon atom. In addition, at least one other reaction channel, which could be identified as the

*This work was supported by the Director, Office of Energy Research, Office of Basic Energy Sciences, Chemical Sciences Division, of the U.S. Department of Energy under Contract No. DE-AC03-76SF00098.

production of vinyl and formyl radicals, occurs. This channel involves the decomposition of acrolein, which is formed by the addition of oxygen to the terminal carbon atom, followed by 1,2-hydrogen migration.

4. The Dissociation Energy and Photochemistry of NO_3 (Publication 5)

H.F. Davis, B. Kim, H.S. Johnston, and Y.T. Lee

The photodissociation of NO_3 was studied using the method of molecular beam photofragmentation translational spectroscopy. The existence of two photodissociation channels was confirmed under collision-free conditions. At excitation energies below $D_0(O–NO_2)$ for internally cold NO_3, we observe a large quantum yield (0.70 ± 0.10 at 588 nm) for a concerted three-center rearrangement resulting in $NO(^2\Pi) + O_2(^3\Sigma_g^-, {}^1\Delta)$. The quantum yield for the $NO + O_2$ channel decreased sharply at wavelengths shorter than 587 nm, falling to <0.01 at 583 nm, while the $NO_2 + O(^3P)$ quantum yield increased to >0.99. On the basis of this wavelength dependence and the product translational energy distributions, we conclude that the wavelength threshold for $NO_3(0,0,0,0) \rightarrow NO_2(0,0,0) + O(^3P_2)$ is 587 nm ± 3 nm; i.e., $D_0(O–NO_2) = 48.69 \pm 0.25$ kcal/mol. From the enthalpies of formation of $O(^3P_2)$ and $NO_2(^2A_1)$, we calculate $\Delta H_f^\circ(NO_3) = 18.87 \pm 0.33$ kcal/mol at 0 K and $\Delta H_f^\circ(NO_3) = 17.62 \pm 0.33$ kcal/mol at 298 K. This is 2.23 kcal/mol higher than the most recent thermochemical value but is consistent with a value calculated indirectly using the most recent values for the electron affinity (EA) of NO_3 and $\Delta H_f^\circ(NO_3^-)$. From the wavelength dependence and translational energy distributions for $NO_3 \rightarrow NO + O_2$, the potential energy barrier for $NO_3(^2A_2) \rightarrow NO(^2\Pi) + O_2(^2\Sigma_g^-)$ was found to be 47.3 ± 0.8 kcal/mol.

5. The Near-Ultraviolet Photodissociation Dynamics of Azomethane (Publication 9)

S.W. North, C.A. Longfellow, and Y.T. Lee

The photodissociation of azomethane following absorption of a single 351-nm photon was studied using the method of molecular beam photofragment translational spectroscopy. The dissociation was observed to proceed via cleavage of both C–N bonds to yield N_2 and two methyl radicals. The measured time-of-flight spectra show evidence that the two methyl radicals possess unequal velocities in the azomethane center of mass, suggesting that the dissociation is not symmetric. The angles between the asymptotic center-of-mass velocities for all three fragments are strongly correlated, implying that the methyldiazenyl radical (CH_3N_2) intermediate decomposes within a fraction of its rotational period. We conclude, therefore, that the dissociation is *concerted*, not stepwise as was inferred from recent time-resolved experiments. The overall translational energy distributions for all the photofragments in the azomethane center of mass reveal that an average of 60% of the total available energy appears as translation. A possible mechanism, consistent with the experimental findings, will be proposed and discussed.

6. Resonance-Enhanced One- and Two-Photon Ionization of Water Molecule: Preliminary Analysis by Multichannel Quantum Defect Theory (Publication 2)

M.J.J. Vrakking, Y.T. Lee, R.D. Gilbert, and M.S. Child

Experimental results are presented for one- and two-photon ionization of the water molecule, obtained using a near-transform-limited XUV laser. The single-photon ionization results show rotationally resolved autoionizing resonances corresponding to members of Rydberg series ($nd \leftarrow 1b_1$; $n = 6$–11) converging on the $H_2O^+(100)$ vibrational state. The two-color (1 + 1) multiphoton ionization results show rotationally resolved structure corresponding to Rydberg series ($nd \leftarrow 1b_1$; $n \geq 6$) converging on the $H_2O^+(000)$ vibrational state. Typical linewidths below and above $H_2O^+(000)$, the ionization threshold, are 1 and 2 cm^{-1}, respectively. The experimental results are simulated by multichannel quantum defect theory (MQDT). The main features in the spectrum are reproduced in a treatment of the rotational channel interactions with partial l mixing. It is argued that remaining discrepancies between experiment and theory arise from perturbative interactions between the ($nd \leftarrow 1b_1$) levels and members of the ($nd \leftarrow 3a_1$) Rydberg series. Also, it is argued that in the (1 + 1) multiphoton ionization spectra lines may be missing due to selective predissociation.

7. Photodissociation Dynamics of CO_2 at 157.6 nm by Photofragment-Translational Spectroscopy (Publication 3)

A. Stolow and Y.T. Lee

The photodissociation of CO_2 at 157 nm was studied by the photofragment-translational spectroscopy technique. Product time-of-flight spectra were recorded and center-of-mass translational energy distributions were determined. Two electronic channels were observed—one forming

$O(^1D)$ and the other $O(^3P)$. With previously determined anisotropy parameters of $\beta = 2$ for the $O(^3P)$ channel and $\beta = 0$ for the $O(^1D)$ channel, an electronic branching ratio of $6\% \pm 2\%$ $O(^3P)$ was obtained, consistent with previous results. The translational energy distribution for the $CO(\upsilon) + O(^3P)$ channel was very broad (over 30 kcal/mol) and appeared to peak near $CO(\upsilon = 0)$. The value of $\beta = 2$ for the $O(^3P)$ channel was confirmed by comparing Doppler profiles, derived from our measured translational energy distribution, with previously measured Doppler profiles. This suggests that the $O(^3P)$ channel arises from a direct transition to an excited triplet state. The $O(^1D)$ channel had a structured time-of-flight that related to rovibrational distributions of the CO product. The influence of the excitation of the $CO_2(\upsilon_2)$ bending mode was investigated and shown to have a small but not negligible contribution. Based upon a comparison of our data with previous vacuum-ultraviolet (VUV) laser-induced fluorescence study, we obtain as our best estimate of the vibrational branching ratio, $CO(\upsilon = 0)/CO(\upsilon = 1) = 1.9$, for the $CO(\upsilon) + O(^1D)$ channel.

8. $Ba(6s6p\ ^1P_{1,m_j}) \rightarrow Ba(6s6p\ ^3P_{2,m'_j})$ Zeeman Cross Sections in Single Collisions with N_2, O_2, and H_2 (Publication 1)

J.-M. Mestdagh, P. Meynadier, P. de Pujo, O. Sublemontier, J.-P. Visticot, J. Berlande, J. Cuvellier, T. Gustavsson, A.G. Suits, and Y.T. Lee

Zeeman cross sections $\sigma_{j,m_j \rightarrow j',m'_j}$ for the spin-changing $6s\ 6p\ ^1P_1 - 6s\ 6p\ ^3P_2$ transition of barium induced by single collisions with N_2, O_2, and H_2 have been measured using a crossed-beam apparatus. State-selective preparation of $6s\ 6p\ ^1P_{1,m_j}$ and detection of $6s\ 6p\ ^3P_{2,m'_j}$ were achieved using the laser excitation technique in the presence of a magnetic field that breaks the degeneracy of the magnetic sublevels. The results showed that the Zeeman cross sections $\sigma(^1P_{1,m_j} \rightarrow {}^3P_{2,m'_j})$ are fairly dependent upon m_j and m'_j for N_2 and H_2, whereas the Zeeman cross sections all have the same value with O_2. Additionally, the flux-velocity contour map of $Ba(6s\ 6p\ ^3P_2)$ for scattering with H_2 depends significantly on the magnetic sublevel of barium in the exit channel. The results for $Ba–(N_2,H_2)$ scattering were accounted for semiquantitatively by a very simple model. The model was then used to stress which physical phenomena are at the origin of the preservation of the orbital alignment and orientation during collisions. The present work also compared the kind of information obtained by the direct measurement of Zeeman cross sections to that found in other experiments that deal with the effect of polarizing the collision partners.

9. Ultrasensitive Detection of Hydrogen Molecules by (2 + 1) Resonance-Enhanced Multiphoton Ionization (Publication 4)

M.J.J. Vrakking, A.S. Bracker, T. Suzuki, and Y.T. Lee

Ultrasensitive detection of molecular hydrogen is reported by using Doppler-free (2 + 1) resonance-enhanced multiphoton ionization through the $E,F\ ^1\Sigma_g^+$ state. By using an arrangement with two near-transform-limited counterpropagating laser beams, a single-shot detection efficiency of 6.8×10^3 molecules/cm^3 has been demonstrated. Frequency scans of the two-photon transitions show that the detection efficiency is limited by AC Stark effects.

10. Work in Progress

Considerable effort is currently directed to an investigation of the dissociation dynamics of hydrocarbon radicals. A Chen-type pulsed pyrolytic source has been developed for generating intense beams of cooled radicals. The first investigation into the photochemistry of the allyl radical suggests the formation of methyl + acetylene as a minor channel in addition to the dominant hydrogen atom elimination. Studies of the photochemistry of methyl and ethyl radicals promise further insight into the thermochemistry and dissociation dynamics of these species. Pyrolytic fragmentation is of central importance in combustion processes, and a study currently under way using IR multiphoton excitation of fluorocarbons promises to yield valuable insight into the ground-state dissociation processes of these molecules.

A very well-defined beam of $O(^1D)$ has recently been developed using photolysis of ozone in the expansion from a high-pressure-pulsed nozzle. The result is a pulsed beam characterized by a very narrow velocity distribution that will yield unprecedentedly high-resolution $O(^1D)$ reactive scattering experiments. Initial studies focus on an understanding of the dynamics of $O(^1D)$ reactions with H_2 and hydrocarbons.

Recent studies in the IR spectroscopy of solvated carbonium ions have been quite fruitful. "Consequence spectroscopy" enables us to record spectra that are mass-specific in both parent and daughter ions. Using this technique with isotope labeling, we have shown that proton exchange is rapid (barrier <9 kcal/mole) between carbons in $CH_5^+(CH_4)$. Further studies of solvation series of carbonium ions, as well as studies of the spectroscopy of radical cations such as CH_3OH^+, $C_2H_5OH^+$ and $CH_3COCH_3^+$, are currently under way.

We have recently succeeded in producing an intense supersonic lithium atomic beam and exciting it to the 2P

state. Studies of the reaction dynamics of these excited atoms and the orbital alignment dependence of the product distributions promise detailed insight into systems that may be directly and meaningfully compared to accurate quantum mechanical calculations.

FY 1993 PUBLICATIONS AND REPORTS

Refereed Journals

1. J.-M. Mestdagh, P. Meynadier, P. de Pujo, O. Sublemontier, J.-P. Visticot, J. Berlande, J. Cuvellier, T. Gustavsson, A.G. Suits, and Y.T. Lee, "Ba($6s6p\ ^1P_{1,mj}$) → Ba($6s6p\ ^3P_{2,mj}$) Zeeman Cross Sections in Single Collisions with N_2, O_2, and H_2," Phys. Rev. A **47**, 241–254 (1993); LBL-33860.
2. M.J.J. Vrakking, Y.T. Lee, R.D. Gilbert, and M.S. Child, "Resonance-Enhanced One- and Two-Photon Ionization of Water Molecule: Preliminary Analysis by Multichannel Quantum Defect Theory," J. Chem. Phys. **98**, 1902–1915 (1993); LBL-32590.
3. A. Stolow and Y.T. Lee, "Photodissociation Dynamics of CO_2 at 157.6 nm by Photofragment-Translational Spectroscopy," J. Chem. Phys. **98**, 2066–2076 (1993); LBL-32651.
4. M.J.J. Vrakking, A.S. Bracker, T. Suzuki, and Y.T. Lee, "Ultrasensitive Detection of Hydrogen Molecules by (2 + 1) Resonance-Enhanced Multiphoton Ionization," Rev. Sci. Instrum. **64**, 645–652 (1993); LBL-32881.
5. H.F. Davis, B. Kim, H.S. Johnston, and Y.T. Lee, "The Dissociation Energy and Photochemistry of NO_3," J. Phys. Chem. **97**, 2172–2180 (1993); LBL-33113.
6. H.F. Davis, A.G. Suits, Y.T. Lee, C. Alcaraz, and J.-M. Mestdagh, "State-Specific Reactions of Ba($^1S_0$) and Ba($^1D_2$) with Water and Methanol," J. Chem. Phys. **98**, 9595–9609 (1993); LBL-33577.
7. A.M. Schmoltner, S.Y. Huang, R.J. Brudzynski, P.M. Chu, and Y.T. Lee, "Crossed Molecular Beam Study of the Reaction of O(^3P) + Allene," J. Chem. Phys. **99**, 1644–1653 (1993); LBL-27917.
8. D.W. Boo and Y.T. Lee, "Infrared Spectra of CH_5^+ Core in CH_5^+ (H_2)," Chem. Phys. Lett. **211**, 358–363 (1993); LBL-34170.
9. S.W. North, C.A. Longfellow, and Y.T. Lee, "The Near-Ultraviolet Photodissociation Dynamics of Azomethane," J. Chem. Phys. **99**, 4423–4429 (1993); LBL-34092.

LBL Reports

10. M.W. Crofton, J.M. Price, and Y.T. Lee, "IR Spectroscopy of Hydrogen-Bonded Charged Clusters," in *Clusters of Atoms and Molecules*, edited by H. Haberland (Springer-Verlag, Berlin, 1993) (submitted); LBL-29681.
11. L.I. Yeh, Y.T. Lee, and J.T. Hougen, "Vibration-Rotation Spectroscopy of the Hydrated Hydronium Ions $H_5O_2^+$ and $H_9O_4^+$," J. Chem. Phys. (submitted); LBL-32591.
12. S.J. Sibener and Y.T. Lee, "The Internal and Translational Energy Dependence of Molecular Condensation Coefficients: SF_6 and CCl_4," J. Chem. Phys. (submitted); LBL-34775.
13. J.D. Myers, "Chemical Dynamics of Time and Energy Space," Ph.D. Thesis, 1993; LBL-34091.
14. J. Zhang, "Crossed Molecular Beam Studies of Atmospheric Chemical Reaction Dynamics," Ph.D. Thesis, 1993; LBL-34297.

Invited Talks

15. Y.T. Lee, "Energetics and Dynamics of Polyatomic Radicals," 13th International CODATA Conference, Beijing, China, October 19, 1992.
16. Y.T. Lee, "Orbital Alignment in Electronically Excited Atoms," Department of Physics, University of Texas, Austin, TX, October 28, 1992.
17. Y.T. Lee, "Steering Chemical Reactions by Laser Excitation," Arizona State University, Tempe, AZ, November 16–19, 1992.
18. Y.T. Lee, "Dynamics of Concerted Decomposition of Organic Molecules," Arizona State University, Tempe, AZ, November 16–19, 1992.
19. Y.T. Lee, "Infrared Absorption Spectroscopy of Solvated Ions in the Gas Phase," Arizona State University, Tempe, AZ, November 16–19, 1992.
20. Y.T. Lee, "Concerted Molecular Elimination in the Dissociation of Polyatomic Molecules," E.K.C. Lecturer, Department of Chemistry, University of California, Irvine, CA, December 1, 1992.
21. Y.T. Lee, "Infrared Multiphoton Excitation of Solvated Ions," Department of Chemistry, University of California, Irvine, CA, December 3, 1992.
22. Y.T. Lee, "Application of Synchrotron Light Source on Molecular Dynamics," Okazaki Conference, Institute of Molecular Sciences, Okazaki, Japan, December 16, 1992.
23. Y.T. Lee, "Application of VUV Undulator Beam Line to Chemical Dynamics at ALS," 46th Okazaki Conference, Institute for Molecular Science, Myodaiji, Okazaki, Japan, December 16–18, 1992.
24. Y.T. Lee, "Steering Chemical Reactions Through Laser Excitations," Institute of Molecular Sciences, Okazaki, Japan, December 17, 1992.
25. Y.T. Lee, "Science and Technology Policy in Taiwan," K.T. Lee Lectureship in Science Policy, National Taiwan University, Taipei, Taiwan, December 21, 1992.
26. Y.T. Lee, "Experimental Studies of State-Resolved Angular Distribution of D + H_2 → DH + H Reaction," Symposium on Physical Chemistry, Institute of Atomic and Molecular Sciences, Taipei, Taiwan, December 28, 1992.
27. Y.T. Lee, "Infrared Spectroscopy of Ionic Complexes of CH_5^+," International Society for Optical Engineers Symposium, Los Angeles, CA, January 21–23, 1993.
28. Y.T. Lee, "Infrared Spectroscopy of $CH_5^+ \rightarrow CH_4$," Workshop on Chemistry of Carbonium Ions, Locker Hydrocarbon Research Institute, University of Southern California, Los Angeles, CA, January 28, 1993.

29. Y.T. Lee, "Report on Conference on Synchrotron Radiation Applications, December 1992, Japan," Workshop on Applications of Synchrotron Radiation in Chemical Dynamics, Oakland, CA, February 5, 1993.
30. Y.T. Lee, "Steering Chemical Reactions Through Laser Excitations," Faculty Research Lecturer, University of California, Berkeley, CA, February 24, 1993.
31. Y.T. Lee, "Bond-Selective and Mode-Selective Chemistry Through Laser Excitation," Xiamen University, Xiamen, China, March 25, 1993.
32. Y.T. Lee, "Steering Chemical Reactions Through Laser Excitation, Molecular Beam Chemistry," Merck Lecturer, Department of Chemistry, Hope College, Holland, MI, April 23, 1993.
33. Y.T. Lee, "Molecular Beam Studies of Elementary Chemical Reactions," Merck Lecturer, Hope College, Holland, MI, April 23, 1993.
34. Y.T. Lee, "Molecular Reaction Dynamics by Lasers and Molecular Beams," Department of Chemistry, Bilkent University, Ankara, Turkey, May 11, 1993.
35. Y.T. Lee, "Application of VUV Photons in Chemical Reaction Dynamics," Institute Molecular Beam Symposium, Berlin, Germany, May 17, 1993.
36. Y.T. Lee, "Molecular Beam Studies of Reaction Dynamics," 1993 Combustion Research Contractors' Meeting, Split Rock Resort and Conference Center, Lake Harmony, PA, June 2–4, 1993.

Molecular Interactions*

William A. Lester, Jr., Investigator

INTRODUCTION

This research program is directed at extending fundamental knowledge of atoms and molecules, including their electronic structure, mutual interaction, collision dynamics, and interaction with radiation. The approach combines the use of *ab initio* basis set methods with the recently developed quantum Monte Carlo (QMC) to describe electronic structure, intermolecular interactions, and other properties. The approach uses various methods for characterizing inelastic and reactive collision processes, including surface-catalyzed processes and photodissociation dynamics. Present activity is focused primarily on the development and application of the QMC method.

1. Random-Walk Approach to Mapping Nodal Regions of *N*-Body Wavefunctions: Ground-State Hartree-Fock Wavefunctions for Li–C (Publication 1)

W.A. Glauser,† W.R. Brown, W.A. Lester, Jr., D. Bressanini,‡ B.L. Hammond,‖ and M.L. Koszykowski¶

Despite the widespread acceptance of the relevance of the nodes of one-body electronic wavefunctions (atomic or molecular orbitals) in determining chemical properties, relatively little is known about the corresponding nodes of many-body wavefunctions. As an alternative to mapping the nodal surfaces present in the ground state of many-electron systems, we have focused instead on the structural domains implied by these surfaces. In the spirit of Monte Carlo techniques, the nodal hypervolumes of a series of atomic *N*-body Hartree-Fock level electronic wavefunctions have been mapped using a random-walk simulation in $3N$-dimensional configuration space. The basic structural elements of the domain of atomic or molecular wavefunctions are identified as nodal regions (continuous volumes of the same sign) and permutational cells (identical building blocks). The algorithm determines both the relationships among nodal regions or cells (topology) and the geometric properties within each structural domain. Results indicate that ground-state Hartree-Fock wavefunctions generally consist of four equivalent nodal regions (two positive and two negative), each constructed from one or more permutational cells. In the course of this research, we have developed an operational method to distinguish otherwise identical permutational cells.

*This work was supported by the Director, Office of Energy Research, Office of Basic Energy Sciences, Chemical Sciences Division, of the U.S. Department of Energy under Contract No. DE-AC03-76SF00098.

†Permanent address: Fujitsu America, Inc., Malvern, Pennsylvania.
‡Permanent address: University of Milan, Milan, Italy.
‖Permanent address: Fujitsu America, Inc., San Jose, California.
¶Permanent address: Sandia National Laboratory, Livermore, California.

2. Computation of Transition Dipole Moments by Monte Carlo (Publication 2)

R.N. Barnett,† P.J. Reynolds,‡ and W.A. Lester, Jr.

Three Monte Carlo methods for computing transition dipole moments have been developed. Two of these approaches are based on the use of multiple Monte Carlo "random walks" to sample different probability distributions. The remaining technique employs a single Monte Carlo walk and averages an analytic approximation of Green's function to sample other distributions. The accuracy and efficiency of each method has been investigated by computing the transition dipole moment between the ls and $2p_z$ states of the hydrogen atom. Monte Carlo parameters, such as the time step size and the convergence time, were varied to study their effect on computed results. It was found that the approach based on a guided Metropolis walk with quantum Monte Carlo "side walks" and also the approach based on Green's function averages yield accurate transition dipole moments efficiently. These two methods also yield accurate energies and expectation values for the individual eigenstates. The approach based on two equivalent quantum Monte Carlo walks, one for each state, was found to be least satisfactory.

†Present address: Department of Chemistry, University of California, Berkeley, California.
‡Permanent address: Physics Division, Office of Naval Research, Arlington, Virginia.

3. Reorientation Cross Sections in Collisions of $He(^1S) + H_2(B\ ^1\Sigma_u^+)$ (Publication 3)

J.A. Odutola,† W.A. Lester, Jr., and R.M. Grimes‡

Reorientation cross sections were computed for the $He(^1S) + H_2(B\ ^1\Sigma_u^+)$ using a potential energy surface and model previously introduced for rovibrational energy transfer.[1] The model consists of restricting the scattering

solely to the excited state potential energy surface and the use of the coupled-channel method. The calculated reorientation cross section is 41.6 Å^2 for the transition ($vjm_j \equiv 0,1,0 \rightarrow v'j'm_{j'} \equiv 0,1,\pm 1$) at room temperature; the corresponding Boltzmann average is 39.2 Å^2. The latter result is in good agreement with a recent measurement by Pibel and Moore of 29.7 ±7.4 Å^2.

[†]Permanent address: Department of Chemistry, Obafemi Awolowo University, Ile-Ife, Nigeria.

[‡]Permanent address: Texas Instruments, Stafford, Texas.

1. R.M. Grimes, W.A. Lester, Jr., and M. Dupuis, J. Chem. Phys. **84**, 5437 (1986).

2. C.D. Pibel and C.B. Moore, J. Chem. Phys. **93**, 4804 (1990)

4. The Effects of Lone Pairs on Charge Distribution in the Tetracyclic Norbornyl Derivatives (Publication 4)

J.W. de M. Carneiro,[†] P.R. Seidl,[‡] J.G.R. Tostes,[||] C.A. Taft,[¶] B.L. Hammond,[§] M.M. Soto, and W.A. Lester, Jr.

Ab initio and MM2 Allinger calculations have been used to investigate charge distributions in different conformations of the hydroxyl groups in unsaturated alcohols containing norbornyl units. The study was undertaken to investigate an intriguing lack of symmetry in the charge distribution on atoms that lie close to the hydroxyl group. Previous examination of the effect of rotating the carbon–oxygen bond revealed that the position of the lone pair is responsible for polarization of carbon–hydrogen and carbon–carbon bonds. The calculated net atomic charges indicate that hydrogens as well as carbons lying between oxygen lone pairs become more positively charged.

[†]Permanent address: Departmento de Fisico-Quimica, Universidade Federal Fluminenes, Niteroi, RJ, Brazil.

[‡]Permanent address: Secao de Quimica, Instituto, Millitar de Engenharia, Rio de Janeiro, RJ, Brazil.

[||]Permanent address: Departmento de Fisico-Quimica, Universidade Federal Fluminenes, Niteroi, RJ, Brazil.

[¶]Permanent address: Centro Brasileiro de Pesquisas Fisicas, Rio de Janeiro, RJ, Brazil.

[§]Permanent address: Fujitsu America, Inc., San Jose, California.

FY 1993 PUBLICATIONS AND REPORTS

Refereed Journals

1. W.A. Glauser, W.R. Brown, W.A. Lester, Jr., D. Bressanini, B.L. Hammond, and M.L. Koszykowski, "Random-Walk Approach to Mapping Nodal Regions of *N*-Body Wavefunctions: Ground-State Hartree-Fock Wavefunctions for Li–C," J. Chem. Phys. **97**, 9200 (1992); LBL-32885.
2. R.N. Barnett, P.J. Reynolds, and W.A. Lester, Jr., "Computation of Transition Dipole Moments by Monte Carlo," J. Chem. Phys. **96**, 2141 (1992); LBL-31146.
3. J.A. Odutola, W.A. Lester, Jr., and R.M. Grimes, "Reorientation Cross Sections in Collisions of $He(^1S) + H_2(B\ ^1\Sigma_u^+)$," J. Chem. Phys. **99**, 2632 (1993); LBL-34011.
4. J.W. de M. Carneiro, P.R. Seidl, J.G.R. Tostes, C.A. Taft, B.L. Hammond, M.M. Soto, and W.A. Lester, Jr., "The Effects of Lone Pairs on Charge Distribution in the Tetracyclic Norbornyl Derivatives," Chem. Phys. Letts. **202**, 278 (1993); LBL-33127.

LBL Reports

5. J.G.R. Tostes, J.W. de M. Carneiro, S.K. Lie, P.R. Seidl, C.A. Taft, M.M. Soto, W.A. Lester, Jr., and B.L. Hammond, "Hyperconjugation and Charge Distribution in Alicyclic Alcohols and EXO and ENDO Norbornol," J. Mol. Struc. (THEOCHEM) (submitted); LBL-35147.
6. A.C. Pavão, M.M. Soto, W.A. Lester, Jr., S.K. Lie, B.L. Hammond, and C.A. Taft, "Molecular States of the CO Interaction with the 3d Metal Surfaces," Phys. Rev. B (submitted); LBL-34391.
7. Z. Sun, M.M. Soto, and W.A. Lester, Jr., "Characteristics of Electron Movement in Variational Monte Carlo Simulations," J. Chem. Phys. (accepted); LBL-35148.

Invited Talks

8. W.A. Lester, Jr., "Theoretical Studies of Molecular Interactions," DOE Office of Basic Energy Sciences Combustion Research Meeting, Split Rock Resort and Conference Center, Lake Harmony, PA, June 1–4, 1993; LBL-35146.

Theory of Atomic and Molecular Collision Processes*

William H. Miller, Investigator

INTRODUCTION

This research primarily involves the development and application of theoretical methods and models for describing atomic and molecular collision processes and chemical reaction dynamics. Specific topics of interest include the theory of inelastic and reactive scattering, collision processes involving electronically excited atoms or molecules, collisional ionization phenomena, statistical theories of chemical reactions, scattering of atoms and molecules from surfaces, and the interactions of molecular systems with high power laser radiation.

The research deals with both development of rigorous theoretical approaches that are applicable to *simple* chemical systems, and more approximate methods that are applicable to *complex* chemical systems, e.g., polyatomic molecules and their reactions. Even in the latter area, however, the goal is to develop approaches that can utilize *ab initio* quantum chemical calculations of the potential energy surface (in the Born–Oppenheimer approximation) as direct input into the dynamical treatment. Thus, to as great an extent as possible, these approaches have a truly predictive theory.

1. A Random Matrix/Transition State Theory for the Probability Distribution of State-Specific Unimolecular Decay Rates: Generalization to Include Total Angular Momentum Conservation and Other Dynamical Symmetries (Publication 6)

R. Hernandez, W.H. Miller, C.B. Moore, and W.F. Polik†

A previously developed random matrix/transition state theory (RM/TST) model for the probability distribution of state-specific unimolecular decay rates has been generalized to incorporate total angular momentum conservation and other dynamical symmetries. The model is made into a predictive theory by using a semiclassical method to determine the transmission probabilities of a nonseparable rovibrational Hamiltonian at the transition state. The overall theory gives a good description of the state-specific rates for the $D_2CO \rightarrow D_2 + CO$ unimolecular decay. In particular, it describes the dependence of the distribution of rates on total angular momentum J. Comparison of the experimental values with results of the RM/TST model suggests that there is mixing among the rovibrational states.

†Department of Chemistry, Hope College, Holland, MI 49423.

2. Semiclassical Transition State Theory—A New Perspective (Publication 10)

R. Hernandez and W.H. Miller

The semiclassical transition state theory (SCTST) introduced by Miller, Hernandez, Handy, Jayatilaka and Willets[1] requires the inversion of an (effectively integrable) Hamiltonian with respect to the action of the reactive coordinate. This paper shows that the inversion may be avoided in computing the thermal rate constant. The resulting expression also provides an appealing link to conventional transition state theory. This reformulation of the SCTST rate is illustrated by application to the bimolecular reaction, $H + H_2 \rightarrow H_2 + H$, and to the unimolecular dissociation, $D_2CO \rightarrow D_2 + CO$.

1. W.H. Miller, R. Hernandez, M.C. Handy, D. Jayatilaka, and A. Willets, Chem. Phys. Lett. 172, 62 (1990).

3. A New Computational Algorithm for Green's Functions: Fourier Transform of the Newton Polynomial Expansion (Publication 13)

S.M. Auerbach and C. Leforestier†

A new iterative method to compute the Green's function for continuum systems is presented here. It is based on a Newton polynomial expansion of the corresponding propagator, followed by accurate half-Fourier transformation. The new technique is remarkably stable and accurate, and can handle very large systems. We apply the new method to the calculation of three-dimensional quantum reaction probabilities for the initial state-selected $D + H_2(n,j) \rightarrow DH + H$ reaction. We find excellent agreement with previous results, requiring very modest amounts of CPU time.

†Laboratoire de Chimie Théorique, Université de Paris-Sud, 91405 Orsay, France

*This work was supported by the Director, Office of Energy Research, Office of Basic Energy Sciences, Chemical Sciences Division, of the U.S. Department of Energy under Contract No. DE-AC03-76SF00098.

4. Efficient Polynomial Expansion of the Scattering Green's Function: Application to the D + $H_2(v = 1)$ Rate Constant (Publication 16)

S.M. Auerbach and W.H. Miller

We apply the absorbing boundary condition (ABC) discrete variable representation (DVR) theory of quantum reactive scattering to the initial state-selected $D + H_2(v = 1,j) \rightarrow DH + H$ reaction. The ABC-DVR Green's function is efficiently computed by a Newton polynomial expansion. We compute accurate reaction probabilities for the total energies and angular momenta required to obtain the thermal rate constants $k_{v=1,j}(T)$. As $T = 310$ K, a thermal average over $j = (0,1,2,3)$ is performed to yield the final result $k_{v=1,j}(310\text{ K}) = 1.87 \times 10^{13}$ cm^3 molecule^{-1} s^{-1}, in *quantitative* agreement with the most recent experimental value $(1.9 \pm 0.2) \times 10^{-13}$ cm^3 molecule^{-1} s^{-1}. The *J*-shifting approximation using accurate $J = 0$ reaction probabilities is tested against the exact results. It reliably predicts $k_{v=1}(T)$ for temperatures up to 700 K, but individual $(v = 1,j)$ selected-rate constants are in error by as much as 41%.

5. State-Specific Reaction Probabilities from a DVR-ABC Green's Function (Publication 5)

W.H. Thompson and W.H. Miller

Seideman and Miller[2] have recently introduced a direct, efficient method for calculating cumulative reaction probabilities by using a discrete variable representation (DVR) to represent the Green's function and absorbing boundary conditions (ABC) to enforce the outgoing wave boundary conditions. The present paper shows that this method for representing the Green's function can also be used to calculate *state-specific* reaction probabilities. Application to the collinear reaction $H + H_2 \rightarrow H_2 + H$ demonstrates that the method is an efficient way to calculate state-to-state and partially state-resolved reaction probabilities. In addition, distorted waves are useful in reducing the size of the DVR basis.

2. T. Seideman and W.H. Miller, J. Chem. Phys. **96**, 4412 (1992); **97**, 2499 (1992).

6. The Cumulative Reaction Probability as Eigenvalue Problem (Publication 9)†

U. Manthe‡ and W.H. Miller

It is shown that the cumulative reaction probability for a chemical reaction can be expressed (absolutely rigorously) as

$$N(E) = \sum_k p_k(E),$$

where $\{p_k\}$ are the eigenvalues of a certain Hermitian matrix (or operator). The eigenvalues $\{p_k\}$ all lie between 0 and 1 and thus have the interpretation of probabilities, *eigen reaction probabilities*, which may be thought of as the rigorous generalization of the transmission coefficients for the various states of the activated complex in transition state theory. The eigen reaction probabilities $\{p_k\}$ can be determined by diagonalizing a matrix that is directly available from the Hamiltonian matrix itself. It is also shown how a very efficient iterative method can be used to determine the eigen reaction probabilities for problems that are too large for a direct diagonalization to be possible. The number of iterations required is much smaller than that of previous methods, approximately the number of eigen reaction probabilities that are significantly different from zero. All of these new ideas are illustrated by application to three model problems: transmission through a one-dimensional (Eckart potential) barrier, the collinear $H + H_2 \rightarrow H_2 + H$ reaction, and the three-dimensional version of this reaction for total angular momentum $J = 0$.

†This work is also supported in part by the National Science Foundation, Grant CHE-89-20690.

‡Fakultät für Physik, University of Freiburg, 7800 Freiburg, Germany.

7. Full Dimensional Quantum Mechanical Calculation of the Rate Constant for the $H_2 + OH \rightarrow H_2O + H$ Reaction (Publication 11)†

U. Manthe,‡ T. Seideman,‖ and W.H. Miller

The cumulative reaction probability (CRP) (the Boltzmann average of which is the thermal rate constant) has been calculated for the reaction $H_2 + OH \rightarrow H_2O + H$ in its full (six) dimensionality for total angular momentum

$J = 0$. The calculation, which should be the (numerically) exact result for the assumed potential energy surface, was carried out by a "direct" procedure that avoids having to solve the complete state-to-state reactive scattering problem. Higher angular momenta ($J > 0$) were taken into account approximately to obtain the thermal rate constant $k(T)$ over the range $300\ \text{K} < T < 700\ \text{K}$. The result is significantly larger than the experimental values (a factor of ~4 at 300 K), indicating that a more accurate potential energy surface is needed in order to provide a quantitative description of this reaction.

†This work is also supported in part by the National Science Foundation, Grant CHE89-20690.
‡Fakultät für Physik, University of Freiburg, 7800 Freiburg, Germany.
||Steacie Institute for Molecular Sciences, National Research Council of Canada, Ottawa, Ontario K1A 0R6, Canada.

8. Quantum Mechanical Calculation of the Rate Constant for the Reaction $H + O_2 \rightarrow OH + O$ (Publication 14)†‡

C. Leforestier|| *and W.H. Miller*

Rigorous three-dimensional quantum mechanical calculations have been carried out for the cumulative reaction probability of the titled reaction for total angular momentum $J = 0$. Higher values of J are included approximately, and the resulting thermal rate constant agrees well with experimental values for $1000\ \text{K} \leq T \leq 3000\ \text{K}$.

†This work is also supported in part by the National Science Foundation, Grant CHE89-20690.
‡Calculations were carried out on the Cray C-90 at the National Energy Research Supercomputer Center (NERSC) at the Lawrence Livermore National Laboratory.
||Laboratoire de Chimie Théorique, Université de Paris-Sud, 91405 Orsay, France.

9. Work in Progress

Rigorous quantum mechanical methods that have been developed recently are very effective for describing dynamical systems with a few degrees of freedom (≤6). One would of course like to be able to carry out calculations for more complex systems. To do this, ways are being explored that allow one to treat a few degrees of freedom in a rigorous quantum framework, while the remaining (perhaps many) degrees of freedom are treated by a semiclassical approximation.

FY 1993 PUBLICATIONS AND REPORTS

Refereed Journals

1. W.H. Miller, "Beyond Transition State Theory—A Rigorous Quantum Theory of Chemical Reaction Rates," Acct. Chem. Res. **26**, 174 (1993).
2. S. Keshavamurthy and W.H. Miller, "A Semiclassical Model to Incorporate Multidimensional Tunneling in Classical Trajectory Simulations Using Locally Conserved Actions," Chem. Phys. Lett. **205**, 96 (1993).
3. P. Saalfrank and W.H. Miller, "Time-Independent Quantum Dynamics for Diatom-Surface Scattering," J. Chem. Phys. **98**, 9040 (1993).
4. S.M. Auerbach and W.H. Miller, "Quantum Mechanical Reaction Probabilities with a Power Series Green's Function," J. Chem. Phys. **98**, 6917 (1993).
5. W. H. Thompson and W. H. Miller, "State-Specific Reaction Probabilities from a DVR-ABC Green's Function," Chem. Phys. Lett. **206**, 123 (1993); LBL-33723.
6. R. Hernandez, W.H. Miller, C.B. Moore, and W.F. Polik, "A Random Matrix/Transition State Theory for the Probability Distribution of State-Specific Unimolecular Decay Rates: Generalization to Include Total Angular Momentum Conservation and Other Dynamical Symmetries," J. Chem. Phys. **99**, 950 (1993); LBL-33750.
7. G. Stock and W.H. Miller, "Classical Formulation of the Spectroscopy of Non-Adiabatic Excited State Dynamics," J. Chem. Phys. **99**, 1545 (1993).
8. A.K. Belyaev, D.T. Colbert, G.C. Groenenboom, and W.H. Miller, "State-to-State Reaction Probabilities for Processes in $H^- + H_2$, D_2 Collisions," Chem. Phys. Lett. **209**, 309 (1993).
9. U. Manthe and W.H. Miller, "The Cumulative Reaction Probability as Eigenvalue Problem," J. Chem. Phys. **99**, 3411 (1993); LBL-35013.
10. R. Hernandez and W.H. Miller, "Semiclassical Transition State Theory—A New Perspective," Chem. Phys. Lett. **214**, 129 (1993); LBL-34585.
11. U. Manthe, T. Seideman, and W.H. Miller, "Full Dimensional Quantum Mechanical Calculation of the Rate Constant for the $H_2 + OH \rightarrow H_2O + H$ Reaction," J. Chem. Phys. **99**, 10078 (1993); LBL-35012.

Other Publications

12. W.H. Miller, "S-Matrix Version of the Kohn Variational Principle for Quantum Scattering Theory of Chemical Reactions," in *Advances in Molecular Vibrations and Collision Dynamics: Quantum Reactive Scattering*, edited by J.M. Bowman (JAI Press, Greenwich, 1994), Vol. IIA.

LBL Reports

13. S.M. Auerbach and C. Leforestier, "A New Computational Algorithm for Green's Functions: Fourier Transform of the Newton Polynomial Expansion," Comp. Phys. Comm. (in press); LBL-34570.
14. C. Leforestier and W.H. Miller, "Quantum Mechanical Calculations of the Rate Constant for the Reaction $H + O_2 \rightarrow OH + O$," J. Chem. Phys. (in press); LBL-34817.
15. S.M. Auerbach and W.H. Miller, "Efficient Polynomial Expansion of the Scattering Green's Function: Application to the $D + H_2$ ($v = 1$) Rate Constant," J. Chem. Phys. (in press); LBL-34739.

Invited Talks

16. W.H. Miller, "Some Recent Developments Related to Quantum Mechanical Transition State Theory," Latsis Symposium on Intramolecular Kinetics and Reaction Dynamics, ETH Zürich, Switzerland, October 20–23, 1992.
17. W.H. Miller, "Direct Calculation of Cumulative and State-to-State Reaction Probabilities," NATO Advanced Research Workshop on Orientation and Polarization Effects in Chemical Reaction Dynamics, Assisi, Italy, November 20–25, 1992.
18. W.H. Miller, "Cumulative and State-to-State Reaction Probabilities," Femtosecond Chemistry—The Berlin Conference, Berlin, Germany, March 1–4, 1993.
19. W.H. Miller, "Calculations of Cumulative and State-to-State Reaction Probabilities via an Absorbing Boundary Condition Green's Function," Symposium on Elementary to Complex Systems, American Physical Society Meeting, Seattle, WA, March 22–26, 1993.
20. W.H. Miller, "Beyond Transition State Theory—a Rigorous Theory of Chemical Reaction Rates," 76th Canadian Society for Chemistry Conference, Sherbrooke, Quebec, Canada, May 30– June 3, 1993.
21. W.H. Miller, "Beyond Transition State Theory—a Rigorous Theory of Chemical Reaction Rates," 8th American Conference on Theoretical Chemistry, Rochester, NY, June 28–July 2, 1993.
22. W.H. Miller, "Recent Advances in the Quantum Theory of Chemical Reaction Rates," 14th European Conference on Few-Body Problems in Physics, Amsterdam, The Netherlands, August 22–27, 1993.

Selective Photochemistry*

C. Bradley Moore, Investigator

INTRODUCTION

The fundamental goals of this work are to elucidate the molecular dynamics of energy-transfer and chemical reaction processes. Lasers are used to prepare molecules in selected excited states, and a variety of spectroscopic probes are used to follow energy transfers and chemical reactions with quantum-state resolution. Ideally, all quantum numbers are resolved in the initial excitation and for each of the product states. By exploring the dependence of processes on quantum state and other experimentally controllable parameters, it is usually possible to establish a physical model for the process. Optimally accurate benchmarks are established for the quantitative test of first principles theory.

Chemical reactions usually require excitations corresponding to ultraviolet photon energies, and hence the initial state is usually an electronically excited one. The first step is then to understand the transfer of electronic (and perhaps vibrational and even rotational) energy to different electronic states and to vibrational, rotational, and translational degrees of freedom. These processes occur both unimolecularly and in collisions. To the extent that initial excitation is randomized among the available degrees of freedom, opportunities for state selectivity may be lost. The simplest stable-molecular excited-electronic state is B-state H_2. In the absence of collisions, the molecule simply radiates. Collisions cause electronic energy transfer to a repulsive potential surface, depositing the energy into translation of the product H-atom fragments. Collisions also cause changes in vibrational and rotational quantum numbers. The dynamics of these processes and the relationship between them are under study.

When the ketene molecule is placed into its first excited electronic state, strong electronic-vibrational and spin-orbit couplings produce a statistical mixture of excited singlet, triplet, and ground-singlet states. The lower the electronic energy, the greater the vibrational energy and the greater the corresponding statistical weight. The lowest threshold for dissociation to CH_2 + CO is on the triplet surface. The total energy and angular momentum can be finely controlled. The microcanonical reaction rate, $k(E,J)$, and reaction product attributes can be studied to reveal the dynamics of the reaction in the transition state region. In this same energy region, unimolecular exchange of the carbon atoms occurs, and thus excitation of $^{13}CH_2CO$ can yield ^{13}CO product. This reaction permits the first study of reaction-rate resonances due to vibrational resonances in the reaction coordinate degree of freedom. These studies are providing an increasingly sharp picture of molecular dynamics in the region of a unimolecular transition state.

Lasers are particularly useful in studying the highly reactive species important in combustion, atmospheric reactions, and homogenous catalysis. Flash photolysis with a laser provides a controlled source of these species for study in gases or liquids. Laser spectroscopy provides excellent wavelength and time resolution for observation of the spectrum and study of the reaction kinetics of reactive species. Studies here concentrate on infrared absorption spectroscopic studies of hydrocarbon radicals important in combustion and atmospheric chemistry and, in collaboration with Robert Bergman, coordinatively unsaturated organometallics important in CH activation chemistry.

1. Structures in the Energy Dependence of the Rate Constant for Ketene Isomerization (Publication 1)

E.R. Lovejoy and C.B. Moore

The isomerization of highly vibrationally excited and rotationally cold ketene has been investigated by monitoring the ^{12}CO and ^{13}CO dissociation products following laser excitation of jet-cooled $^{12}CH_2$ ^{13}CO, $^{13}CH_2$ ^{12}CO, and $^{12}CD_2$ ^{13}CO. The rate constants for the reactions $^{12}CH_2$ $^{13}CO \leftrightarrow$ $^{13}CH_2$ ^{12}CO and $^{12}CD_2$ $^{13}CO \leftrightarrow$ $^{13}CD_2$ ^{12}CO are reported as a function of energy with a resolution of 1 cm^{-1}. The rate constants exhibit pronounced peaks as a function of energy near the reaction threshold (see Figure 1-1). This is the first time that an elementary reaction rate

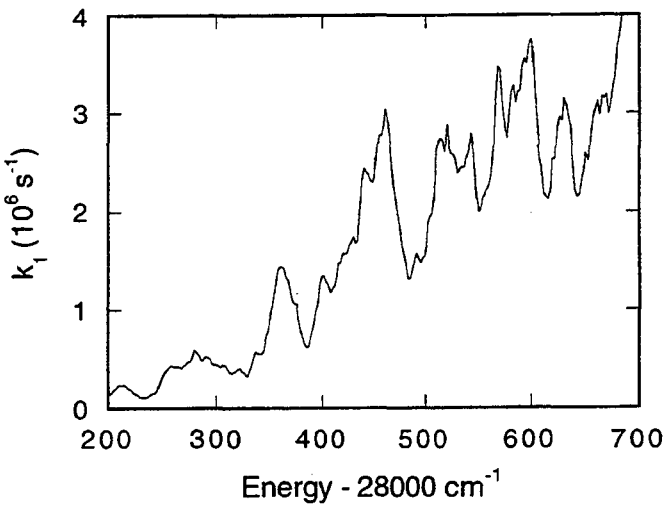

Figure 1-1. Isomerization rate constant (k_1) derived from data for ^{12}CO and ^{3}CO products based on the mechanism of Figure 1-2. (XBL 947-4204)

*This work was supported by the Director, Office of Energy Research, Office of Basic Energy Sciences, Chemical Sciences Division, of the U.S. Department of Energy under Contract No. DE-AC03-76SF00098.

constant has been observed to decrease markedly with increasing energy or to show structure on such a fine energy scale. This structure is attributed to quasistable motion along the reaction coordinate in the vicinity of the isomerization transition state. The dip in the potential surface (Figure 1-2) at the oxirene configuration may support levels below the barrier top that would give resonances in the tunneling probability. The multidimensionality of the reaction coordinate may support resonances above the barrier top as well that lead to structure in the rate constant.

Theoretical treatments of this system are being carried out by W.H. Miller (Chemical Sciences Division, LBL) with *ab initio* potential energy surfaces from H.F. Schaefer, III (Georgia) and L. Radom (Canberra).

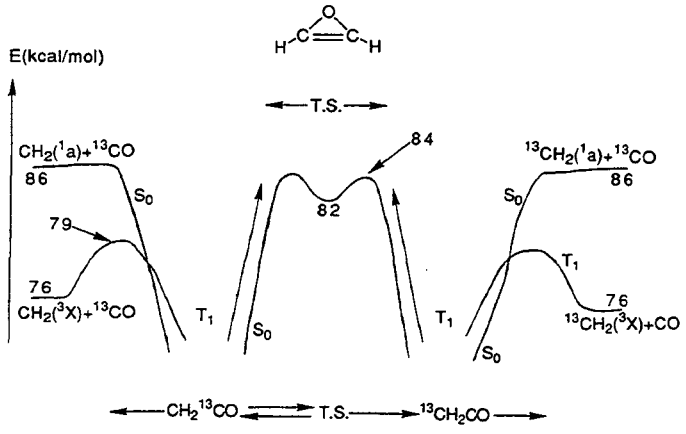

Carbon Isotope Exchange in Ketene

Figure 1-2. Potential-energy/reaction-coordinate diagram for ketene. The oxirene configuration, center, in which the carbon atoms are symmetric, is the midpoint for the isomerization reaction. (XBL 987-4205)

2. Absolute Yields of CO, CO_2, and H_2CO from the Reaction $CH2(\tilde{X}\ ^3B_1) + O_2$ by IR Diode Laser Flash Kinetic Spectroscopy (Publication 6)

R.A. Alvarez and C.B. Moore

The absolute yields of the stable carbon-containing products CO, CO_2, and H_2CO, formed in the reaction of triplet methylene ($\tilde{X}\ ^3B_1 \equiv CH_2$) with O_2, have been determined using a flash kinetic spectrometer. The CH_2 radicals were generated by excimer laser photolysis of ketene, and product formation was monitored by time-resolved infrared diode laser absorption. The reaction was carried out in a static gas cell at room temperature (T = 298 ± 3 K) with total pressures in the range of 1–25 torr. The measured product yields were as follows: CO, 0.34 ± 0.06; CO_2, $0.40^{+0.09}_{-0.07}$; H_2CO, 0.16 ± 0.04. The rate constants for production of CO and CO_2 were equivalent to the published rate constant for removal of CH_2.

The reaction may lead to many possible products:

$$\begin{aligned} CH_2 + O_2 &\rightarrow (CH_2O_2) \rightarrow HCO + OH \\ &\rightarrow CO + H_2O \\ &\rightarrow H_2CO + O(^3P) \\ &\rightarrow H + CO + OH \\ &\rightarrow HOCO + H \\ &\rightarrow CO_2 + 2H \\ &\rightarrow CO_2 + H_2 \\ &\rightarrow HC(O)O + H \\ &\rightarrow H_2CO + O(^1D) \\ &\rightarrow HCOOH \cdot \end{aligned}$$

The stable C-containing products from the reaction $^3CH_2 + O_2$ have been measured. The branching steps are key inputs to the modeling of acetylene combustion. This study reaffirms the accepted near-equality of CO and CO_2 yields and identifies the modest production of H_2CO. On the basis of indirect evidence obtained in this work and previous studies, it appears likely that the OH yield in this system amounts to 30 ± 5%. Since the O-atom yield is equivalent to that of H_2CO, the only remaining uncertainty is the branching between molecular and atomic hydrogen production.

3. Kinetics and Product Branching Ratios for the Reaction HCO + NO_2 (Publication 8)

Y. Guo, S.C. Smith, C.B. Moore, and C.F. Melius

The kinetics and product branching of the HCO + NO_2 reaction have been studied at room temperature using laser flash kinetic spectroscopy and have been modeled with microcanonical variational RRKM theory. The rate constant for the disappearance of the HCO radical at 296 K is (5.7 ± 0.9) × 10^{-11} cm^3 $molecule^{-1}s^{-1}$, and it is independent of the pressure of SF_6 buffer gas up to 700 torr. The CO_2 yield is 52 ± 14%. Less than 10% of the reaction goes through the most exothermic product channel, HNO + CO_2. The least exothermic product channel, H + CO_2 + NO, is responsible for the remaining CO_2. HONO has been observed, though not quantitatively, as a reaction product corresponding to the HONO + CO product channel. It must account for the 48 ± 14% of reaction that does not yield CO_2. The rates of formation of the collision complexes HCO(ONO) and HCO(NO_2) are calculated by variational RRKM theory to be comparable and only weakly temperature-dependent. Branching ratios for the decomposition of these complexes are also calculated. They are found to match most experimental observations from 300–1600 K.

4. Work in Progress

Unimolecular reaction studies on triplet ketene are being initiated with full rotational state resolution in the initial excitation. An IR optical parametric oscillator is being set up to select a single excited rovibrational state that will then be further excited to the reaction threshold by a UV laser pulse. Quantitative theoretical analysis of the resonances in the isotopic exchange rate is being carried out by William Miller's group with a multidimensional reaction coordinate. Ultimately, these resonances will be studied experimentally with complete rotational resolution.

The B-state of hydrogen is being produced by tunable vacuum UV laser excitation. Experiments use a monochromator to disperse fluorescence and study collision-induced, vibration-rotation energy transfers as a function of the initial quantum state. Future studies are planned using a second vacuum UV laser to probe the velocity distribution of H-atom fragments from collision-induced electronic curve crossing. William Lester's group is carrying out *ab initio* theoretical work on these systems.

The mechanism of atmospheric photochemical degradation of CH_3NCS, an important agricultural chemical, is being studied using a diode laser infrared flash kinetic spectrometer. Reaction rates for radical–radical reactions are being measured. Infrared spectra and chemical reaction kinetics of intermediates in organometallic photochemistry in gas and liquid phase are being studied jointly with R.G. Bergman. Emphasis is on CH activation chemistry. Studies of CH activation systems in liquid Kr and Xe are proceeding well.

FY 1993 PUBLICATIONS AND REPORTS

Refereed Journals

1. E.R. Lovejoy and C. Bradley Moore, "Structures in the Energy Dependence of the Rate Constant for Ketene Isomerization," J. Chem. Phys. **98**, 7846 (1993); LBL-33087.
2. B.H. Weiller, E.P. Wasserman, C.B. Moore, and R.G. Bergman, "Organometallic CO Substitution Kinetics in Liquid Xe by Fast Time-Resolved IR Spectroscopy," J. Am. Chem. Soc. **115**, 4326 (1993); LBL-32834.
3. R. Hernandez, W.H. Miller, C.B. Moore, and W.F. Polik, "A Random Matrix/Transition State Theory for the Probability Distribution of State-Specific Unimolecular Decay Rates: Generalization to Include Total Angular Momentum Conservation and Other Dynamical Symmetries," J. Chem. Phys. **99**, 950 (1993); LBL-33750.

Other Publications

4. S.K. Kim, "Unimolecular Photodissociation Dynamics of Ketene (CH_2CO): The Singlet/Triplet Branching Ratio and Experimental Observation of the Vibrational Level Thresholds of the Transition-State," Ph.D. Thesis, University of California, Berkeley, CA, June 1993; LBL-34251.
5. R.A. Alvarez, "Infrared Diode Laser Studies of the Products from the Reaction $CH_2(\tilde{X}\ ^3B_1) + O_2$ and from the Near-UV Photolysis of CH_3NCS," Ph.D. Thesis, University of California, Berkeley, CA, December 1993; LBL-34918

LBL Reports

6. R.A. Alvarez and C.B. Moore, "Absolute Yields of CO, CO_2, and H_2CO from the Reaction $CH_2(\tilde{X}\ ^3B_1) + O_2$ by IR Diode Laser Flash Kinetic Spectroscopy," J. Phys. Chem. (in press); LBL-34762.
7. R.A. Alvarez and C.B. Moore, "Quantum Yield for Production of CH_3NC in the Photolysis of CH_3NCS," Science (in press); LBL-34995.
8. Y. Guo, S.C. Smith, C.B. Moore, and C.F. Melius, "Kinetics and Product Branching Ratios for the Reaction of HCO + NO_2," J. Phys. Chem. (submitted December 1993); LBL-35090.

Invited Talks

9. C.B. Moore, "Vibrational Dynamics of Dissociating Molecules," Department of Chemistry, Massachusetts Institute of Technology, MA, November 1992
10. C.B. Moore, "Vibrations at Unimolecular Reaction Transition States," National Institute of Standards and Technology, Gaithersburg, MD, December 1992.
11. C.B. Moore, "Breaking Chemical Bonds—The Structure and Dynamics of Unimolecular Transition States," Vanderbilt University, Nashville, TN, January 1993.
12. C.B. Moore, "Breaking Chemical Bonds—The Structure and Dynamics of Unimolecular Transition States," Annual Meeting of the Korean Physical Society, Seoul, Korea, April 1993.
13. C.B. Moore, "Breaking Chemical Bonds—The Structure and Dynamics of Unimolecular Transition States," Seoul University, Korea, April 1993.
14. C.B. Moore, "Breaking Chemical Bonds—The Structure and Dynamics of Unimolecular Transition States," Korean Advanced Institute for Science and Technology, Korea, April 1993.
15. C.B. Moore, "Vibrations at Unimolecular Transition States," Opening Lecture at the Gordon Research Conference on Molecular Energy Transfer, NH, June 1993.
16. C.B. Moore, "Dynamics at Transition States for Unimolecular Reactions," 14th Conference on Dynamics of Molecular Collisions, Unicoi State Park, GA, June 1993.

17. C.B. Moore, "Dynamics in the Transition State Region for Unimolecular Reactions," International Symposium on Molecular Energy Transfer and Reaction Dynamics, University of Tokyo, Tokyo, Japan, August 1993.
18. C.B. Moore, "Transition States in Unimolecular Reactions," Hitachi Advanced Research Laboratory, Hatoyama, Japan, August 1993.
19. C.B. Moore, "Infrared Flash Kinetic Spectroscopy Studies of Reaction Intermediates and Reaction Mechanisms," Hitachi Research Laboratory, Hitachi City, Japan, August 1993.
20. C.B. Moore, "Energy States and Energy Flow in Chemical Bond Breaking," Department of Chemistry, Rice University, September 1993.
21. C.B. Moore, "Energy States and Energy Flow in Chemical Bond Breaking," Department of Chemistry, University of Texas, Austin, TX, September 1993.

Other Work

22. C.B. Moore, "Unimolecular Reaction Dynamics," National Science Foundation, November 1, 1993–October 31, 1996.

Photodissociation of Free Radicals*

Daniel M. Neumark, Investigator

INTRODUCTION

While many photodissociation studies of stable molecules have been performed in recent years, it has proved difficult to extend these experiments to studies of reactive-free radicals. This is largely due to the difficulty of implementing a clean, well-characterized source of free radicals. We have developed a novel approach to this problem by setting up an experiment in which free radicals are generated by photodetachment of a mass-selected anion beam, rather than by adhering to the more conventional strategies in which radicals are formed by photolysis of a stable precursor or by a chemical reaction. Since nearly all radicals have a positive electron affinity, this approach should be quite general.

In the experiment, an 8 keV beam of cold mass-selected anions is photodetached with a pulsed laser. The resulting neutral radicals are photodissociated with a second pulsed laser, and the photofragments are detected with high (~50%) efficiency using a microchannel plate detector, which lies about 100 cm downstream from the photodissociation laser. The center of the detector is blocked so that the undissociated radicals do not impinge on it, but the photofragments move off the beam axis and strike the detector. The experiment can be operated in several modes. We can measure the total photofragment signal as a function of dissociation laser wavelength, thereby mapping out the dissociative electronic transitions of the radical. We can measure the time-of-flight distribution of the photofragments, thereby obtaining an approximated kinetic energy distribution at a fixed photodissociation wavelength. Finally, using a two-particle position and time-sensing detector, we can determine detailed photofragment energy and angular distributions.

*This work was supported by the Director, Office of Energy Research, Office of Basic Energy Sciences, Chemical Sciences Division, of the U.S. Department of Energy under Contract No. DE-AC03-76SF00098.

1. Photodissociation Dynamics of the N_3 Radical (Publication 7)

R.E. Continetti,† D.R. Cyr, D.L. Osborn, and D.M. Neumark

The dissociation dynamics of the $B^2\Sigma_u^+$ excited state of N_3 were investigated, using fast radical beam photodissociation coupled with a new coincidence wedge-and-strip-anode particle detector. With this detector, detailed photofragment kinetic energy and angular distributions can be measured as a function of excitation energy. The design of the detector is discussed, along with its calibration using predissociation of the O_2 $B^3\Sigma_u^-$ state. The results for N_3 show that both spin-allowed [$N_3 \rightarrow N(^2D) + N_2(^1\Sigma_g^+)$] and spin-forbidden [$N_3 \rightarrow N(^4S) + N_2(^1\Sigma_g^+)$] dissociation processes occur from the vibrationless level of the $B^2\Sigma_u^+$ state in N_3. Bend excitation in the $B^2\Sigma_u^+$ state, however, enhances the spin-allowed dissociation process considerably. The implications of these results for the predissociation mechanism are discussed.

†Department of Chemistry, University of California, San Diego, La Jolla, CA 92093-0314.

2. Fast-Beam Studies of the CH_2NO_2 Radical (Publication 10)

D.R. Cyr, D.J. Leahy, D.L. Osborn, R.E. Continetti,† and D.M. Neumark

The photodissociation of the nitromethyl radical, CH_2NO_2, has been studied using a fast-beam photofragment translational spectrometer. In these experiments, a fast beam of mass-selected, internally cold nitromethyl radicals is formed via negative ion photodetachment of $CH_2NO_2^-$ and subsequently dissociated. The recoiling photofragments are detected in coincidence using a microchannel plate detector equipped with a time- and position-sensing anode. Two dissociation product channels are observed at each of three dissociation wavelengths investigated in the range of 240–270 nm, and are identified as: (I) $CH_2NO_2 \rightarrow CH_2NO + O$, and (II) $CH_2NO_2 \rightarrow H_2CO + NO$. In marked contrast to the ultraviolet photodissociation of CH_3NO_2, no evidence is found for simple C–N bond fission to give (III) $CH_2NO_2 \rightarrow CH_2 + NO_2$. Translational energy and angular distributions have been obtained for the two observed channels. The translational energy distribution of channel I peaks at only 5–8 kcal/mol, while the distribution for channel II peaks at around 60 kcal/mol. The angular distribution for both channels is largely isotropic. The nature of the electronic excitation

and dissociation dynamics is considered at length. The upper state in the electronic transition is assigned to the $1\ ^2B_1$ state. Results of attempts to model various aspects of the dissociation dynamics as statistical processes on the ground state surface indicate this mechanism is very unlikely. Instead, both dissociation channels are believed to occur primarily on excited-state surfaces, and mechanisms for these processes are proposed.

†Department of Chemistry, University of California, San Diego, La Jolla, CA 92093-0314.

3. Observation of the Correlated O $^3P_{j1}$, $^3P_{j2}$ State Distribution from the Predissociation of O_2 $B^3\Sigma_u^-$

D.J. Leahy, D.R. Cyr, D.L. Osborn, and D.M. Neumark

We present a fast-beam photofragment translational spectroscopy study of the predissociation of the O_2 $B^3\Sigma_u^-$ state. The $B^3\Sigma_u^-$ $(v' = 7) \rightarrow X\ ^3\Sigma_g^-$ $(v'' = 4)$ transition of the Schumann–Runge band is then excited, resulting in predissociation to two O ^3P_j atoms. We determine the photofragment kinetic energy and angular distribution using a time- and position-sensitive detector. Our energy resolution (10 meV) is sufficient to resolve the energy splittings of the O-atom spin-orbit levels, enabling us to determine the *correlated* $(j_1 j_2)$ fine structure distribution for the photofragments. These results do not appear to be consistent with predictions based on a recent model of O_2 $B^3\Sigma_u^-$ state predissociation.

4. Work in Progress

We have studied the predissociation dynamics of O_2 in considerably more detail. The O-atom spin-orbit distributions have been measured for several vibrational levels of the O_2 $B^3\Sigma_u^-$ state. These measurements disagree significantly with what would be expected, based on previous models of the B-state predissociation dynamics.

In addition, we have developed a new negative ion source that combines a pulsed molecular beam with a pulsed high-voltage discharge. This has proved to be an intense source of many ions that we were unable to make previously, and has thereby expanded the range of free radicals accessible to our experiment. We are currently investigating the photodissociation dynamics of the CH_3O radical.

FY 1993 PUBLICATIONS AND REPORTS

Refereed Journals

1. D.M. Neumark, "Transition State Spectroscopy via Negative Ion Photodetachment," Acct. Chem. Res. **26**, 33 (1993).
2. S.E. Bradforth, E.H. Kim, D.W. Arnold, and D.M. Neumark, "Photoelectron Spectroscopy of CN^-, NCO^-, and NCS^-," J. Chem. Phys. **98**, 800 (1993).
3. D.J. Leahy, D.R. Cyr, D.L. Osborn, and D.M. Neumark, "Fast-Beam Studies of Free Radical Photodissociation: The CH_2NO_2 Radical," SPIE Proc. Ser. **1858**, 49 (1993).
4. Y. Zhao, C.C. Arnold, and D.M. Neumark, "Study of the $I{\cdot}CO_2$ van der Waals Complex by Threshold Photodetachment Spectroscopy of I^-CO_2," J. Chem. Soc. Far. Trans. **89**, 1449 (1993).
5. C.C. Arnold, T.N. Kitsopoulos, and D.M. Neumark, "Reassignment of the Si Photodetachment Spectra," J. Chem. Phys. **99**, 766 (1993).
6. C.C. Arnold and D.M. Neumark, "Reply to Comment on: Study of C_6^- and C_6 with Threshold Photodetachment Spectroscopy and Autodetachment Spectroscopy," J. Chem. Phys. **99**, 1442 (1993).
7. R.E. Continetti, D.R. Cyr, D.L. Osborn, D.J. Leahy, and D.M. Neumark, "Photodissociation Dynamics of the N_3 Radical," J. Chem. Phys. **99**, 2616 (1993); LBL-33584.
8. C.C. Arnold and D.M. Neumark, "Study of Si_4 and Si_4^- Using Threshold Photodetachment (ZEKE) Spectroscopy," J. Chem. Phys. **99**, 3353 (1993).
9. S.E. Bradforth, D.W. Arnold, D.M. Neumark, and D.E. Manolopoulos, "Experimental and Theoretical Studies of the $F + H_2$ Transition State Region via Photoelectron Spectroscopy of FH_2^-," J. Chem. Phys. **99**, 6345 (1993).
10. D.R. Cyr, D.J. Leahy, D.L. Osborn, R.E. Continetti, and D.M. Neumark, "Fast Beam Photodissociation of the CH_2NO_2 Radical," J. Chem. Phys. **99**, 8751 (1993); LBL-34583
11. D.E. Manolopoulos, K. Stark, H.-J. Werner, D.W. Arnold, S.E. Bradforth, and D.M. Neumark, "The Transition State of the $F + H_2$ Reaction," Science **262**, 1852 (1993).

Other Publications

12. T.N. Kitsopoulos and D.M. Neumark, "Studying the Low Lying Electronic States of Small Silicon and Carbon Clusters Using Negative Ion Photodetachment Techniques," in *On Clusters and Clustering, From Atoms to Fractals*, edited by P. J. Reynolds (Elsevier Sci. Pub., 1993), pp. 33–45.

LBL Reports

13. D.J. Leahy, D.R. Cyr, D.L. Osborn, and D.M. Neumark, "Observation of the Correlated O $^3P_{j1}$, $^3P_{j2}$ State Distribution from the Predissociation of O_2 $B^3\Sigma_u^-$," Chem. Phys. Lett. (in press); LBL-34820.
14. S.E. Bradforth, Ph.D. Thesis, "Bimolecular Reaction Dynamics from Photoelectron Spectroscopy of Negative Ions," University of California, Berkeley, CA, 1992; LBL-33328.

Invited Lectures

15. D.M. Neumark, "Studies of Transient Species Using Negative Ion Photodetachment," University of British Columbia, Vancouver, Canada, October 1992.
16. D.M. Neumark, "Studies of Transient Species Using Negative Ion Photodetachment," University of Victoria, Canada, October 1992.
17. D.M. Neumark, "Studies of Transition State Species and Clusters with Negative Ion Photodetachment," AFOSR Molecular Dynamics and Ceramics Contractor's Conference, Washington, DC, October 1992.
18. D.M. Neumark, "Fast Beam Photodissociation Studies of Reactive Free Radicals," American Chemical Society Senior Technical Meeting, Mayagüez, Puerto Rico, November 1992.
19. D.M. Neumark, "Studies of Anisotropic Atom–Molecule Interaction Potentials with Negative Ion Photodetachment," NATO Advanced Research Workshop, Orientation and Polarization Effects in Chemical Reaction Dynamics, Assissi (Perugia), Italy, November 1992.
20. D.M. Neumark, "Fast Beam Studies of Free Radical Photodissociation," International Society for Optical Engineering Symposium on Laser Techniques for State-Selected and State-to-State Chemistry, Los Angeles, CA, January 1993.
21. D.M. Neumark, "Photodissociation Dynamics of Free Radicals," The 5th Australian Conference on Chemical Reactions, Armidale, Australia, February 1993.
22. D.M. Neumark, "Transition State Spectroscopy of the $F + H_2$ Reaction," Femtosecond Chemistry—The Berlin Conference, Berlin, Germany, March 1993.
23. D.M. Neumark, "Studies of Transient Species with Negative Ion Photodetachment," Gordon Conference on Structures, Energetics, and Reaction Dynamics of Gaseous Ions, Ventura, CA, March 1993.
24. D.M. Neumark, "Studies of Transient Species Using Negative Ion Photodetachment," Frontiers in Chemistry Colloqium, Wayne State University, Detroit, MI, March 1993.
25. D.M. Neumark, "Studies of Transient Species with Negative Ion Photodetachment," University of California, Berkeley, CA, March 1993.
26. D.M. Neumark, "Photodissociation Dynamics of Free Radicals," University of California, Riverside, CA, April 1993.
27. D.M. Neumark, "Fast Beam Studies of Free Radical Photodissociation," Department of Energy Combustion Research Meeting, Lake Harmony, PA, June 1993.
28. D.M. Neumark, "Photodissociation Dynamics of Free Radicals," 14th Conference on the Dynamics of Molecular Collisions, Helen, GA, June 1993.
29. D.M. Neumark, "Photodissociation Dynamics of Free Radicals," Université Paris-Sud, Orsay, France, June 1993.
30. D.M. Neumark, "Transition State Spectroscopy of the $F + H_2$ Reaction," Université Paris-Sud, Orsay, France, July 1993.
31. D.M. Neumark, "Photodissociation Dynamics of Free Radicals," Université Paul Sabatier, Toulouse, France, July 1993.
32. D.M. Neumark, "Fast Beam Studies of Free Radical Photodissociation," 22nd International Symposium on Free Radicals, Doorwerth, Netherlands, September 1993.
33. D.M. Neumark, "Transition State Spectroscopy of the $F + H_2$ Reaction," Iowa State University, Ames, IA, September 1993.

Physical Chemistry with Emphasis on Thermodynamic Properties*

Kenneth S. Pitzer, Investigator

INTRODUCTION

The purpose of this program is to discover and develop methods of calculation of thermodynamic and related properties of important chemical systems by the use of quantum and statistical mechanics, together with experimental measurements for key systems. Current emphasis is on fluid systems that include ionic or strongly dipolar components in novel ranges of conditions, including near-critical and supercritical temperatures and compositions extending from pure water or other polar solvents to pure fused salt. Reported in item 1 below are relatively simple equations of state for Ar–H_2O and Xe–H_2O that predict remarkably large volumetric effects near the critical point of water. Item 2 is a comprehensive equation of state for the system NaCl–KCl–H_2O, including the two aqueous binaries, that is very important geologically and industrially and very complex theoretically. A related interest concerns novel ionic systems with a critical point near room temperature where it is possible to measure with high precision the near-critical properties, including the critical exponents. Further work in this field continues. Earlier advances yielded improved equations for electrolyte solutions that are now being applied to a wide variety of systems of industrial or geological interest, including geothermal brines. Other recent research has involved the development of a feasible method of relativistic quantum mechanical calculation for molecules containing very heavy atoms and the application of this method to important examples. This method is now in wide use.

1. On the Apparent Molar Volumes of Nonelectrolytes in Water (Publication 6)

A. Anderko,† J.P. Chan, and K.S. Pitzer

Apparent molar volumes of aqueous solutions of argon and xenon have been calculated using a comprehensive equation of state for nonelectrolyte systems that was developed previously in this project. The equation consists of a virial expansion truncated after the fourth virial coefficient and a closed-form term approximating higher coefficients. Mixing rules are based on the composition dependence of virial coefficients, which is known from statistical mechanics. The equation accurately represents vapor–liquid and gas–gas equilibria for the Ar + H_2O and Xe + H_2O systems over wide ranges of pressure and temperature using two binary parameters. With the binary parameters determined from phase equilibrium data, the equation accurately predicts apparent molar volumes V_ϕ in the near-critical and far-from-critical regions. Apart from reproducing experimental V_ϕ data, the equation reveals remarkable maxima of V_ϕ as a function of pressure and temperature in the near-critical region. The implications of this equation with respect to the Ar–H_2O intermolecular potential are discussed via the second virial coefficient. Figure 1-1 shows the experimental data fitted for Ar–H_2O. Figure 1-2 shows the remarkably large apparent molar volumes of Ar and the accuracy of the prediction (these data were not used in fitting the equation). The results for Xe–H_2O are very similar.

†Present address: Simulation Sciences Inc., 601 South Valencia Avenue, Brea, CA 92621.

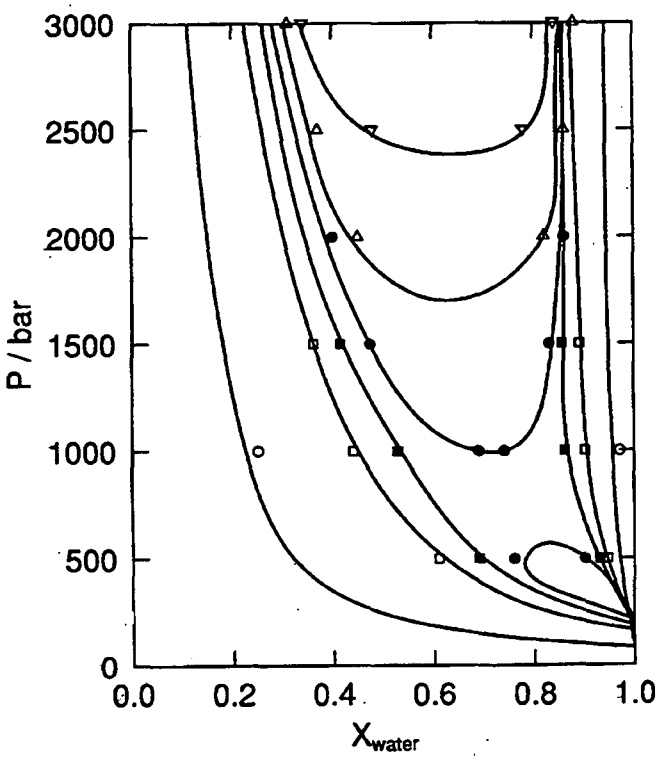

Figure 1-1. Phase equilibria in the water + argon mixture at 573 K (○), 623 K (□), 633 K (■), 638 K (●), 643 K (△), and 653 K (▽). The symbols show the experimental data, while the lines are calculated.

*This work was supported by the Director, Office of Energy Research, Office of Basic Energy Sciences, Chemical Sciences Division, of the U.S. Department of Energy under Contract No. DE-AC03-76SF00098.

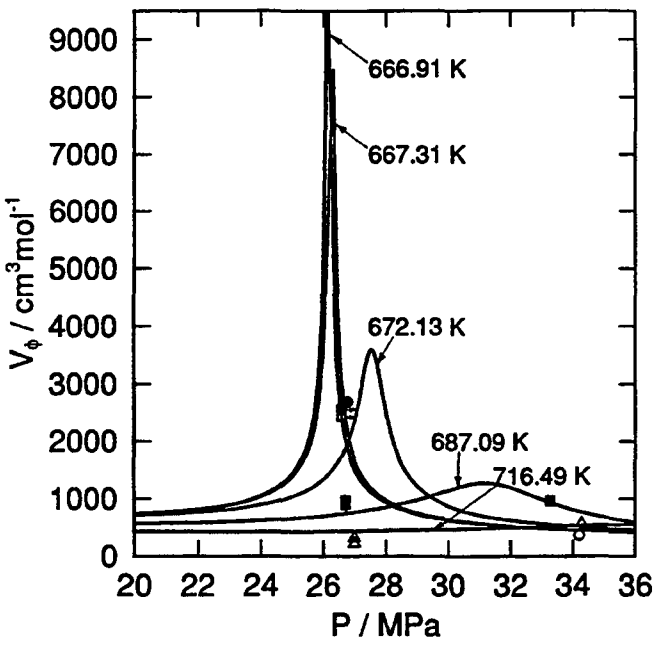

Figure 1-2. Comparison of the predicted apparent molar volumes of aqueous argon from the equation of state (lines) with experimental measurements for T = 666.91 K and m = 0.0770 mol/kg (●), T = 667.31 and m = 0.0770 (○), T = 672.13 and m = 0.0905 (□), T = 687.09 and m = 0.0885 (■), and T = 716.49 and m = 0.0791 (△).

2. Phase Equilibria and Volumetric Properties of the Systems KCl–H_2O and NaCl–KCl–H_2O Above 573 K: Equation-of-State Representation (Publication 8)

A. Anderko and K.S. Pitzer

A comprehensive equation of state has been developed for the system KCl–H_2O at high temperatures and pressures. The equation is based on a theoretical model developed for the system NaCl–H_2O that was reported last year. Experimental vapor–liquid equilibrium, solid–liquid equilibrium, and density data have been critically evaluated and used to fit the adjustable parameters of the model. The equation of state reproduces these properties within experimental uncertainty. It is valid for temperatures between 573 K and 973 K and for pressures up to 5 kbar. Graphs are presented to provide recommended values of phase compositions and volumetric properties. Furthermore, the equations for NaCl–H_2O and KCl–H_2O have been combined to yield an equation for the ternary system NaCl–KCl–H_2O. The equation reproduces solid–liquid equilibrium data for the ternary system and agrees with the available semiquantitative information about the relative concentration of Na and K in the vapor phase.

3. Thermodynamics of Na_2SO_4(aq) at Temperatures T from 273 K to 373 K and of $[(1 - y)H_2SO_4 + yNa_2SO_4]$(aq) at T = 298.15 K (Publication 3)

J.K. Hovey,[†] K.S. Pitzer, and J.A. Rard[‡]

New isopiestic vapor-pressure measurements on $\{(1 - y)H_2SO_4 + yNa_2SO_4\}$(aq), along with earlier experimental investigations that span the range from y = 0 to y = 1 and infinitely dilute to supersaturated molalities, have been analyzed in terms of the Pitzer ion-interaction model. Refined ion-interaction parameters for Na_2SO_4(aq) valid over the temperature range of 273 to 373 K have been calculated and used for analyzing results for $[(1 - y)H_2SO_4 + yNa_2SO_4]$(aq) at 298.15 K. Analysis of experimental results for these aqueous mixtures required explicit consideration of the dissociation reaction of HSO. Previous treatments of H_2SO_4(aq) and the subsequent equilibrium for the dissociation of HSO valid in the range of 273 to 343 K were employed as a first approximation in representing the mixed solutions. Two sets of Pitzer ion-interaction parameters are presented for $[(1 - y)H_2SO_4 + yNa_2SO_4]$(aq). The validity of the first set is limited in ionic strength to I = 12 mol·kg^{-1} or to saturation with respect to Na_2SO_4. The second set corresponds to a slightly less precise representation but is valid over the entire range of experimental results considered. Both sets of parameters provide a more complete description of solutions of H_2SO_4 because of the removal of various redundancies in ion-interaction parameters. The specific ion-interaction terms used and the overall fitting procedure are described, as well as selected examples of relevant thermodynamic calculations for $[(1 - y)H_2SO_4 + yNa_2SO_4]$(aq).

[†]Present address: Institut für Mineralogie und Petrographie, Sonneggstrasse 5, ETH-Zentrum, CH-8092 Zürich, Switzerland.
[‡]Lawrence Livermore National Laboratory, University of California, Livermore, CA 94550.

4. Work in Progress

Instrumentation has been acquired, set up, and tested for turbidity measurements under very precisely controlled temperatures. Initial measurements have been made for the ionic system comprising tetra-n-butylammonium picrate as the salt and 1 dodecanol as the solvent. The phase diagram was first measured; then the turbidity was measured for the critical composition at temperatures ranging upward from T_c. The results are interpreted to yield the critical exponent γ. It might be expected to have the Ising value 1.24 typical

of most liquid–liquid systems. Recent research in this project yielded the classical value, however, for the exponent β for a similar system dominated by ionic forces, and others subsequently found $\gamma = 1.0$, the classical value, for the same system.

In contrast, with water as a solvent, systems with similar salts yield Ising exponents. The high dielectric constant of water greatly reduces the ionic forces, and the phase separation must be caused by hydrophobic effects. The current program is designed to explore systems of intermediate character and to determine whether there is a "crossover" from the Ising γ very near T_c to the classical γ at higher temperature. Theory suggests, but as yet does not prove, that such a crossover should occur.

FY 1993 PUBLICATIONS AND REPORTS

Refereed Journals

1. A. Anderko and K.S. Pitzer, "Equation-of-State Representation of Phase Equilibria and Volumetric Properties of the System NaCl–H_2O Above 573 K," Geochim. Cosmochim. Acta **57**, 1657 (1993); LBL-32429.
2. R.N. Roy, K.M. Vogel, C.E. Good, W.B. Davis, L.N. Roy, D.A. Johnson, A.R. Felmy, and K.S. Pitzer, "Activity Coefficients in Electrolyte Mixtures: HCl + $ThCl_4$ + H_2O for 5–55 °C," J. Phys. Chem. **96**, 11065 (1992); LBL-32731.†
3. J.K. Hovey, K.S. Pitzer, and J.A. Rard, "Thermodynamics of Na_2SO_4(aq) at Temperatures T from 273 K to 373 K and of $\{(1-y)H_2SO_4 + yNa_2SO_4\}$(aq) at T = 298.15 K," J. Chem. Thermodynamics **25**, 173 (1993); LBL-31194.
4. K.S. Pitzer, "Thermodynamics of Natural and Industrial Waters," J. Chem. Thermodynamics **25**, 7 (1993); LBL-31210.‡
5. K.S. Pitzer and Y. Shi, "Thermodynamics of Calcium Chloride in Highly Concentrated Aqueous Solution and in Hydrated Crystals," J. Solution Chem. **22**, 99 (1993); LBL-33134.†
6. A. Anderko, J.P. Chan, and K.S. Pitzer, "On the Apparent Molar Volumes of Nonelectrolytes in Water," J. Sol. Chem. **22**, 369 (1993); LBL-33030.
7. K.S. Pitzer and S.M. Sterner, "Equations of State for Solid NaCl–KCl and Saturated Liquid NaCl–KCl–H_2O," Thermochimica Acta **218**, 413 (1993); LBL-30916.†
8. A. Anderko and K.S. Pitzer, "Phase Equilibria and Volumetric Properties of the Systems KCl–H_2O and NaCl–KCl–H_2O Above 573 K: Equation of State Representation," Geochim. Cosmochim. Acta **57**, 4885 (1993); LBL-33169.

LBL Reports

9. S.L. Clegg, J.A. Rard, and K.S. Pitzer, "Thermodynamic Properties of 0–6 mol kg^{-1} Aqueous Sulphuric Acid from 273.15 to 328.15 K," J. Chem. Soc. Faraday Trans. (submitted); LBL-34579.
10. K.S. Pitzer and C.S. Oakes, "Thermodynamics of Calcium Chloride in Concentrated Aqueous Solutions and in Crystals," J. Chem. & Eng. Data (submitted); LBL-34806.†
11. C.S. Oakes, R.J. Bodnar, J.M. Simonson, and K.S. Pitzer, "Critical and Supercritical Properties for 0.3 to 3.0 mol·kg^{-1} $CaCl_2$(aq)," Geochim. Cosmochim. Acta (submitted); LBL-34907.†

†This work was supported by the Director, Office of Energy Research, Office of Basic Energy Sciences, Division of Engineering and Geosciences of the U.S. Department of Energy under Contract No. DE-AC03-76SF00098.

‡This work was supported by both the Division of Engineering and Geosciences and the Division of Chemical Sciences of DOE under Contract No. DE-AC03-76SF00098.

Chemical Physics at High Photon Energies*

David A. Shirley, Investigator

INTRODUCTION

This program addresses both experimental and theoretical aspects of electron spectroscopy for the investigation of electronic structure of matter in the gaseous and condensed phases. Research is conducted using both laboratory sources at Lawrence Berkeley Laboratory (LBL) and synchrotron radiation in the 5–5,000-eV energy range available at the Stanford Synchrotron Radiation Laboratory (SSRL) and the National Synchrotron Light Source (NSLS). Completion of the Advanced Light Source (ALS) at LBL and moving beamline 6-1 from SSRL to the ALS as beamline 9.3.2 will allow us to carry out most of the experiments at LBL. A considerable effort is placed on developing the high-resolution spectroscopy in the 20–1,500-eV energy range by using both modified toroidal grating monochromator (TGM) and spherical grating monochromators at the ALS (beamline 9.3.2). Effects are emphasized that can be refined and extended with the advent of third-generation light sources, e.g., threshold and near-edge photoexcitation phenomena, very fast processes, and processes requiring very high intensity and energy resolution. Electron correlations in atoms and molecules are studied, especially in the adiabatic (low-energy) limit, where the electronic structure of the continuum is important. Time-of-flight measurements with synchrotron radiation are used to measure angular distributions of photoelectrons and resonant photoemission phenomena in the gas phase. Of special interest are ultra-high-resolution absorption and threshold photoemission studies. Ultra-high-resolution photoelectron spectroscopy based on molecular beams is yielding new information about small molecules and about the transition from single-metal atoms to behavior characteristic of a three-dimensional solid. Employing angle-resolved, variable-energy photoemission, this program examines the electronic structure of solids. The program also studies the geometric and electronic structure of surface-adsorbate systems using photoelectron diffraction, angle-resolved photoemission, extended fine structure (ARPEFS).

1. Near-Edge Sodium and Fluorine Photoabsorption of Alkali Halides (Publication 4)

E. Hudson, E. Moler, Y. Zheng, S. Kellar, P. Heimann, Z. Hussain, and D.A. Shirley

The x-ray absorption near-edge structure (XANES) of single-crystal alkali halide salts has been measured at low temperature ($T \approx 80$ K) with high energy resolution. By employing the electron partial-yield detection technique, spectra of NaF, NaCl, and NaBr were obtained near the sodium K-edge, and spectra of LiF, NaF, and KF were obtained near the fluorine K-edge. All spectra showed sharp absorption features at the absorption threshold and broader features extending 50–80 eV above threshold. Some narrow features close to threshold are attributed to core-level excitations. Contributions from atomic multi-electron excitations, estimated by a comparison to the K-edge photoabsorption spectrum of Ne in the gas phase, are found to be very small. Thus the intense, broader peaks observed further above threshold arise from single-electron scattering resonances. These highly structured spectra of well-characterized ordered crystals provide a set of standard data that is used to test the multiple-scattering x-ray absorption code FEFF V. For some spectra, at photon energies more than ≈ 10 eV above threshold, the calculations achieve very sound agreement with the experiment. The dependence of the calculation on cluster size, order of scattering, and choice of self-energy is demonstrated.

*This work was supported by the Director, Office of Energy Research, Office of Basic Energy Sciences, Chemical Sciences Division, of the U.S. Department of Energy under Contract No. DE-AC03-76SF00098. It was performed at the National Synchrotron Light Source and Stanford Synchrotron Radiation Laboratory, which are supported by the Department of Energy's Office of Basic Energy Sciences.

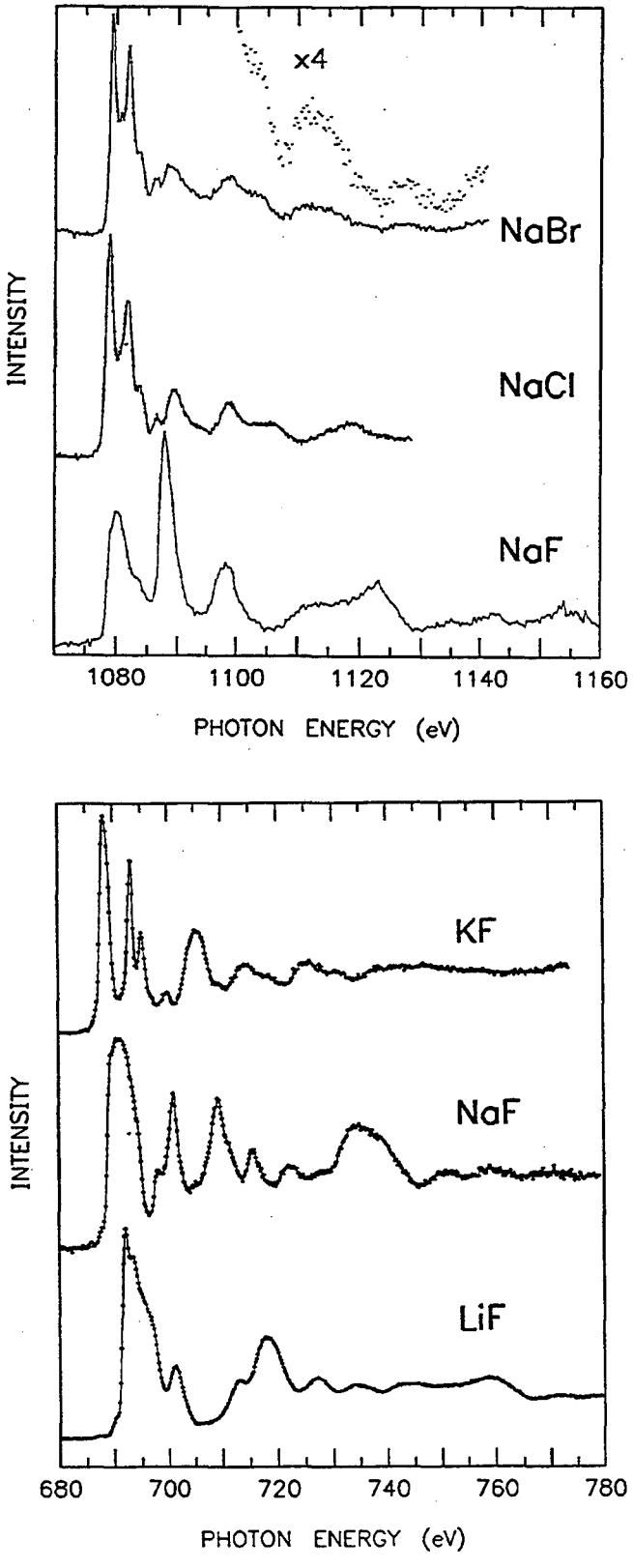

Figure 1-1. (a) Photoabsorption spectra of sodium halide salts near the sodium *K*-edge. For NaBr, weaker absorption features are also shown with an expanded vertical scale. (b) Photoabsorption spectra of alkali fluoride salts near the fluorine *K*-edge. (XBL 947-4183)

2. High-Resolution Photoabsorption Near the Sulfur $L_{2,3}$ Thresholds: H_2S and D_2S (Publication 5)

E. Hudson, D.A. Shirley, M. Domke, G. Remmers, and G. Kaindl

The x-ray absorption near-edge structure (XANES) of gas-phase H_2S, hydrogen sulfide, and D_2S, deuterium sulfide, at the sulfur $L_{2,3}$ ionization thresholds has been measured using synchrotron radiation with high-energy resolution from the SX700/II soft x-ray monochromator at BESSY. Previously unobserved fine structure is resolved. The spectra of both molecules are characterized by multi-electron excitations 8–14 eV above the L_2 threshold energy, broad valence-shell absorption features 5–8 eV below the L_2 edge, and many narrower Rydberg excitations 0–5 eV below the L_2 edge. Comparison of the H_2S and D_2S spectra allows the identification of transitions that include vibrational excitation caused by the isotopic dependence of vibrational energies. For the $(2p)^{-1}$ core-excited Rydberg states, a least-squares analysis was employed, which deconvoluted the core-level and excited-orbital splittings. Results show that the two-fold degeneracy of the sulfur $2p_{3/2}$ core level is removed by the molecular field, with a resulting splitting of 115 meV for the higher-energy core-excited Rydberg states. The energies of the higher Rydberg states were well described by the Rydberg formula with the quantum defects $\delta_p = 1.63$ and $\delta_d = 0.32$. Fine structure was resolved in the transitions to the dissociative $(2p)^{-1}$ core-excited valence-shell states. The regular spacing and isotopic dependence of this structure clearly identifies it as a vibrational progression.

3. Photoelectron Holography of Pt(111) at 351 eV (Publication 8)

B.L. Petersen, L.J. Terminello, J.J. Barton, and D.A. Shirley

A 351-eV photoelectron hologram of a Pt(111) surface was collected by detection of photoelectrons from the $4f_{5/2}$ subshell in a display analyzer and was Fourier-analyzed. The real-space image showed sensitivity to the fourth atomic layer, excellent reproduction of the fcc lattice, and sixteen source-atom neighbors. Transverse atomic positions were located to 0.1 Å. Photoelectron holography using low-energy electrons is thus shown to be capable of imaging lattices and interfaces.

4. High-Resolution Photoelectron Spectroscopy of CH_2F_2, CH_2Cl_2 and CF_2Cl_2 Using Supersonic Molecular Beams (Publication 10)

T. Pradeep and D.A. Shirley

Molecular beam photoelectron spectroscopy using HeI radiation (584 Å) has been used to study the electronic structures of CH_2F_2, CH_2CL_2, and CF_2CL_2. The spectra obtained at a resolution of 13 meV show a number of new features, in addition to those reported earlier in the literature. Accurate values of the ionization potentials were obtained, and many new vibrational progressions were resolved and assigned. The first four ionic states are discussed in more detail on the basis of reported configuration interaction calculations and photoionization measurements. Ambiguities regarding the ordering of these states have been resolved. Although the agreement between theory and experiment is good in CF_2Cl_2, there are significant differences in CH_2F_2 and CH_2Cl_2.

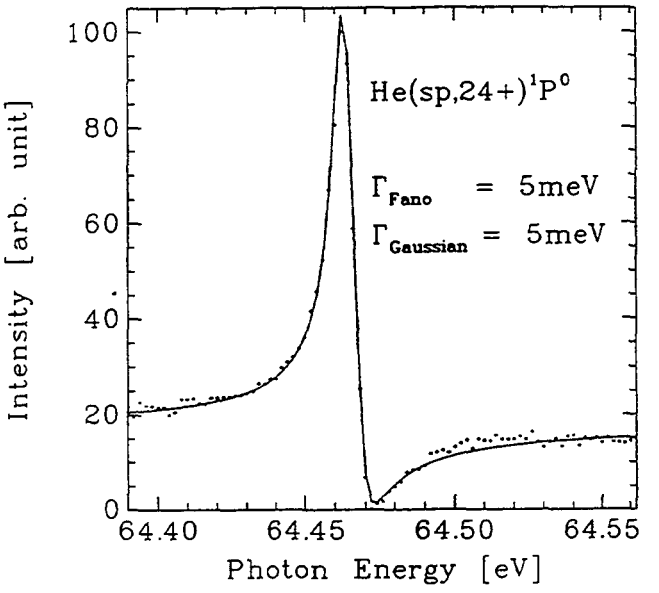

Figure 5-1. Photoionization spectrum from He gas showing the autoionizing double-excitation state of He(sp,24+)$^1P^0$. The spectrum was obtained with entrance and exit slits of 10 μm and a 32% mask opening of the grating. The solid curve is a fit. (XBL 947-4184)

5. High Resolution in the Soft X-ray Range from a Toroidal Grating Monochromator (Publication 12)

T. Reich, Z. Hussain, E. Moler, M. Blackwell, G. Kaindl, D.A. Shirley, and M.R. Howells

A resolving power, E/ΔE, of ≥13,000 has been achieved with the modified 6m/160° toroidal grating monochromator (TGM) installed on beamline 8-1 at the Stanford Synchrotron Radiation Laboratory (SSRL). The resolving power of the TGM was increased by replacing the entrance and exit slits with high-precision slits, masking the horizontal part (short radius) of the grating and improving the TGM scanning mechanisms. To determine the performance of the monochromator, we measured the dependencies of resolution and photon flux on the entrance and exit slitwidths, the exit slit position, and the masking of the grating. The monochromator resolution in the energy range of 25–65 eV was derived from photoionization measurements of extremely narrow core-excitation resonances in He and Ne. With 10-μ vertical entrance and exit slitwidths and a 32% mask opening of the grating, the monochromator has a resolution (FWHM) of 5.0 ± 0.7 meV at a photon energy of 64.5 eV and a flux of 2×10^7 photons/s/100 mA. The results suggest a simple procedure for converting a TGM with moderate resolution into a high-resolution monochromator with a moderate reduction in photon flux due to masking the grating, beyond the reduction attributable to the slitwidths.

6. Structural Determination of NH_3 Adsorbed on Ni(001) Using Angle-Resolved Photoemission Extended Fine-Structure Spectroscopy (Publication 14)

Y. Zheng, E. Moler, E. Hudson, Z. Hussain, and D.A. Shirley

The structure of NH_3 adsorbed on the Ni(001) surface was studied using the angle-resolved photoemission extended fine-structure (ARPEFS) technique. The ARPEFS data were taken along the surface normal-emission direction at a sample temperature of 100 K. Multiple-scattering spherical-wave data analysis determined that NH_3 adsorbs at the atop site of the Ni(001) surface with the N–Ni bond length of 2.01 Å and a 2.8% expansion of the topmost Ni–Ni interlayer spacing.

7. Toward a Soft X-ray Fourier-Transform Spectrometer (Publication 15)

M.R. Howells, K. Frank, Z. Hussain, E. Moler, T. Reich, D. Moller, and D.A. Shirley

The use of Fourier-transform spectroscopy (FTS) in the soft x-ray region is advocated as a possible route to spectral resolution superior to that attainable with a grating system. A technical plan is described for applying FTS to the study

of the absorption spectrum of helium in the region of double ionization around 60–80 eV. The proposed scheme includes a Mach–Zehnder interferometer deformed into a rhombus shape to provide grazing incidence reflections. The path difference between the interfering beams is to be tuned by translation of a table carrying four mirrors over a range of ±1 cm that, in the absence of errors generating relative tilts of the wave fronts, would provide a resolving power equal to the number of waves of path difference: half a million at 65 eV, for example. The signal-to-noise ratio of the spectrum is analyzed, and for operation on an Advanced Light Source bending magnet beamline, it should be about 330.

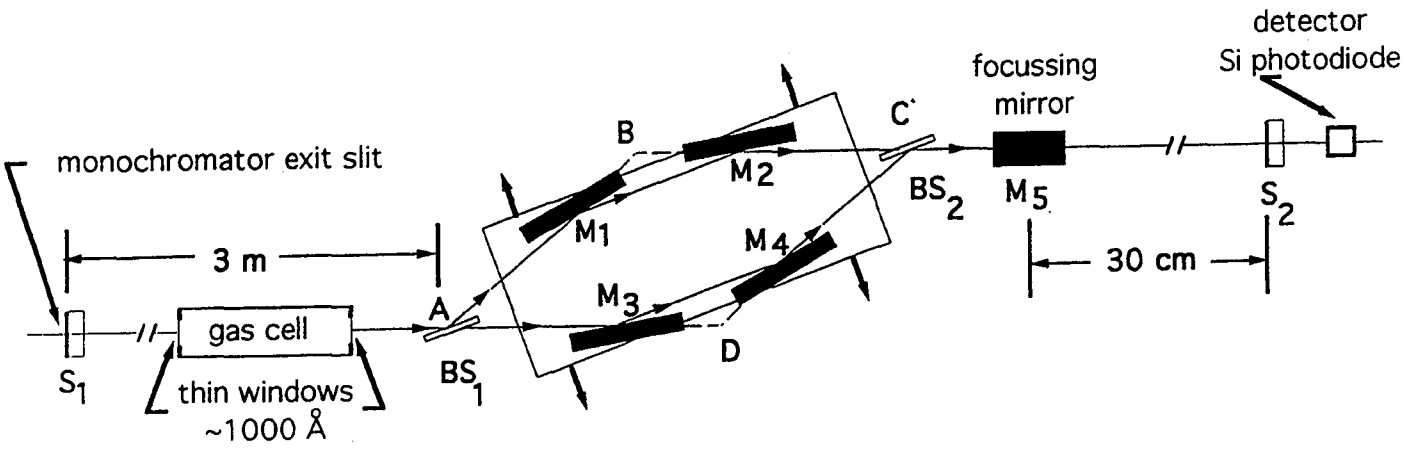

Figure 7-1. Schematic diagram of the soft x-ray interferometer experiment. S_1: beamline monochromator exit slit; BS_1 and BS_2: beamsplitters; M_1, M_2, M_3, M_4: flat mirrors; M_5: spherical focusing mirror; S_2: slit for rejecting orders other than zero diffracted by the beamsplitters. ABCD is a rhombus of 15-cm sides. (XBL 974-4185)

FY 1993 PUBLICATIONS AND REPORTS

Refereed Journals

1. Z.Q. Huang, L.Q. Wang, A.E. Schach von Wittenau, Z. Hussain, and D.A. Shirley, "Angle-Resolved Photoemission Extended Fine-Structure Study of the Structure of p(2×2)K/Ni(111)," Phys. Rev. B **47**, 13626 (1993).
2. Z.Q. Huang, Z. Hussain, W.T. Huff, E. Moler, and D.A. Shirley, "Structural Determination of p2mg(2×1)CO/Ni(110) with the Use of Angle-Resolved Photoemission Extended Fine-Structure Spectroscopy," Phys. Rev. B **48**, 1696 (1993).
3. E. Hudson, D.A. Shirley, M. Domke, G. Remmers, A. Puschmann, T. Mandel, C. Xue, and G. Kaindl, "High-Resolution Measurements of Near-Edge Resonances in the Core-Level Photoionization Spectra of SF_6," Phys. Rev. A **47**, 361 (1993).
4. E. Hudson, E. Moler, Y. Zheng, S. Kellar, P. Heimann, Z. Hussain, and D.A. Shirley, "Near-Edge Sodium and Fluorine *K*-Shell Photoabsorption of Alkali Halides," Phys. Rev. B **49**, 370 (1994).
5. E. Hudson, D.A. Shirley, M. Domke, G. Remmers, and G. Kaindl, "High-Resolution Photoabsorption Near the Sulfur $L_{2,3}$ Thresholds: H_2S and D_2S," Phys. Rev. A **49**, 161 (1994).
6. B. Niu, D.A. Shirley, and Y. Bai, "High-Resolution Photoelectron Spectroscopy and Femtosecond Intramolecular Dynamics of H_2CO^+ and D_2CO^+," J. Chem. Phys. **98**, 4377 (1993).
7. B. Niu, Y. Bai, and D.A. Shirley, "High-Resolution Photoelectron Spectroscopy and Femtosecond Intramolecular Dynamics of H_2CCO^+ and D_2CCO^+," J. Chem. Phys. **99**, 2520 (1993).
8. B.L. Petersen, L.J. Terminello, J.J. Barton, and D.A. Shirley, "Photoelectron Holography of Pt(111) at 351 eV," Chem. Phys. Lett. **213**, 412 (1993).
9. T. Pradeep, B. Niu, and D.A. Shirley, "Photoelectron Spectroscopy of Rare Gas Dimers Revisited: Vibrationally Resolved Photoelectron Spectrum of Argon Dimer," J. Chem. Phys. **98**, 5269 (1993).
10. T. Pradeep and D.A. Shirley, "High-Resolution Photoelectron Spectroscopy of CH_2F_2, CH_2Cl_2 and CF_2Cl_2 Using Supersonic Molecular Beams," J. Elec. Spec. and Related Phenomena **66**, 125 (1993).
11. G. Remmers, M. Domke, A. Puschmann, T. Mandel, G. Kaindl, E. Hudson, and D.A. Shirley, "High-Resolution Inner-Shell Photoionization of NO," Chem. Phys. Lett. **214**, 241 (1993).
12. T. Reich, Z. Hussain, E. Moler, M. Blackwell, G. Kaindl, D.A. Shirley, and M.R. Howells, "High Resolution in the Soft X-ray Range from a Toroidal Grating Monochromator," Rev. Sci. Instrum. **64**, 2552 (1993).
13. Y. Zheng, Z. Hussain, and D.A. Shirley, "The Influence of Calculated Phase Shifts on the Precision and Accuracy of ARPEFS-Derived Structural Parameters," Chem. Phys. Lett. **206**, 161 (1993).

14. Y. Zheng, E. Moler, E. Hudson, Z. Hussain, and D.A. Shirley, "Structural Determination of NH_3 Adsorbed on Ni(001) Using Angle-Resolved Photoemission Extended Fine-Structure Spectroscopy," Phys. Rev. B **48**, 4760 (1993).

LBL Reports

15. M.R. Howells, K. Frank, Z. Hussain, E. Moler, T. Reich, D. Moller, and D.A. Shirley, "Toward a Soft X-ray Fourier-Transform Spectrometer," Nucl. Instr. and Meth. (submitted); LBL-34798.
16. E. Hudson, "High-Resolution Soft X-ray Photoionization Studies of Selected Molecules," Ph.D. Thesis; LBL-34483.
17. B.L. Petersen, L.J. Terminello, J.J. Barton, and D.A. Shirley, "Multiple-Wave Number Photoelectron Holography of Pt(111)," Chem. Phys. Lett. (submitted); LBL-34567.
18. T. Reich, P. Heimann, B.L. Petersen, E. Hudson, Z. Hussain, and D.A. Shirley, "Near-Threshold Behavior of the *K*-Shell Satellites in CO," Phys. Rev. A (submitted); LBL-34936.
19. Y. Zheng and D.A. Shirley, "Simple Surface Structure Determination from Fourier Transforms of Angle-Resolved Photoemission Extended Fine Structure," LBL-34608.
20. Y. Zheng, E. Moler, W.R.A. Huff, S.A. Kellar, Z. Hussain, and D.A. Shirley, "Angle-Resolved Photoemission Extended Fine-Structure Study of a Cu(111) Surface," LBL-34944.

Invited Talks

21. E. Hudson, "High-Resolution XANES of Selected Molecules," Sandia National Laboratory, May 1993.
22. E. Hudson, "High-Resolution XANES of Selected Molecules," Los Alamos National Laboratory, May 1993.
23. E. Hudson, "High-Resolution XANES of Selected Molecules," Glenn T. Seaborg Institute for Transactinium Science, Lawrence Livermore National Laboratory, March 1993.
24. T. Reich, P.A. Heimann, B.L. Petersen, E. Hudson, Z. Hussain, and D.A. Shirley, "Threshold Behavior of the *K*-Shell Satellites in CO," Annual Meeting of the Division of Atomic, Molecular, and Optical Physics, Reno, NV 1993; APS Bulletin **38**, No. 3 (1993), p. 1147.
25. B.L. Petersen, L.J. Terminello, J.J. Barton, and D.A. Shirley, "Photoelectron Holography of Platinum (111)," 1993 Spring Meeting of the Materials Research Society, April 12–16, 1993.
26. B.L. Petersen, L.J. Terminello, J.J. Barton, and D.A. Shirley, "3-Dimensional Photoelectron Holography of Surfaces," Joint Meeting of the 29th Annual Symposium of the American Vacuum Society/New Mexico Chapter and 18th DOE Surface Studies Conference, April 27–30, 1993.
27. Y. Zheng, E. Moler, E. Hudson, Z. Hussain, and D.A. Shirley, "Structural Determination of NH_3 Adsorbed on Ni(001) Using Angle-Resolved Photoemission Extended Fine-Structure Spectroscopy," 1993 APS March Meeting, Seattle, WA.
28. Y. Zheng, E. Moler, Z. Hussain, and D.A. Shirley, "The Effect of Calculated Atomic Scattering Phase Shifts on the Data Analysis of Angle-Resolved Photoemission Extended Fine Structure," 1993 Spring Meeting of the Materials Research Society, San Francisco, CA, April 12–16, 1993.
29. T. Reich, P.A. Heimann, B.L. Petersen, E. Hudson, Z. Hussain, and D.A. Shirley, "High-Resolution Photoelectron Spectroscopy of the Core-Level Satellites in CO, C_2H_2, and C_2H_4," 1993 Spring Meeting of the Materials Research Society, San Francisco, CA, April 12–16, 1993.
30. E.J. Moler, Y. Zheng, E.A. Hudson, Z. Hussain, and D.A Shirley, "Surface Structure Determination of c(2×2) N_2/Ni(100) by Angle-Resolved Photoemission Extended Fine Structure," 1993 Spring Meeting of the Materials Research Society, San Francisco, CA, April 12–16, 1993.
31. E. Hudson, E. Moler, Y. Zheng, S. Kellar, P. Heimann, Z. Hussain, and D.A. Shirley, "High-Resolution Core-Level Photoabsorption of Alkali Halides," 1993 Spring Meeting of the Materials Research Society, San Francisco, CA, April 12–16, 1993.
32. Z. Hussain, Y. Zheng, L.-Q. Wang, A.E. Schach von Wittenau, "Low-Temperature Angle-Resolved Photoemission Extended Fine Structure: A Technique for High-Precision Surface Structure Determination," 1993 Spring Meeting of the Materials Research Society, San Francisco, CA, April 12–16, 1993.

Experimental Search for the Electron Electric Dipole Moment*

Eugene D. Commins, Investigator

INTRODUCTION

An atom in a nondegenerate state cannot possess a permanent electric dipole moment (EDM) unless parity (P) and time reversal invariance (T) are both violated. If an atomic EDM were to exist, it could arise from one or more of the following causes:

1. An intrinsic EDM of the neutron and/or proton.
2. A P,T odd component of the nucleon–nucleon interaction.
3. An intrinsic EDM of the electron.
4. A P,T odd component of the electron–nucleon interaction.

Experimental searches for the free-neutron EDM and atomic (or molecular) EDM's are motivated by the fact that charge conjugation and parity (CP) violation in neutral kaon decay, equivalent to T violation, still has no satisfactory explanation in spite of 30 years of detailed investigation. Thus, a variety of theoretical models of CP violation have been proposed, including some that predict nucleonic or atomic EDM's within experimental range.

One searches for an EDM by exposing the neutral system of interest (atom, neutron) to an external electric field and looking for an energy shift proportional to this field (linear Stark effect). Efforts to observe an electron EDM are aided greatly by the following: It can be shown that, in suitable heavy paramagnetic atoms where relativistic effects are large, the ratio, R, of the atomic EDM (d_a) to the EDM of the unpaired electron (d_e) is approximately 100 to 1000 in magnitude. For example, in the ground $6^2P_{1/2}$ state of thallium [atomic number (Z), 81], $R = -580$. Thus, in practice, one carries out an experiment to search for d_a and interprets the result in terms of d_e.

The present experiment utilizes two counter-propagating atomic beams of ^{205}Tl, laser optical pumping for state selection and analysis, two separated rf fields for magnetic resonance, and an intense electric field **E** (approximately 120,000 V/cm) between these separated rf fields. The entire experiment is immersed in a uniform magnetic field, **B**, parallel to **E**. The observed signal is fluorescence in the second optical pumping region, and the signature of an EDM is an asymmetry in the fluorescence signal proportional to **E**·**B**. The best limit on the electron EDM has been obtained in this experiment, with the following published result[1]:

$$d_e = (-2.7 \pm 8.3) \cdot 10^{-27} \text{ e cm} \qquad (1)$$

Several theoretical models of considerable current interest predict that d_e should be in the range of 10^{-26} e cm to 10^{-28} e cm, and thus it is very important to improve the precision of our result. Since publication in 1990, we have devoted ourselves to improving the sensitivity of the apparatus, reducing noise, and eliminating sources of systematic error. In section 1, we describe the consequences of these efforts for the present experiment. About one year ago, we also arrived at a new scheme for major improvement of the experiment. Progress along these lines is described in section 2.

*This work was supported by the Director, Office of Energy Research, Office of Basic Energy Sciences, Chemical Sciences Division, of the U.S. Department of Energy under Contract No. DE-AC03-76SF00098.

1. K. Abdullah *et al.*, Phys. Rev. Lett. 65, 2347 (1990).

1. Progress on the Present Experiment

S.B. Ross, B.C. Regan, and E.D. Commins

By January, 1993, we had already achieved substantial improvements in noise reduction and sensitivity, and we had also gained much improved control over many sources of systematic error. (This was, in fact, described in the 1992 Annual Report). We demonstrated that it was possible to arrive at a statistical precision of 3×10^{-27} e cm in d_e in about 10 hours of data taking, and thus we began what we thought would be a final set of data runs. Unfortunately, the data we acquired in early 1993 revealed a fluctuating systematic effect, the origin of which eluded us for many months, despite much determined effort. Finally, we discovered the cause of this effect, and also its cure, in December 1993. We found that our analysis of the "$\mathbf{E} \times \mathbf{v}$" effect, which we had thought was complete, contained a subtle flaw. The difficulty arose from a combination of two things: a very slight angular misalignment of the "up" and "down" atomic beams and a slight "wedging" distortion of the electric field that reverses direction from one end of the electric field to the other. The auxiliary experiments that we had previously devised to test for various manifestations of the $\mathbf{E} \times \mathbf{v}$ effect had failed to account for this particular problem. Once this problem was clearly recognized, however, in December of 1993, a solution became readily apparent. It required the construction of a set of coils to

generate a test magnetic field of rather peculiar geometry. With this new set of coils, we have eliminated the angular misalignment of the atomic beams to very good precision, and the troublesome problem has now been solved. We have thus at last embarked on final data runs, which will complete this phase of the experiment.

2. Progress on the New Phase of the Experiment

D. DeMille, B.C. Regan, and E.D. Commins

The basic idea here is to employ simultaneous beams of atoms in the $6P_{1/2}$, F = 1 and $6P_{3/2}$, F = 2 states and to switch rapidly back and forth between their fluorescence signals in the analyzer region. Comparison of these two signals by rapid switching can eliminate low-frequency magnetic and atomic beam noise. When used in conjunction with the up–down beam technique, it can lead to cancellation of a variety of systematic errors, giving high precision. During the past year we have devoted ourselves to planning and design and to ordering the necessary new equipment. Many of the required components have arrived, but we are still not ready to begin construction and modification of the apparatus. We hope to move into that stage by April 1994.

FY 1993 PUBLICATIONS AND REPORTS

Refereed Journals

1. D. Budker, D. DeMille, E.D. Commins, and M. S. Zolotorev, "Investigation of Nearly Degenerate Opposite Parity States in Atomic Dysprosium," Phys. Rev. Lett. **70**, 3019 (1993).

High-Energy Atomic Physics*

Harvey Gould, Investigator

INTRODUCTION

The goals of this program are to understand relativistic atomic collisions and to search for a charge-parity-violating permanent electric dipole moment (EDM) of the electron. Recent results include the discovery of a new relativistic atomic collisions process—electron capture from pair production—and the first measurement of its cross section. This is the process in which an electron–positron pair is produced by the strong transient electromagnetic field of a relativistic atomic collision and the electron emerges from the collision *bound to the ion.* This process is unique because its cross section increases with energy at relativistic energies, and because it has no electron in the initial state. It is predicted to be the dominant mechanism for beam loss for the heaviest ions at the Relativistic Heavy Ion Collider (RHIC) being built at Brookhaven National Laboratory. Present activities include (1) developing a calculation that can accurately predict the cross sections for capture from pair production at relativistic and ultrarelativistic energies, (2) setting up an experiment to measure capture from pair production at 10 GeV/u at the Brookhaven Alternating Gradient Synchrotron, (3) constructing an EDM experiment using trapping and cooling of francium to reach a sensitivity of 10^{30} e-cm or better, and (4) continued adherence to applicable standards for environment, health, safety, and procedure in all activities.

1. Measurement of Electron Capture from Electron–Positron Pair Production in Relativistic Heavy Ion Collisions (Publication 1)

A. Belkacem, H. Gould, B. Feinberg, R. Bossingham, and W.E. Meyerhof†

We report the first observation and measurement of electron capture from electron–positron pair production in relativistic heavy ion collisions. This is the process in which an electron–positron pair is produced by the strong transient electromagnetic field of a relativistic atomic collision and the electron emerges from the collision *bound to the ion.*

Figure 1-1 shows a schematic of our experiment, which was performed at Lawrence Berkeley Laboratory's Bevalac accelerator using 0.956 GeV/u U^{92+} (bare uranium ions) incident on thin fixed targets. The experimental signature for capture from electron–positron pair production is the capture of the electron, changing the charge of the U^{92+} to U^{91+}, in coincidence with the detection of the emitted positron. The U^{91+} is magnetically separated from the main U^{92+} beam, and each charge state is detected, at the end of the beamline by a plastic scintillator-photomultiplier detector. The positron is detected, and its energy is measured, by another plastic scintillator-photomultiplier detector.

The Advanced Positron Spectrometer (APS) is used to measure the energy and angular distribution of the positrons emitted at the target. The APS contains a solenoid magnet with a dipole magnet at each end. The solenoid generates a strong (B = 0.8 T, maximum), but adiabatically decreasing, longitudinal magnetic field that transports the positrons and electrons away from the target and, most importantly, converts much of the positron (electron) transverse motion into a longitudinal motion with respect to the axis of the solenoid. Tests of the APS show an acceptance close to unity for emission angles of up to 75° forward and backward. This acceptance is independent of the electron or positron energy in the energy range of interest (100 keV to 2,500 keV).

For a given positron (electron) energy, larger emission angles result in a longer time of flight through the strong field of the solenoid, and this time of flight is used to determine the emission angle with respect to the beam direction. The energy resolution of the positrons (electrons) is about 17% and the angular resolution is about 15°.

Additional discrimination is made by detecting of one of the two 511-keV positron-annihilation photons emitted back-to-back in the plastic scintillator in which the positron is stopped. This is important, because at 1 GeV/u, an average of 3 to 4 knock-on electrons (delta rays) with an

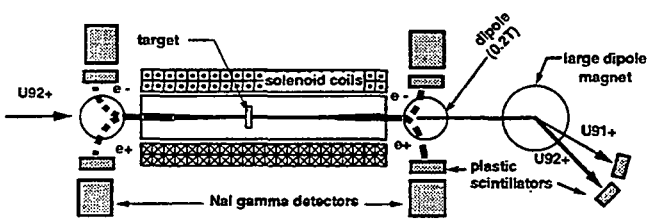

Figure 1-1. Schematic of the electron capture from pair production experiment. (XBL 947-4180)

*This work was supported by the Director, Office of Energy Research, Office of Basic Energy Sciences, Chemical Sciences Division, of the U.S. Department of Energy under Contract No. DE-AC03-76SF00098.

energy above 100 keV are ejected from a 1-mg/cm^2 gold target by each uranium ion, while only one positron from the same target is expected for every 10^6 uranium ions. Roughly 0.2% to 0.3% of these knock-on electrons backscatter from the electron scintillator into the positron scintillator-detector, simulating a positron. With the addition of the 511-keV photon, we accept only about 1 in 10^8 (knock-on) electrons.

Figure 1-2 shows the observed energy spectra of the positrons emitted in coincidence with the U^{91+}, produced by a 0.956-GeV/u U^{92+} beam incident on a 1-mg/cm^2 Au target. The spectra show a relative lack of low-energy positrons. This is due to the repulsion of the positrons by the gold target nuclei, which are at rest in the laboratory frame. Comparing the two spectra bin by bin suggests that positrons emitted at higher energies are also emitted at smaller (more forward) angles.

Our measured total cross section for capture from pair production by a 0.956-GeV/u U^{92+} on a gold target is 2.19 (0.25) barns. We also obtain a cross section of 3.30 (0.65) barns for the free pair process (for this process the positron is detected in coincidence with the U^{92+}). We find it striking that, at 1 GeV/u, the electron of the electron–positron pair is almost as likely to emerge from the collision bound to the uranium ion as it is to emerge free.

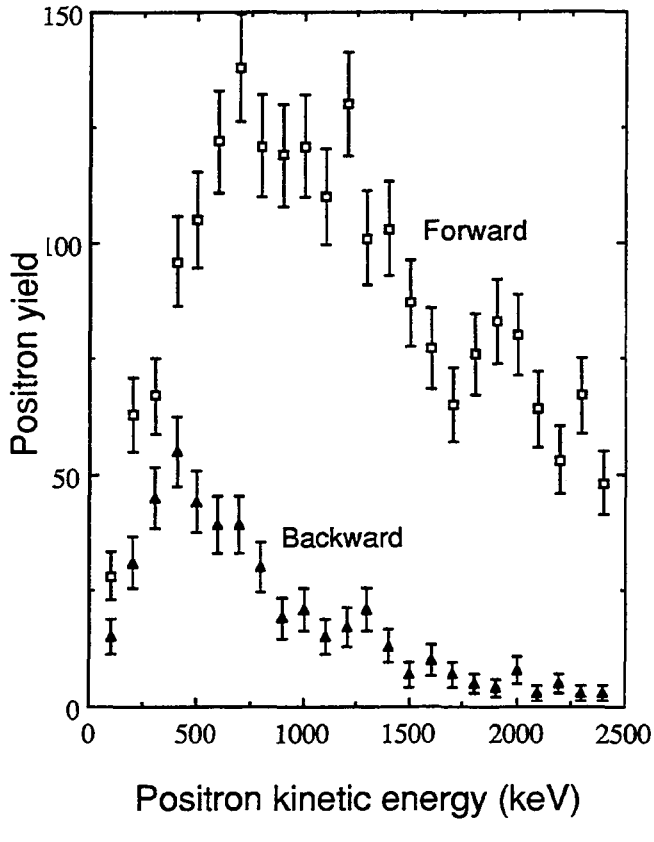

Figure 1-2. Yield of positrons vs. positron kinetic energy measured for electron capture from pair production by 956 MeV/u U^{92+} beam on Au target. (XBL 947-4181)

†Stanford University, Stanford, CA 94305.

2. Relativistic Coulomb Wave Functions in Momentum Space (Publication 2)

A. Sørensen† and A. Belkacem

Momentum-space wave functions for single electrons bound in a Coulomb potential have been provided by many authors both for nonrelativistic and relativistic motion. The situation for unbound motion in a Coulomb field is quite different. Motivated by this apparent deficiency and by the importance of these waves in the description of atomic processes at relativistic energies, we report below a computation of Coulomb wave functions in momentum space for unbounded relativistic motion. The waves appear highly localized. This feature is of a substantial advantage in calculations including evaluation of certain matrix elements that one encounters in relativistic atomic collision processes: capture from pair production, ionization, charge transfer, etc.

To obtain momentum-space wave function, we perform a Fourier transformation on configuration-space wave functions. This procedure makes use of the availability, in the literature, of the configuration-space wave functions.

Let a source of the Coulomb field be a charge Ze and let the total energy of the electron of mass m be $E = Wmc^2$, where $|W| > 1$. The partial waves corresponding to a total angular momentum quantum number j are characterized by the quantum number $k = +(j + 1/2)$ and a magnetic number m, which assumes the values $m = -j, -(j - 1), \ldots, j - 1, j$. They read

$$\Psi(\mathbf{r},t) = \begin{bmatrix} g(r)\Omega_\kappa^\mu(\Theta,\Phi) \\ if(r)\Omega_\kappa^\mu(\Theta,\Phi) \end{bmatrix} \exp(-iWct/\lambda_c) \ .$$

The Ω functions are the usual spin-angular momentum functions. The Fourier transform of the wave function $\Psi(\mathbf{r},t)$ and subsequent integration over angles transforms the above equation into

$$\Psi(\mathbf{k}) = -i^{-1} \begin{bmatrix} g(k)\Omega_\kappa^\mu(\Theta_\kappa,\Phi_\kappa) \\ -S_\kappa f(k)\Omega_\kappa^\mu(\Theta_\kappa,\Phi_\kappa) \end{bmatrix}$$

with (Θ,Φ) denoting the polar and azimuthal angles of the momentum vector $\mathbf{k}$ and S_κ is the sign of κ. To obtain $\Psi(\mathbf{k})$ for all values of $\mathbf{k}$, we apply an integral representation of the confluent hypergeometric function that appears in $g(k)$ and $f(k)$. The function is calculated numerically using a

contour integration. Figure 2-1 reveals a standard example with $Z = 92$, $W = 2$, $\kappa = -3$ and the convergence parameter introduced in the contour integration $\varepsilon = 1.10^{-3}$. The major features observed are:

1. The large excursions for k attaining values near k_0, where k_0 is the momentum corresponding for a free electron with energy W. This feature is a result of the electron being unbound and nearly free.
2. A substantial weight in the region above k_0 extending up to roughly 1.5 k_0. This feature derives from the acceleration of the electron near the attracting Coulomb center. In contrast, for negative values of the energy W, Coulomb waves show a substantial weight in the region below k_0, which corresponds to the slowing down of a positron by the repulsive Coulomb center.

† Permanent address: Institute of Physics and Astronomy Aarhus University, DK-8000 Aarhus C, Denmark.

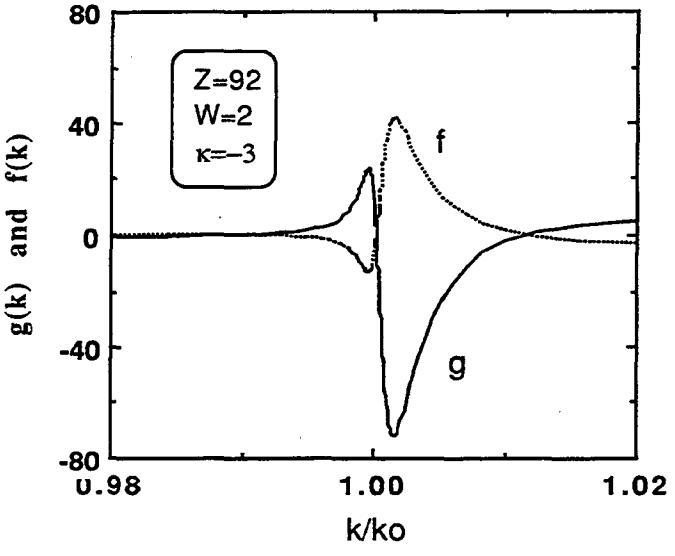

Figure 2-1. Functions $g(k)$ and $f(k)$ computed by contour integration for the case of $Z = 92$, $W = 2$, $\kappa = -3$. The convergence parameter ε is 0.001. (XBL 947-4182)

3. Work in Progress: Electron EDM Measurement by Trapping and Cooling of Francium

We are building an experiment to search for a charge-parity-violating permanent electric dipole moment (EDM) of the electron using laser trapping and cooling of francium. Compared to earlier techniques, this method reduces the major systematic effects as well as increases the sensitivity of the experiment. Consequently, an experimental limit of 10^{-30} ecm—a factor of 10,000 improvement over the current upper limit—may be reached. The first steps will be to construct a fountain atomic clock using cesium (which is less sensitive to an EDM than francium but easier to work with) and a francium trap. The francium is obtained as a decay product of ^{229}Th, eliminating the need to use an accelerator to produce the francium. The Cs fountain is presently under construction and a ^{229}Th source is being fabricated from a large stock of recently obtained ^{229}Th.

FY 1993 PUBLICATIONS AND REPORTS

Refereed Journals

1. A. Belkacem, H. Gould, B. Feinberg, R. Bossingham, and W.E. Meyerhof, "Measurement of Electron Capture from Electron–Positron Pair Production in Relativistic Heavy Ion Collisions," Phys. Rev. Lett. **71**, 1514 (1993); LBL-34021.
2. A.H. Sørensen and A. Belkacem, "Relativistic Coulomb Wave Functions in Momentum Space," Phys. Rev. A **49**, 81 (1994); LBL-34546.

Other Publications

3. A. Belkacem, H. Gould, B. Feinberg, R. Bossingham, and W.E. Meyerhof, "First Measurement of Capture from e^+e Pair Production in Relativistic Heavy Ion Collisions," Bull. Am. Phys. Soc. **38**, 1170 (1993); LBL-33588a.
4. A. Belkacem, H. Gould, B. Feinberg, R. Bossingham, and W.E. Meyerhof, "First Measurement of Capture from Pair Production in Relativistic Heavy Ion Collisions," in *ICPEAC 1993: Abstract Papers of the 18th International Conference on the Physics of Electronic and Atomic Collisions*, edited by T. Andersen, B. Fastrup, F. Folkmann, and H. Knudsen (Aarhus University, Aarhus, Denmark), Vol. II, 629; LBL-35189.
5. A. Belkacem, H. Gould, B. Feinberg, R. Bossingham, and W. Meyerhof, "Measurement of Energy Dependence, Projectile Z Dependence, and Target Z Dependence of Electron Capture from Pair Production," in *Abstracts of the XIV DOE Atomic Physics Workshop* (Charlottesville, VA, October 15–16, 1993); LBL-35190.
6. A. Belkacem and A.H. Sørensen, "Relativistic Coulomb Wave Functions in Momentum Space," Bull. Am. Phys. Soc. **38**, 1126 (1993); LBL-33590a.
7. B. Feinberg, A. Belkacem, R. Bossingham, H. Gould, and W.E. Meyerhof, "Capture from Pair Production as a Beam Loss Mechanism for Heavy Ions at RHIC," *Proceedings of the 1993 Particle Accelerator Conference* (Washington, DC, May 1993), IEEE 93CH3279-7, Vol. 5, 3751 (1993); LBL-34072, UC-410.
8. B. Feinberg, A. Belkacem, R. Bossingham, Harvey Gould, and W.E. Meyerhof, "Capture from Pair Production as a Beam Loss Mechanism for Heavy Ions at RHIC," Bull. Am. Phys. Soc. **38**, 1265 (1993); LBL-33212.

9. K. Momberger, A. Belkacem, and A.H. Sørensen, "Nonperturbative Treatment of the Evolution of the Momentum Distribution for Capture from Pair Production," Bull. Am. Phys. Soc. **38**, 1102 (1993); LBL-33589a.

Invited Talks

10. H. Gould, "Measurement of Electron Capture from Pair Production," 9th High-Energy Heavy Ion Study, Lawrence Berkeley Laboratory, Berkeley, CA, October 28, 1993.
11. H. Gould, "Measurement of Electron Capture from Electron–Positron Pair Production," Physics Department, University of California, Davis, CA, October 25, 1993.
12. A. Belkacem, "Time-Dependent Dirac Equation in Momentum Space and Application to Capture from Pair Production," XIV DOE Atomic Physics Workshop, Charlottesville, VA, October 16, 1993.
13. A. Belkacem, "Experimental Evidence of the Highly Nonperturbative Aspect of Capture from Pair Production," XIII ISIAC Conference, Manne Siegbahn Institute of Physics, Stockholm, Sweden, July 29, 1993.
14. A. Belkacem, "Measurement of Electron Capture from e^+e Pair Production by 0.956 GeV/u U^{92+} on Au, Ag, Cu, and Mylar Targets," XVII International Conference on the Physics of Electronic and Atomic Collisions, Aarhus University, Aarhus, Denmark, July 27, 1993.
15. H. Gould, "First Measurement of Electron Capture from Pair Production," Workshop on the Atomic/Nuclear Frontier, Sparks, NV, May 15, 1993.
16. A. Belkacem, "Electron Capture from Pair Production," Institute for Nuclear Theory, University of Washington, Seattle, WA, April 23, 1993.
17. H. Gould, "Capture from Pair Production at 10 GeV/u," Brookhaven National Laboratory, February 25, 1993.
18. A. Belkacem, "Measurement of Electron Capture from Pair Production at the Bevalac," Lawrence Berkeley Laboratory, Nuclear Science Division Colloquium, Berkeley, CA, January 25, 1993.

Atomic Physics*

Michael H. Prior, Investigator

INTRODUCTION

This program studies the structures and interactions of atomic systems in order to provide detailed descriptions of their behavior and to challenge and stimulate theoretical understanding. Emphasis is upon research topics that are best addressed with unique research tools and expertise available at LBL. Often these topics have relevance to plasma behavior and diagnostics in fusion devices or advanced laser technology. Collaborative associations with investigators from outside of LBL are a means of bringing resources to the program, stimulating scientific exchange, and efficiently utilizing experimental facilities.

The program currently exploits the ability of state-of-the-art electron cyclotron resonance (ECR) ion sources at LBL to produce intense, highly charged beams for the conducting of ion-neutral collision and Auger spectroscopic studies. This work is carried out using the atomic physics facilities jointly established by LBL and LLNL at the two LBL ion sources. Two beamlines are currently in operation at the original LBL ECR ion source; a third beamline is attached to the recently completed Advanced ECR (AECR) ion source located nearby. These ion sources were constructed by the LBL Nuclear Science Division for use by the 88-Inch Cyclotron; their availability for atomic physics research is by cooperative agreement with that Division. The proximity of the two sources and facilities allows efficient use of instrumentation at either site and quick switchover from one ion source to the other.

Current emphasis is upon providing the most detailed experimental description of multiple-electron capture in slow ion–atom collisions. In the past, nearly all multiple-electron-capture experiments consisted of total cross-section measurements into unresolved or only partially resolved final states. Thus, whereas theorists can calculate population amplitudes into fully defined quantum states of the products, summing and averaging over much of this detail are required to obtain a total or partial cross section to compare with the much less detailed experimental data. A substantial fraction of our research consists of experiments that describe double- (or more) electron transfer between uniquely characterized final states so that theoretical predictions can be tested at the finest scale possible.

*This work was supported by the Director, Office of Energy Research, Office of Basic Energy Sciences, Chemical Sciences Division, of the U.S. Department of Energy under Contract No. DE-AC03-76SF00098.

The research also provides energy level structure and decay modes of highly excited states, as well as insight into novel population mechanisms in ion–atom collisions, for a wide range of multiply charged ions.

1. Magnetic Substate Alignment in Double-Electron-Capture Collisions (Publication 1)

M.H. Prior, R.A. Holt,† D. Schneider,‡ K.L. Randall,|| and R. Hutton¶

This work reports measurements of the magnetic substate alignment produced in double-electron capture by H-like projectiles B^{4+} and C^{5+} from He atoms by measuring the anisotropy of the Auger electron emission from the doubly excited projectile states formed in the collision, that is, the process:

$$A^{(Z-1)+}(1s) + He(1s^2) \rightarrow A^{(Z-3)+}(1s2l2l'\ ^2L) + He^{2+} \quad ,$$

which is rapidly ($\approx 10^{-12}$ s) followed by the Auger decay:

$$A^{(Z-3)+}(1s2l2l'\ ^2L) \rightarrow A^{(Z-2)+}(1s^2) + e(\varepsilon L) \quad .$$

Analysis of the anisotropy of the angular distribution of the decay electrons, with respect to the projectile beam direction (z-axis), provides values for the population of the aligned magnetic substates $|L,M_L\rangle$. This work adds the results of measurements on the B^{4+},He system to previous and extended measurements on the isoelectronic system C^{5+},He. These are the first such measurements for a multiple-electron-capture collision.

We have concentrated on the Li-like 1s2l2l′ states because the ^2L lines are resolved and the spectrum includes an S state for normalization. In addition, for these collision partners, the 1s2l2l′ ^2L states are directly produced in the collision (there is no significant radiative feeding). The final ion state following the Auger decay is an S state, which ensures that the electron angular distribution contains complete information regarding the alignment of the initial state. The relatively high energy of the electrons and the lifetimes of the initial states preclude significant perturbations by postcollision interaction effects, and the relative size of the fine-structure and level widths leads to small de-alignment corrections for fine structure coupling of L and S.

We have determined the alignment of the population of the $|LM_L\rangle$ substates for the $1s(2s2p\ ^1P)^2P$ and $1s2p^2\ ^2D$ levels for both projectiles at four collision velocities. This is done by measuring the intensity of Auger emission from each of these states, normalized to that from one of the two 1s2l2l′ S states at nine angles between 20° and 160° with respect to the projectile beam direction. The normalized anisotropy is given by:

$$W(\theta) = 1 + \sum_{1}^{k=L} D_{2k} A_{2k} P_k(\cos\theta) \quad ,$$

where the P_{2k} are Legendre polynomials, the A_{2k} are the alignment parameters, and D_{2k} are factors, near unity, that correct for de-alignment of the M_L populations caused by spin-orbit mixing. From the A_{2k} we extract the fractional population in each $|LM_L\rangle$ substate. Figures 1-1 and 1-2 summarize the results for the fractional population of each $1s2l2l'$ ^2L level and for the $1s(2s2p\ ^2P)^2P$ and $1s2p^2\ ^2D$ magnetic sublevels. The figures include results of calculations by W. Fritsch (Hahn Meitner Inst. Berlin) and C.D. Lin (Kansas State Univ.), and by J.P. Hansen (U. Norway, Bergen) and K. Taulbjerg (U. Aarhus, Denmark). The theoretical treatments utilize close-coupling methods with limited two-electron-basis sets, and treat the screening

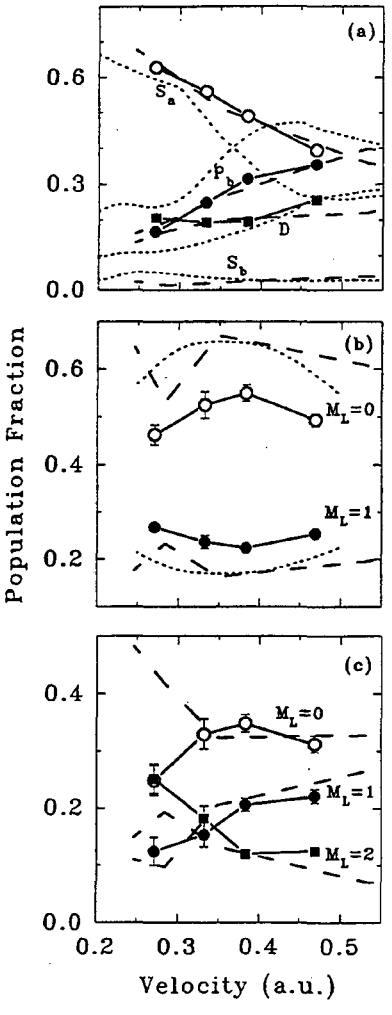

Figure 1-1. Results for the B^{4+}, He system. (a) shows the L-state population fractions; (b) and (c) show the ^2P and ^2D state magnetic sublevel fractions $|a_{M_L}|^2$ versus collision velocity. The long dashed lines are the results of calculations by Fritsch and Lin,[1] and the short dashed lines are those by Hansen and Taulbjerg.[2] (XBL 947-4194)

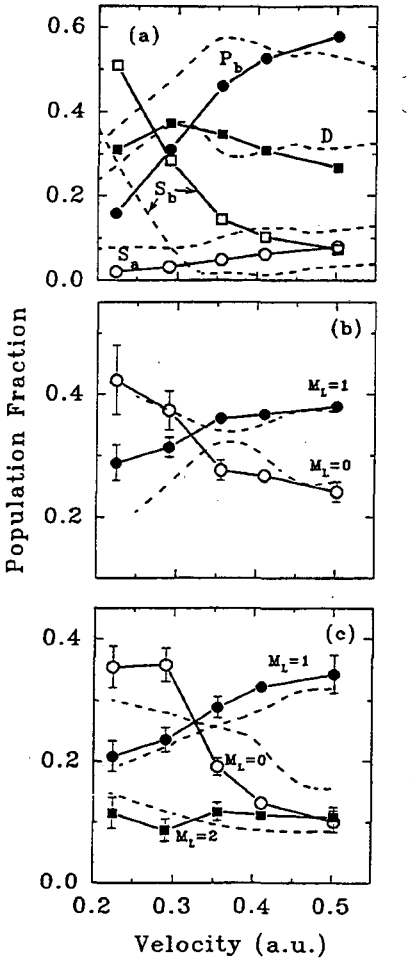

Figure 1-2. Results for the C^{5+},He system. (a) shows the L-state population fractions; (b) and (c) show the ^2P and ^2D state magnetic sublevel fractions, $|a_{M_L}|^2$, versus collision velocity. The dashed lines are the results of calculations by Hansen and Taulbjerg. (XBL 947-4195)

of the projectile nucleus by its 1s electron via model potentials. The work of Hansen and Taulbjerg has stressed the importance of using a correlated set for the doubly excited states of the Li-like projectile state formed in the collision. When compared to calculations using a simpler basis set made up of products of hydrogenic functions for the $n = 2$ state, the superiority of the correlated basis is clearly evident. Of course, as pointed out by Hansen and Taulbjerg, it is well known that doubly excited states often show a high degree of correlation, and thus it is not surprising that a limited basis set that includes the lowest order effects of the interelectronic repulsion performs better than one that treats the two electrons as independent particles moving in a screened central Coulomb potential. On the other hand, Fritsch and Lin have obtained good agreement for the distribution of population among the L-states for B^{4+},He using an atomic basis expansion in products of modified hydrogenic functions.

With regard to the M_L sublevel populations, generally there is fair agreement between the calculations and the measurements for the higher velocities. However, there is substantial deviation at low velocities for the ^2D state formed in the B^{4+}, He collision and the ^2P state formed in the C^{5+}, He collision. In the latter case, Hansen and Taulbjerg predict a population distribution favoring $M_L = 1$ near $v = 0.2$ au. This is directly opposite to the measured results.

†Department of Physics, University of Western Ontario, London, Ontario, Canada.
‡V-Division, Lawrence Livermore National Laboratory.
||Department of Chemistry, University of Toronto, Canada.
¶Department of Physics, U. Lund, Lund, Sweden.

1. W. Fritsch and C.D. Lin, Phys. Rev. A 45, 4611 (1992).
2. J.P. Hansen and K. Taulbjerg, Phys. Rev. A 47, 2987 (1993).

2. Quasimolecular X-ray Spectrum from 117-keV Ne^{9+} + Ne Collisions (Publication 2)

M.H. Prior, R. Doerner,† H. Berg,† H. Schmidt-Boecking,‡ J.O.K. Pedersen,‡ and C.L. Cocke‡

It is well established theoretically and experimentally that the 1sσ-quasimolecular x-ray (QMOX) emission spectra from swift H-like ion–atom collisions show, at fixed impact parameters, a characteristic interference structure. This oscillating variation of intensity with photon energy can yield information on the level spacing of states in the transient quasimolecular collision system. The interference follows from a coherent superposition of nondistinguishable amplitudes for transitions on the incoming half (at collision time $-t_0$) and outgoing half ($+t_0$) of the collision trajectory for the same transition energy. Note that to observe interference in the x-ray spectrum, a unique (or narrow) range of impact parameters must be selected. This is accomplished by measuring the x-ray spectrum in coincidence with particles scattered by a chosen angle (or narrow range of angles). In addition, the velocity of the H-like ion must be small enough so that the phase differences ($\Delta\phi$) between the interfering amplitudes can exceed π (constructive) or 2π (destructive interference).

Interference structure was observed at other laboratories in the 1sσ-QMOX emission spectra from collisions of S^{15+} and Cl^{16+} on Ar and for Ge^{31+} on Kr. In these works, the swift H-like ions were produced by the "accel-stripping-decel" technique. At present, this method cannot be applied to much heavier (e.g., Pb^{81+}) or much lighter (e.g., Ne^{9+}) ions. Recent improvements in the electron cyclotron resonance (ECR) ion sources, however, make possible similar studies with beams of, for example, Ne^{9+} or Si^{13+}.

We observed the 1sσ-QMOX emission from a 117-keV Ne^{9+} collision with Ne using a photon-particle coincidence technique. The Ne^{9+} ions were produced by the LBL ECR ion source at the 88-Inch Cyclotron and transported to the apparatus using the joint LLNL/LBL atomic physics beamline facilities. Projectiles scattered within the range of 17°–26° by a Ne gas-jet target struck a position-sensitive detector (PSD). The jet target region was viewed by a SiLi detector placed at 90° to the beam-jet plane. The x-ray signals from the SiLi detector provided start pulses for a time-to-amplitude (TAC) converter, which was stopped by fast pulses from the particle PSD. A data acquisition computer with mass storage collected and recorded each event (x-ray energy, TAC output, and particle position).

Figure 2-1 is a plot of the x-ray energy versus the projectile time-of-flight for a portion of the data collected. The preponderance of counts uncorrelated with projectile flight time are accidental coincidences caused by the large flux of Ne K x-ray photons that follow from electron capture collisions. The rectangular area in the figure, outlining higher x-ray energies, contains the real QMOX events. The data in this figure are for all particle-scattering angles included by the masked PSD.

A total of 1.56×10^7 events were collected, 4,771 of which fell inside the QMOX box in the x-ray versus time-of-flight two-dimensional spectrum (e.g., Figure 2-1). Figure 2-2 presents the QMOX energy spectrum integrated over all particle scattering angles. The solid line is a computed spectrum that includes the averaging effect of the finite (≈200 eV) x-ray detector resolution. The amplitude of the computed spectrum has been adjusted to approximate the data.

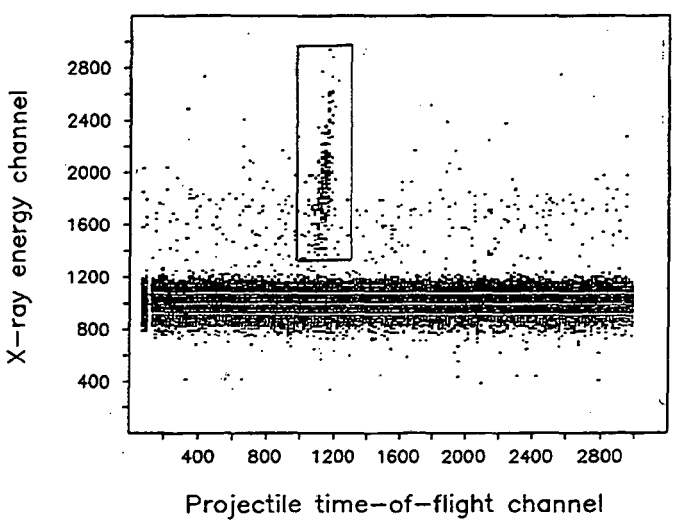

Figure 2-1. Scatter plot of the x-ray energy versus projectile flight time. The QMOX events are those inside the box. (XBL 947-4194)

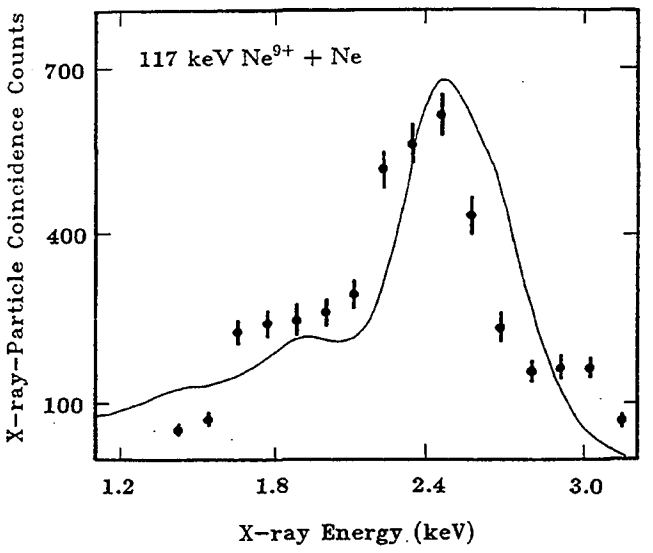

Figure 2-2. The QMOX spectrum summed over the angular range of the projectile detector. The curve is a calculated shape, averaged over the angular range and the SiLi detector resolution (see text). (XBL 947-4195).

The spectral shape has been calculated following the uniform asymptotic approximation approach, as presented by Schuch, *et al.*,[3] utilizing results of calculations of the energy separation of the $2p\pi$ and $1s\sigma$ levels versus internuclear separation by U. Wille[4] and a straight-line trajectory. The solid curve in Figure 2-2 is the sum of calculations at three angles spanning the projectile detector that have been averaged over the SiLi detector resolution of 200 eV. The computed spectral shape agrees substantially with the observed one, predicting an interference structure that is essentially washed out by the x-ray detector resolution. Some indication of oscillatory structure appears on the low energy side of the QMOX peak and is in reasonable agreement in magnitude and location with the averaged calculated spectrum. Although the experiment contains information on the impact parameter dependence of the QMOX spectrum (i.e., the dependence on scattering angle) when smoothed by the detector resolution, the structure is substantially reduced, certainly below the statistical uncertainty in our angle-sorted spectra. Substantially improved x-ray detector resolution and/or higher projectile velocities would provide more clearly resolved interference structure. Nonetheless, this work demonstrates that beams from modern ECR ion sources will be useful in future studies of the quasimolecular-level structure and collision dynamics in these peculiar transient systems.

†Institut für Kernphysik, U. Frankfurt, Germany.
‡Department of Physics, Kansas State University, Manhatten, KS.

3. R. Schnch *et al.*, Phys. Rev. A 37, 3313 (1988).
4. U. Wille (private communication).

3. Work in Progress: Impact Parameter Dependence of Substate Complex Amplitudes Populated in Double-Electron-Capture Collisions

H. Khemliche,† M.H. Prior, and D. Schneider‡

We are extending our study (Publication 1) of the anisotropy of Auger electron emission following double-electron capture to determine not only the magnitudes of the complex amplitudes of the doubly excited $|LM_L\rangle$ sublevels, but their relative phases and the dependence of both on the scattering angle of the projectile. The scattering angle can be related to details of the collision trajectory (impact parameter or distance of closest approach) via an appropriate calculation or model. At this fine detail, theoretical calculations are addressed at their core; that is, unmeasured quantities or quantum numbers need not be averaged or summed to make comparisons with the results of these measurments. The technique measures the electron spectrum emitted into a known small solid angle with respect to the projectile beam in coincidence with the position of arrival (differential scattering angle) of the projectile product. From this we reconstruct the electron anisotropy with respect to the beam direction and the scattering plane.

We are concentrating on the C^{5+},He system at 25 keV and have completed a preliminary analysis of the $1s2s2p\ ^2P$ state formed in C^{3+} by the double-capture process. For a P state, there are only two independent parameters, since the amplitudes are aligned (i.e., $a_{M_L} = a_{-M_L}$), and hence, $2|a_1|^2 + |a_0|^2 = 1$. Thus, one may choose, say, $|a_0|$ and the relative phase, $\arg(a_0^* a_1)$. Our preliminary results show that, at this energy, $|a_0|$ and $|a_1|$ are nearly equal over most of the scattering angle range (for small scattering $|a_0|$ approaches unity, as it must). This is in agreement with our earlier measurements of the impact-parameter-averaged alignment (Publication 1). However, the relative phase varies substantially over the scattering angle range. Analysis of the $1s2p^2\ ^2D$ state is more complex, as here

there are four independent parameters, two magnitudes and two relative phases. To extract these, more data must be collected at appropriate orientations of the electron spectrometer with respect to the projectile beam chosen specifically to address the ^2D level.

†Graduate student, U. Pierre et Marie Curie, Paris, France.
‡V-Division, Lawrence Livermore National Laboratory.

4. Work in Progress: Multiply Charged Fullerenes

J. Jian, M.H. Prior, and H. Khemliche†

We have initiated a study aimed at determining the lifetime of C_{60}^{q+} and C_{70}^{q+} ions with $q = 1 - 6$. Production of these ions is detected by time-of-flight and rf quadrupole analysis, following impact by ion beams (e.g., Ar^{Q+}, $Q = 2 - 12$) at impact energies of 10 keV/Q, and electrons with energies up to ≈200 eV, on a thermal beam of C_{60} and C_{70} molecules. The time-of-flight analyzer used with ion-beam production measures the arrival time of positively charged products following detection of an electron or XUV photon from the collision. We observe C_{60} ions up to $q = 6$ using ions with high Q (e.g., $Q = 8 - 12$), and, interestingly, we also observe fullerene ions with $q > Q$ for low Q (e.g., $Q =$ 2,3). This is not expected if simple charge capture onto the projectile (with minimal excitation of the fullerene) were the production mechanism. To measure lifetimes, the positively charged collision products are held in an ion trap for periods of up to several seconds. Decay of the trapped population is monitored by emptying the trap into an rf quadrupole or time-of-flight analyzer at a selected time following the pulsed production beam (electron or ion).

†Graduate student, U. Pierre et Marie Curie, Paris, France.

1993 PUBLICATIONS AND REPORTS

Refereed Journals

1. M.H. Prior, R.A. Holt, D. Schneider, K.L. Randall, and R. Hutton, "Alignment of Magnetic Substates in Double-Electron-Capture Collisions," Phys. Rev. A **48**, 1964 (1993).
2. M.H. Prior, R. Doerner, H. Berg, H. Schmidt–Boecking, J.O.K. Pedersen, and C.L. Cocke, "Quasimolecular X-ray Spectrum from 117-keV Ne^{9+} + Ne Collisions," Phys. Rev. A **47**, 2964 (1993).

Other Publications

3. D. Cordes, R. Bruch, H. Wang, D. Schneider, L.A. Vainshtein, T. Brage, D. Ridder, and M. Prior, "Autoionization of Multiply-Charged Si, Ar, Sc, Ti, Fe and Cu Ions: The Sodium Isoelectronic Sequence," Bull. Am. Phys. Soc. **38**(3), 1128 (1993).
4. H. Khemliche, M.H. Prior, V.L. Plano, R.R. Haar, J.A. Tanis, P.A. Zavodszky, L. Sarkadi, J. Palinkas, and D. Berenyi, "Low-Energy Electrons from Multiple-Electron Transfer to Slow O^{8+} Ions," Bull. Am. Phys. Soc. **38**(3), 1160 (1993).

PROCESSES AND TECHNIQUES

CHEMICAL ENERGY

High-Energy Oxidizers and Delocalized-Electron Solids*

Neil Bartlett, Investigator

INTRODUCTION

The main aim of this program is the synthesis and characterization of new materials that may have utility in efficient storage or usage of energy. The novel materials include two-dimensional networks of light π-bonding atoms (boron, carbon, and nitrogen) with structures akin to graphite. Of these, the more metallic ones have possible applications as electrode materials for high-energy-density batteries and those that are semiconducting could be useful in converting light to electrical energy. Good ionic conductors are also being sought, with emphasis on lithium-ion and fluoride-ion conductors, since batteries based on lithium and fluorine would be unsurpassed in their energy density features. In addition, novel oxidation-state fluorides are being synthesized and structurally characterized to provide a comprehensive basis for better theoretical models, from which an improved capability to predict physical and chemical behavior ought to be forthcoming. Previously unknown or little-studied high-oxidation-state species constitute a large part of this effort. Such species are also investigated for their efficiency and specificity as chemical reagents.

1. Synthesis and Some Oxidizing Properties of Novel Thermodynamically Unstable Nickel Fluorides (Publication 2)

L. Chacón, J. Allman, B. Žemva, C. Shen, J. Münzenberg, and N. Bartlett

It has long been conjectured that the anodic oxidation of hydrocarbons and other molecules in anhydrous hydrogen fluoride (AHF) at a nickel anode (Simons Process) could be occurring via a higher fluoride of nickel than NiF_2. Although earlier work by others had attempted to identify such a material, no convincing evidence for a higher nickel fluoride of known composition and structure had been obtained. The fluorides described here are the first clear examples of higher nickel fluorides than NiF_2. They are thermodynamically unstable and are powerful oxidizers and fluorinators. Nickel tetrafluoride precipitated with BF_3 as a yellow-brown solid from a solution of K_2NiF_6 in AHF,

$$K_2NiF_6 + 2BF_3 \rightarrow 2KBF_4 + NiF_4 \ ,$$

has been shown to be stable in the presence of that solvent at temperatures below –45 °C, but to lose fluorine above that temperature. If the tetrafluoride is dried by removal of AHF at –45 °C or below, it does not begin to liberate elemental fluorine until ~0 °C.

Decomposition of NiF_4 in AHF at 0 °C yields black rhombohedral NiF_3, which is insoluble in AHF, the KBF_4 salt associated with the NiF_4 synthesis being removed by washing with AHF at that temperature:

$$NiF_4 \xrightarrow[AHF]{0°C} R\text{-}NiF_3 + 1/2\ F_2 \ .$$

If the interaction of BF_3 with K_2NiF_6 in AHF is carried out at room temperature, with slow addition of the BF_3, the evolution of fluorine occurs to produce NiF_3 directly, but this material is of the hexagonal tungsten–bronze structure, i.e., H-NiF_3 (see Publication 3 for the structure types). Again, in bulk, the solid appears to be black, but it shows a deep red reflectance in strong light. This H-NiF_3 is also the major phase (it is accompanied by R-NiF_3) when NiF_3 is precipitated from AHF by mixing solutions of K_2NiF_6 and $Ni(AsF_6)_2$ at ~25 °C:

$$Ni(AsF_6)_2 + K_2NiF_6 \xrightarrow[AHF]{25°C} 2NiF_3 + 2KAsF_6 \ .$$

This last synthetic route is a convenient one for the production of large quantities of NiF_3. The pyrochlore form (see Publication 3) of the trifluoride, P-NiF_3, is generated when the dry tetrafluoride is rapidly heated from <0 °C to 40 °C. As so obtained, it is a deep brown solid.

All three forms of NiF_3 lose fluorine on heating. The R- and H-NiF_3 each initially produce a red solid and finally the difluoride (yellow green). The close-packed R-NiF_3 shows least kinetic stability (with decomposition beginning at 40 °C), and acetonitrile burns in contact with it at –60 °C or above. The more open–structure materials H-NiF_3, (decomposes above 76 °C) and P-NiF_3 interact much less

*This work was supported by the Director, Office of Energy Research, Office of Basic Energy Sciences, Chemical Sciences Division, of the U.S. Department of Energy under Contract No. DE-AC03-76SF00098.

violently but are also reduced in their interaction with acetonitrile to NiF_2.

The oxidizing power of the three forms of NiF_3 is indicated by their interaction with xenon (Xe). All three oxidize Xe (present in excess of that required to form NiF_2) to XeF_2 at 25 °C in contact with liquid AHF:

$$Xe + 2NiF_3 \xrightarrow[AHF]{25°C} NiF_2 + XeF_2 \quad .$$

Dry R-NiF_3, in a Pyrex glass container, will also oxidize Xe to XeF_2 at 25 °C, but several days are required for complete reduction of the R-NiF_3 to NiF_2. This reaction proceeds in the dark, unlike that between F_2 and Xe, which requires light (to produce F atoms). Thus R-NiF_3 is a more effective fluorinator than F_2. An intermediate red solid, possibly Ni_2F_5, is first formed in the R-NiF_3/Xe reaction, and such a red intermediate is also seen in the AHF-promoted reactions with all three forms of NiF_3. The dry forms of H-NiF_3 and P-NiF_3 interact much more slowly with xenon, although some XeF_2 is observed after several days in the H-NiF_3 case. R-NiF_3 with liquid AHF also oxidizes XeF_2 to XeF_4:

$$XeF_2 + 2R\text{-}NiF_3 \xrightarrow[AHF]{0°C} XeF_4 + 2NiF_2 \quad .$$

The interaction of solid H-NiF_3 with solid LiCl to form chlorine (and possibly chlorine fluoride, ClF) occurs with great violence when the dry solids are mixed. In contact with liquid AHF at –35 °C, the reaction is moderated but is quickly completed:

$$LiCl + NiF_3 \rightarrow LiF + NiF_2 + 1/2\ Cl_2 \quad .$$

This interaction with H-NiF_3 does not produce Li_xNiF_3 even though the large tunnel running through the H-NiF_3 structure (parallel to c_0) could accommodate cations up to the size of K^+.

As a test of the fluorinating capability of the R-NiF_3 toward unsaturated carbon compounds, the solid, in Pyrex glass apparatus, was exposed to perfluoropropene vapor and the progress of the reaction was monitored by IR spectroscopy. The black R-NiF_3 rapidly became red brown (showing an NiF_2 diffraction pattern) and the perfluoropropene was quickly (within an hour at 25 °C) converted to perfluoropropane. Traces of CF_4 indicate a small amount of C–C bond cleavage:

$$2R\text{-}NiF_3 + C_3F_6 \rightarrow 2NiF_2 + 6C_3F_8 \quad .$$

Without precise structural data (such data are being sought) one cannot rule out the possibility that the NiF_3 solids could be the mixed-valence materials Ni(II)Ni(IV)F_6. The blackness of R-NiF_3 is in harmony with this, but the magnetic data for the microcrystalline solid do not discriminate between Ni(III) and Ni(II), (IV). The interaction of both R- and H-NiF_3 with KF in AHF to produce NiF_2 and K_2NiF_6,

$$2NiF_3 + 2KF \rightarrow NiF_2 + K_2NiF_6 \quad ,$$

shows, however, that if it is Ni(III), it is at least close to disproportionation to Ni(II) and Ni(IV). Formulation of the NiF_3 as Ni(II)Ni(IV)F_6 also is in accord with the high oxidizing power of NiF_3 in acid AHF.

Although R-NiF_3 and H-NiF_3 will not oxidize the anion RuF_6^- to RuF_6 in neutral AHF, they do so when the AHF is acidified with the strong fluoride-ion acceptor AsF_5:

$$RuF_6^- + NiF_3 + 3AsF_5 \rightarrow Ni^{2+}_{(solv)} + 3AsF_6^- + RuF_6 \quad .$$

Earlier work in these laboratories had shown that Ni(IV) was able to oxidize RuF_6^- to RuF_6, and this may be the oxidizing species here also. Since the RuF_6 product of this reaction is identified by its ability to oxidize oxygen,

$$O_2 + RuF_6(g) \rightarrow O_2^+\ RuF_6^-(c) \quad ,$$

it is clear that NiF_3 in AHF acidified with AsF_5 must also be able to oxidize O_2 to O_2^+.

2. The Structural Forms of the Thermodynamically Unstable Trifluoride of Nickel (Publication 3)

L. Chacón, J. Allman, C. Shen, B. Žemva, and N. Bartlett

Rhombohedral (R), hexagonal tungsten–bronze (H), and pyrochlore (P) forms of the commonly occurring trifluorides of the first transition series are known. The novel fluoride, nickel trifluoride, has been shown to adopt each of these structure types. A synthesis for each form is given in Publication 2. Their structural relationships and the possible reasons for the formation of each are the concern of this paper.

The x-ray powder diffraction data for each of the three forms are set out in Tables 2-1, 2-2, and 2-3, and their structures are illustrated in Figures 2-1, 2-2, and 2-3. In each structure, the Ni atom is at the center of an octahedron of six F ligands. In accord with the NiF_3 stoichiometry, each apex of the NiF_6 octahedron is shared with one other octahedron. The figures illustrate the way in which this apex sharing occurs in each structure type. In the R-NiF_3 (Figure 2-1), each octahedron is close-packed with its neighbors and the atomic arrangement is almost exactly one in which the F ligands are in hexagonal close-packed array, with the metal atoms (Ni) occupying one-third of the octahedral holes in ordered fashion. The formula-unit volume of 43.8 $Å^3$ is the smallest of any trifluoride of the first transition series—an observation in accord with the high oxidizing power of NiF_3, which must reflect a high

Table 2-1. X-ray Powder Data (Cu Kα Radiation, Ni Filter) for the NiF_3 Rhombohedral Unit Cell ($a_0 = 5.17$ Å, $\alpha = 55.7°$).

	$1/d^2 \times 10^4$		
I/I_0	Observed	Calculated	$h\,k\,l$
vs (br)	804	809	1 1 0
ms	1,514	1,515	$\bar{2}$ 1 1
m	1,723	1,719	$\bar{1}$ 1 0
s	2,248	2,249	2 0 1*
mw	2,536	2,528	2 0 0
m	3,237	3,234	2 2 0
s	3,836	3,838	3 2 $\bar{1}$
		4,247	2 1 $\bar{1}$
w (br)	4,281		
		4,340	3 3 2
w	4,963	4,954	3 $\bar{1}$ $\bar{0}$
w	5,162	5,158	2 1 $\bar{1}$
vw	6,053	6,059	4 2 2
vw	6,488	6,487	4 3 $\bar{2}$
vvw	6,867	6,878	2 0 $\bar{1}$
vw	7,394	7,407	3 1 $\bar{1}$
vvw	7,699	7,686	3 0 $\bar{1}$
vw	8,477	8,475	4 4 4
vvw	9,001	8,996	4 2 $\bar{0}$
vvw	9,431	9,405	2 2 $\bar{1}$
vvw	9,967	9,897	5 3 2

Note: br = broad.

Table 2-2. X-ray Powder Data (Cu Kα Radiation, Ni Filter) for the NiF_3 Hexagonal Unit Cell ($a_0 = 7.11$, $c_0 = 7.20$ Å).

	$1/d^2 \times 10^4$		
I/I_0	Observed	Calculated	$h\,k\,l$
s	264	264	1 0 0
s	772	773	0 0 2
w	807	793	1 1 0
		1,038	1 0 2
vs (br)	1,052		
		1,058	2 0 0
m+	1,566	1,566	1 1 2
m–	1,840	1,851	2 1 0
		2,004	1 0 3
m (br)	2,019		
		2,044	2 1 1
w	2,390	2,380	3 0 0
ms	3,096	3,093	0 0 4
ms	3,179	3,174	2 2 0
		3,357	1 0 4
w–	3,362		
		3,367	2 2 1
vvw	3,468	3,438	3 1 0
m (br)	3,943	3,947	2 2 2
ms	4,151	4,151	2 0 4
w (v br)	5,000	5,005	4 0 2
vwd	5,469	5,474	3 0 4
vwd	5,773	5,798	3 2 2
w (v br)	6,264	6,267	2 2 4
vvw	6,695	6,684	2 1 5

Note: br = broad.

effective positive charge at the nickel atom. This fluoride, to be formed free of H-NiF_3, must be generated slowly from NiF_4 in AHF at 0 °C.

The H-NiF_3 structure is much less close-packed than R-NiF_3, the formula-unit volume being 52.3 Å^3. This is a consequence of open channels of approximate diameter 2.6 Å, which run through the structure, parallel with c_0. These channels arise as a consequence of the particular way in which the octahedra are clustered. In the R-NiF_3 the apex sharing of the octahedra gives rise to eight membered rings of alternating Ni and F atoms (four of each). In H-NiF_3 the eight-membered Ni_4F_4 rings have disappeared and the octahedra are now linked through tighter six-membered Ni_3F_3, rings, of alternating Ni and F atoms. This squeezing together of the octahedra provides for the formation of the 2.6-Å-diameter channels already referred to. As may be seen from Figure 2-2, these channels (labeled A) are defined by rings of six octahedral edges, each octahedron linked *cis* to its two neighbors. Such rings are superimposed exactly one on top of the other. Each NiF_6 octahedron in the H-NiF_3 structure has two opposite edges, located nearly in the xy plane, each of which is a component of a six-edge 2.6-Å-diameter ring. The apical F atoms of each octahedron, however, are shared each with an octahedron above or below, along z. These dispositions generate the hexagonal channels running along z.

The formation of the low-density H-NiF_3 structure is probably a consequence of the particular way in which the NiF_4 precursor decomposes. The structure of NiF_4 is still unknown, but like other transition element tetrafluorides from the right-hand side of the transition series, the coordination about the Ni atom is probably six, two F ligands being unshared. In the elimination of fluorine from NiF_4 to generate NiF_3, there must therefore also be a condensation of the octahedra as well as F-atom or F_2 release. Certainly the hexagonal cavities are large enough to accommodate the F atom, or F_2, or even F^-, and such

Table 2-3. X-ray Powder Data (Cu Kα Radiation, Ni Filter) for the Pyrochlore NiF_3 Cubic Unit Cell.

	$1/d^2 \times 10^4$		
I/I_0	Observed	Calculated	$h\,k\,l$
vs (br)	302	302	1 1 1
s (br)	1,103	1,108	3 1 1
s (br)	1,207	1,208	2 2 2
m (br)	2,709	2,718	3 3 3 5 1 1
m (br)	3,222	3,222	4 4 0
m (br)	3,524	3,524	5 3 1
vw (br)	4,436	4,430	6 2 2
vw	5,136	5,135	7 1 1 5 5 1
vw	5,973	5,940	7 3 1 5 5 3

Note: br = broad.

may be their origin. It is of interest that H-NiF_3 has a specific conductivity suggestive of an ionic conductor. There could be some F^- in the channels, although the analytical data indicate that the stoichiometry of the nickel fluoride is close to that of NiF_3.

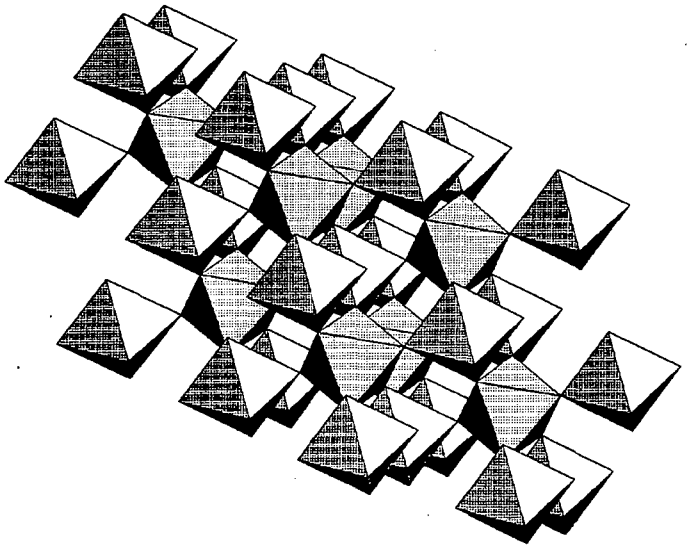

Figure 2-1. Connectivity of NiF_6 octahedra in R-NiF_3. (XBL 947-4176)

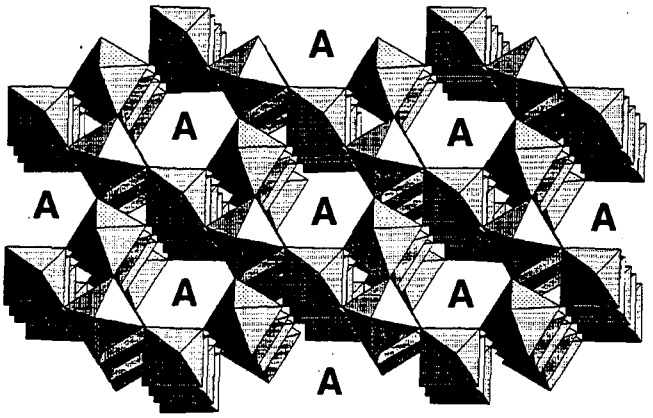

Figure 2-2. Connectivity of NiF_6 octahedra in H-NiF_3. (XBL 947-4177)

As seen in Figure 2-3, the most rapidly formed nickel trifluoride, P-NiF_3 (by decomposition of NiF_4 at 40 °C), is the most open. Again we see the octahedra squeezed together, with formation of Ni_3F_3 six-membered rings, but here this process results in tetrahedral clusters of the octahedra, with even more large-channel space made available than in the case of H-NiF_3. The fast release of fluorine, from the precursor NiF_4, generates the cubic open pyrochlore structure. Here the type of channel seen in the hexagonal structure now runs along each threefold axis of the cubic structure. The formula-unit volume of P-NiF_3 (61.8 $Å^3$) is larger than that of R-NiF_3 (43.8 $Å^3$) by effectively the size of an F ligand—indeed, the formula-unit volume is that to be expected for a close-packed tetrafluoride!

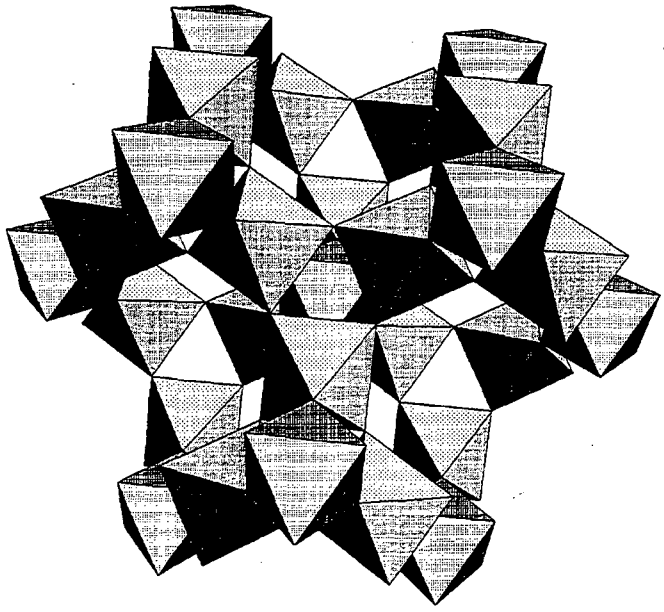

Figure 2-3. Connectivity of NiF_6 octahedra in P-NiF_3. (XBL 947-4178)

3. The Fluorine-Bridged Species $W_2O_2F_9^-$

C. Shen, R. Hagiwara, and N. Bartlett

The fluorine-bridged symmetrical anion $W_2O_2F_9^-$ has been structurally defined and the parent fluoride ion acceptor WOF_4 shown to be only a moderate fluoroacid in anhydrous hydrogen fluoride (AHF), the WOF_5^- species being readily solvolyzed by that solvent to yield $W_2O_2F_9^-$.

Few fluoro-anions are sufficiently stable with respect to electron loss, or F^- loss, to the cation, to be able to stabilize either Ag^{2+} or the chain polymer cation $(AgF)_n^{n+}$. The pseudo-octahedral WOF_5^- is not oxidized by Ag(II), but attempts to prepare $AgF^+WOF_5^-$ in AHF invariably produce $AgF^+W_2O_2F_9^-$, the temperature-independent paramagnetism of which in the temperature range of 50–300 K shows that it is a salt of the polymeric cation $(AgF)_n^{n+}$. Crystals of the salt suitable for structural analysis have not been obtained, but crystals of the Ag(I) salt, $AgW_2O_2F_9$, have been and the structural details derived. The $W_2O_2F_9^-$ occupies two different crystallographic sites, but the two geometries are essentially the same and are represented in Figure 3-1.

In addition to its oxidative stability, the $W_2O_2F_9^-$ anion is of interest for its W–F–W bridge. Fluorine bridging evidently provides better overall bond energy than would be the case if tungsten-to-oxygen multiple bonding were sacrificed. Multiple bonds to oxygen and nitrogen are particularly favorable in high-oxidation-state tungsten, rhenium, and osmium compounds, and the bonding preference seen in $W_2O_2F_9^-$ is evidently another instance of this.

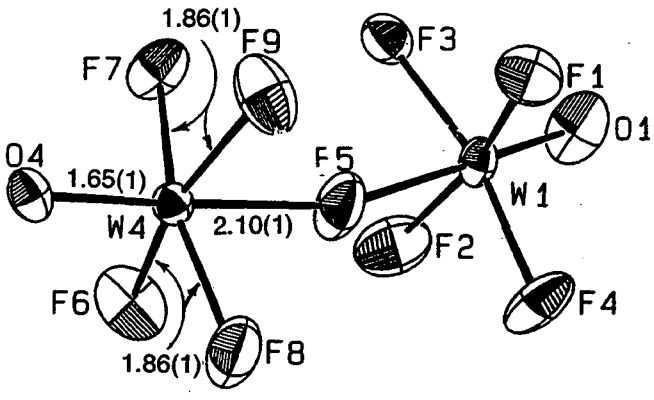

Figure 3-1. The structure of $W_2O_2F_9^-$. (XBL 974-7179)

4. Work in Progress

Investigation of the remarkable oxidizing properties of Ag(II) and Ag(III) in AHF continues to be a major research interest, and with the recent demonstration in these laboratories of the disproportionation of Ag(II) to Ag(I) and Ag(III) at certain acidities, in AHF, an attempt was made to prepare the salt isomer of AgF_2, i.e., $Ag^+AgF_4^-$. The salt $Ag^+AuF_4^-$ has long been known, and AgF_4^- is similar in size and shape to AuF_4^-. When the salts $KAgF_4$ and $AgBF_4$ are mixed in AHF between –30 and –60 °C, a red brown solid is formed along with KBF_4. This solid, suspended in AHF, as the temperature approaches 0 °C, converts exothermally to light brown AgF_2 (which is ferromagnetic). If the solid is washed free of KBF_4 with AHF below –30 °C, the extent of this conversion can be kept small. SQUID magnetometer measurements on samples made in this way reveal only a minor component of AgF_2 (which is also revealed by x-ray powder photography). These data indicate that $Ag^+AgF_4^-$ is diamagnetic, as expected. Material prepared in this way is not sufficiently crystalline to give an x-ray powder pattern.

The solvolysis in AHF of K_3CuF_6, prepared as described by others, appears to yield the trifluoride of copper below –40 °C. The red solid formed at such temperatures decomposes to CuF_2 and F_2 when warmed above –40 °C. The red solid, treated with xenon gas (in large excess) at –78 °C, is rapidly reduced to CuF_2, and the yield of xenon difluoride recovered, based on the known quantity of K_3CuF_6 precursor, amounts to 58% of that expected for the reaction

$$2CuF_3 + Xe \rightarrow 2CuF_2 + XeF_2 \ .$$

The temperature at which the conjectured CuF_3 decomposes in the absence of AHF is not yet known.

1993 PUBLICATIONS AND REPORTS

Refereed Journals

1. F. Okino and N. Bartlett, "Hexafluoroarsenates of Graphite from Its Interaction with AsF_5, $AsF_5 + F_2$, and O_2AsF_6, and the Structure of $C_{14}AsF_6$," J. Chem. Soc. Dalton Trans. **14**, 2081 (1993).

LBL Reports

2. L. Chacón, J. Allman, B. Žemva, C. Shen, J. Münzenberg, and N. Bartlett, "The Synthesis and Some Oxidizing Properties of Novel Thermodynamically Unstable Nickel Fluorides, NiF_4, R-NiF_6, H-NiF_3, and P-NiF_3," LBL-35159.
3. L. Chacón, J. Allman, C. Shen, B. Žemva, and N. Bartlett, "Three Structural Forms of the Novel Thermodynamically Unstable Trifluoride of Nickel," LBL-35160.
4. C. Shen, R. Hagiwara, and N. Bartlett, "The Fluorine-Bridged Species $W_2O_2F_9^-$," LBL-35161.
5. W.J. Casteel, Jr., "The Synthesis and Structural Characterization of Novel Transition Metal Fluorides," LBL-32892; UC-401.
6. C. Shen, "Preparation and Characterization of Novel Graphite-Like Materials and Some High-Oxidation-State Fluorine Chemistry," LBL-35162.

Invited Talks

7. N. Bartlett, "Some Advances in High-Oxidation-State Fluorine Chemistry of the Past Forty Years," Bonner Chemiepreis Lecture, Bonn, Germany, October 19, 1992.
8. N. Bartlett, "Concerning the Stabilization of High Oxidation States and Relevant Synthetic Strategies to Attain Them," American Chemical Society Eleventh Winter Fluorine Conference, January 25, 1993.
9. N. Bartlett, "Synthesis of Thermodynamically Unstable and Powerfully Oxidizing Fluorides," ACS Symposium, New Directions in Solid-State Synthesis, Denver, CO, March 29, 1993.
10. N. Bartlett, "A Chemistry in Which Oxygen Acts as a Reducing Agent," Simon Fraser University, June 4, 1993.
11. N. Bartlett, "The Greenhouse Gas CO_2 and Our Energy Future," Convocation Address, Simon Fraser University, June 4, 1993.

Catalytic Conversion of C_1 Compounds*

Alexis T. Bell, Investigator

INTRODUCTION

The purpose of this program is to develop an understanding of the fundamental processes involved in the catalytic conversion of C_1 compounds, such as CO, CO_2, and CH_4, to fuels and chemicals. Attention is focused on defining the factors that limit catalyst activity, selectivity, and resistance to poisoning and on the relationship between catalyst composition or structure and performance. To meet these objectives, a variety of surface diagnostic techniques are used to characterize supported and unsupported catalysts before, during, and after reaction. The information thus obtained is combined with detailed studies of reaction kinetics to elucidate reaction mechanisms and the influence of modifications in catalyst composition and structure on the elementary reactions involved.

1. Infrared Studies of the Mechanism of Methanol Decomposition on Cu/SiO_2 (Publication 9)

D.B. Clarke, D.-K. Lee, M.J. Sandoval, and A.T. Bell

The mechanism of methanol decomposition on silica-supported Cu has been investigated by means of infrared spectroscopy and temperature-programmed desorption spectroscopy. Infrared spectra taken during both isothermal and temperature-programmed experiments reveal the following species: methanol, methoxy groups, formaldehyde, methylenebis(oxy) groups, and format groups. The only products observed during temperature-programmed decomposition are methanol, formaldehyde, carbon dioxide, and hydrogen. Based on the sequence in which adsorbed species appear and disappear and on the correlation of these species with the appearance of products in the gas phase, a comprehensive mechanism has been deduced for the decomposition of methanol. Simulations based on the proposed decomposition scheme provide an accurate representation of the observed variations in the concentrations of adsorbed species. Activation energies for the elementary processes involved in the decomposition of methanol are also obtained from the simulation.

*This work was supported by the Director, Office of Energy Research, Office of Basic Energy Sciences, Chemical Sciences Division, of the U.S. Department of Energy under Contract No. DE-AC03-76SF00098.

2. Estimates of Rate Coefficients for Elementary Processes Occurring during Fischer–Tropsch Synthesis Over Ru/TiO_2 (Publication 5)

T. Komaya and A.T. Bell

The dynamics of elementary processes involved in Fischer–Tropsch synthesis of hydrocarbons over Ru/TiO_2 have been determined from an analysis of data for both steady-state and transient-response experiments. Both types of experiments were carried out with different catalyst-bed residence times to assess the effects of olefin readsorption on the dynamics of chain initiation, propagation, and termination. Strong evidence was found for the rapid re-entry of ethylene into the chain growth process. The re-entry of C_{3+} olefins, however, is negligible for the conditions studied. The holdup of hydrocarbons in a weakly adsorbed state was found to be insignificant for C_{6+} products and must be accounted for in the simulation of transient-response experiments. When the effects of ethylene readsorption and C_{6+} holdup are properly taken into account, the rate coefficients for chain initiation, propagation, and termination, determined from simulations of the transient-response experiments, are independent of carbon number and catalyst-bed residence time. Rate coefficients for the readsorption of ethylene, the depolymerization of adsorbed ethyl groups, and the dehydrogenation of methyl to methylene groups were also determined from simulations of the transient-response experiments.

3. The Influence of Metal–Support Interactions on the Accurate Determination of Ru Dispersion for Ru/TiO_2 Catalysts (Publication 10)

T. Komaya, A.T. Bell, Z. Weng-Sieh, R. Gronsky, F. Engelke, T.S. King, and M. Pruski

Quantitative measurements have been made of the partial coverage of the surface of Ru particles supported on TiO_2 by amorphous titania. The average particle size was determined from high-resolution electron micrographs of Ru/TiO_2 catalysts, and the amount of atomic hydrogen adsorbed on the portions of the Ru particles not covered by amorphous titania was determined by H NMR. After reduction at 573 K, about 50% of the surface of the Ru particles (average diameter, 15 Å) was found to be covered by a thin layer (about 7–8 Å thick) of amorphous titania. Reduction at 773 K resulted in an increase in the fraction of the Ru particles' surface covered by titania to 85%. When Na is present, it reacts with the titania support to form a sodium titanate. Since sodium titanate has a much lower Tamman temperature than titania, the migration of titania

onto the surface of the Ru particles occurs at a lower temperature. Thus, 80% of the surface of titania is covered by an amorphous sodium titanate when the catalyst is reduced at 573 K.

4. Raman Studies of the Structure of Nb_2O_5/TiO_2 (Publication 5)

R.M. Pittman and A.T. Bell

The structure of titania-supported niobia has been investigated by means of Raman spectroscopy. Well-dispersed monomeric and oligomeric species are observed at low Nb loadings corresponding to 0.13 of a theoretical Nb_2O_5 monolayer, whereas amorphous islands of Nb_2O_5 are the dominant species at Nb loadings corresponding to >0.5 of a theoretical Nb_2O_5 monolayer. Water vapor coordinates reversibly with Nb=O groups at the surface of the dispersed niobia through the formation of Lewis acid–base adducts. The Nb–O–Nb bonds in the oligomeric species appear to undergo hydrolysis upon water exposure unlike the Nb–O–Nb bonds in the amorphous Nb_2O_5 islands, most of which are in the bulk of the oxide and, hence, are less accessible to interaction with water. Calcination between 500 and 700 °C does not affect the structure of the supported Nb_2O_5, although some of the amorphous Nb_2O_5 is transformed into $TiNb_2O_7$. It is proposed that the amorphous Nb_2O_5 is stabilized on the surface of TiO_2 by the formation of Ti–O–Nb linkages. The dispersed Nb_2O_5 is found to stabilize the transformation of the TiO_2 support from anatase to rutile and the coincident loss in surface area of the support. Further calcination to 800 °C and 950 °C results in the formation of $TiNb_2O_7$.

5. Raman Investigations of NH_3 Adsorption on TiO_2, Nb_2O_5, and Nb_2O_5/TiO_2 (Publication 7)

R.M. Pittman and A.T. Bell

A study has been carried out on the interaction of NH_3 with TiO_2, Nb_2O_5, and Nb_2O_5/TiO_2. Raman spectroscopy was used to characterize the structure of the adsorbed NH_3 and the perturbations of species present at the surface of the adsorbent. On each oxide, NH_3 adsorbs predominantly at Lewis acid sites. Hydrogen bonding occurs between the adsorbed NH_3 and OH groups present on the surface of TiO_2. A small concentration of NH_4^+ is observed, consistent with the relatively low concentration of Bronsted acid sites compared to Lewis acid sites on each of the samples investigated. Exposure of Nb_2O_5/TiO_2 to NH_3 at temperatures up to 500 °C does not result in partial reduction of the supported niobia.

6. ^{129}Xe NMR Study of TiO_2(Anatase)-Supported V_2O_5 Catalysts (Publication 8)

J. Kritzenberger, H.C. Gaede, J.S. Shore, A. Pines, and A.T. Bell

TiO_2(anatase); V_2O_5/TiO_2(anatase) catalysts with 1.3%, 3.0%, and 9.8% weight loadings of V_2O_5; and pure V_2O_5 have been investigated by temperature-dependent xenon-129 NMR spectroscopy. The chemical shift of xenon adsorbed on the surface of TiO_2(anatase) and V_2O_5 is interpreted by means of a model of chemical exchange between gaseous and adsorbed phases. Intrinsic chemical shift values were obtained for xenon surface interactions: 109 ± 3 ppm for TiO_2(anatase) and 93 ± 5 ppm for V_2O_5. In contrast, the V_2O_5/TiO_2 catalysts provide a strong adsorption site for xenon. This causes an initial drop of the chemical shift values at low xenon loadings. Crystallites of pure V_2O_5 contain micropores that result in two distinct environments for the xenon atoms. Two-dimensional exchange spectroscopy was used to monitor the exchange between xenon enclosed in these pores and xenon outside the pores, making it possible to determine the rate of exchange and the activation energy.

FY 1993 PUBLICATIONS AND REPORTS

Refereed Journals

1. K.R. Krishna and A.T. Bell, "Estimates of the Rate Coefficients for Chain Initiation, Propagation, and Termination during Fischer–Tropsch Synthesis over Ru/TiO_2," J. Catal. **139**, 104 (1993); LBL-31801.
2. D.B. Clarke, I. Suzuki, and A.T. Bell, "An Infrared Study of the Interactions of CO and CO_2 with Cu/SiO_2," J. Catal. **142**, 27 (1993); LBL-33129.
3. M.J. Sandoval and A.T. Bell, "Temperature-Programmed Desorption Studies of the Interactions of H_2, CO and CO_2 with Cu/SiO_2," J. Catal. **144**, 227 (1993); LBL-33564.
4. B.F. Chmelka, G.F. Went, R. Csencsits, A.T. Bell, E.E. Petersen, and C.J. Radke, "Oxidation of Reduced Platinum Clusters in Pt–NaY," J. Catal. **144**, 506 (1993).

5. R.M. Pittman and A.T. Bell, "Raman Studies of the Structure of Nb_2O_5/TiO_2," J. Phys. Chem. **97**, 12178; LBL-34383.

LBL Reports

6. T. Komaya and A.T. Bell, "Estimates of Rate Coefficients for Elementary Processes Occurring during Fischer–Tropsch Synthesis over Ru/TiO_2," J. Catal. (in press); LBL-34334.
7. R.M. Pittman and A.T. Bell, "Raman Investigation of NH_3 Adsorption on TiO_2, Nb_2O_5, and Nb_2O_5/TiO_2," Catal. Lett. (in press); LBL-34518.
8. J. Kritzenberger, H.C. Gaede, J.S. Shore, A. Pines, and A.T. Bell, "^{129}Xe NMR Study of TiO_2(Anatase)-Supported V_2O_5 Catalysts," J. Phys. Chem. (submitted); LBL-35048.
9. D.B. Clarke, D.-K. Lee, M.J. Sandoval, and A.T. Bell, "Infrared Studies of the Mechanism of Methanol Decomposition on Cu/SiO_2," J. Catal. (submitted); LBL-35149.
10. T. Komaya, A.T. Bell, Z. Weng-Sieh, R. Gronsky, F. Engelke, T.S. King, and M. Pruski, "The Influence of Metal-Support Interactions on the Accurate Determination of Ru Dispersion for Ru/TiO_2 Catalysts," J. Catal. (submitted); LBL-35150.

Invited Talks

11. A.T. Bell, "Applications of Molecular Spectroscopies to Problems in Catalysis," Engineering Foundation Conference, Palm Coast, FL, February 21–26, 1993.
12. A.T. Bell, "Mechanisms of NO Reduction by NH_3 over Pt/Al_2O_3 and V_2O_5/TiO_2," ACS meeting, Denver, CO, March 28–April 2, 1993.
13. A.T. Bell, "Research Needs in the Field of Environmental Catalysis," 13th North American Meeting, The Catalysis Society, Pittsburgh, PA, May 2–7, 1993.
14. A.T. Bell, "Industry–University Collaborations: What Can We Expect," 13th North American Meeting, The Catalysis Society, Pittsburgh, PA, May 2–7, 1993.
15. A.T. Bell, "Applications of In Situ and Ex Situ NMR Spectroscopy to the Study of Catalytic Processes," Colloque Ampere, Menton, France, September 6–11, 1993.

Contributed Talks

16. A.T. Bell, "Raman Studies of Titania-Supported Niobia and Its Interactions with H_2, H_2O, and NH_3," ACS meeting, Denver, CO, March 28–April 2, 1993.
17. A.T. Bell, "Isotopic Tracer Studies of the Effects of Olefin Reincorporation on the Dynamics of Fischer–Tropsch Synthesis," 6th U.S.A.–Japan–China Trilateral Symposium on Catalysis, Tsinghua University, Beijing, Peoples' Republic of China, June 8–11, 1993.
18. A.T. Bell, "Isotopic Tracer Studies of the Effects of Olefin Reincorporation on the Dynamics of Fischer–Tropsch Synthesis," 3rd U.S.–Korea Workshop on Catalysis, Seoul National University, Seoul, Korea, June 14–15, 1993.
19. A T. Bell, "Raman Studies of Titania-Supported Niobia and its Interactions with H_2, H_2O, and NH_3," AIChE Meeting, St. Louis, MO, November 7–12, 1993.
20. A.T. Bell, "Isotopic Tracer Studies of the Effects of Olefin Reincorporation on the Dynamics of Fischer–Tropsch Synthesis," AIChE Meeting, St. Louis, MO, November 7–12, 1993.
21. A.T. Bell, "The Influence of Metal Oxide Composition on the Promotion of CO and CO_2 Hydrogenation over Pt and Rh," AIChE Meeting, St. Louis, MO, November 7–12, 1993.
22. A.T. Bell, "Applicability of BOC–MP Estimates of Surface Energetics to Problems in Catalysis," AIChE Meeting, St. Louis, MO, November 7–12, 1993.

Transition-Metal-Catalyzed Conversion of CO, NO, H_2, and Organic Molecules to Fuels and Petrochemicals*

Robert G. Bergman, Investigator

INTRODUCTION

The goals of this program are the development of new chemical reactions in which transition metals interact with organic materials and the understanding of how these reactions work. A recent discovery in this project was the finding that certain cyclopentadienyliridium and -rhodium complexes undergo oxidative addition into the carbon–hydrogen bonds of completely saturated hydrocarbons (M + R–H → R–M–H). This finding was the first example of a long-sought alkane C–H activation reaction. Research is now being directed at examining the scope, selectivity, and mechanism of the process; extending it to other systems; and developing ways to convert the activated metal complexes X–M–H into functionalized organic molecules. During the current year, two important breakthroughs were made. In one, the first instance of reaction of alkanes, including methane, with the relatively high-oxidation-state metal center Ir^{3+} was observed. A second important finding came out of a collaborative study with Dr. R.A. Andersen; in this work, the first intermolecular abstraction of fluorine atoms (i.e., C–F activation) from simple secondary saturated fluorocarbons was uncovered. Finally, in a collaborative study with Drs. B.H. Weiller and C.B. Moore, rate constants for the very fast reactions of rhodium–xenon complexes with carbon monoxide were measured, and evidence for an associative mechanism in this process was presented.

1. Organometallic CO Substitution Kinetics in Liquid Xe by Fast Time-Resolved IR Spectroscopy

B.H. Weiller, E.P. Wasserman, C.B. Moore, and R.G. Bergman

In earlier experiments, the highly reactive but spectroscopically detectable noble gas complexes Cp*Rh(CO)Xe and Cp*Rh(CO)Kr (Cp* = η^5-C_5Me_5) were generated at low temperatures in liquid rare gas solutions. In the present work, the reaction of Cp*Rh(CO)Xe with CO was studied with time-resolved IR spectroscopy. Infrared spectra for Cp*Rh(CO)Xe were obtained with pulsed UV laser photolysis of Cp*Rh$(CO)_2$ in liquid Xe and a rapid-scan FTIR spectrometer with 0.09-s time resolution. Assignment to the Xe complex was confirmed from the similarity of the spectra and the lifetime of the complex when a mixture of Xe in liquid Kr was used (Figure 1-1). The reaction of Cp*Rh(CO)Xe with added CO is very fast, and the rate constant was measured by fast time-resolved IR spectroscopy (Figure 1-2) to be $(5.7 \pm 0.6) \times 10^5$ to $(1.9 \pm 0.2) \times 10^6$ $M^{-1}s^{-1}$ over the temperature range 202 to 242 K. The observed rate constants show a linear dependence on the CO concentration (Figure 1-3) and are therefore consistent with an associative substitution mechanism with activation parameters for the bimolecular rate constant of $\log(A) = 8.8 \pm 0.3$ ($\Delta S^{\ddagger} = -20 \pm 1$ cal/mol K) and $E_a = 2.8 \pm 0.3$ kcal/mol ($\Delta H^{\ddagger} = 2.4 \pm 0.3$ kcal/mol). The very small barrier to substitution suggests that the reaction occurs by direct displacement of Xe at the metal center by CO rather than by a stepwise mechanism involving the initial formation of a "ring-slipped" η^3-cyclopentadienyliridium intermediate.

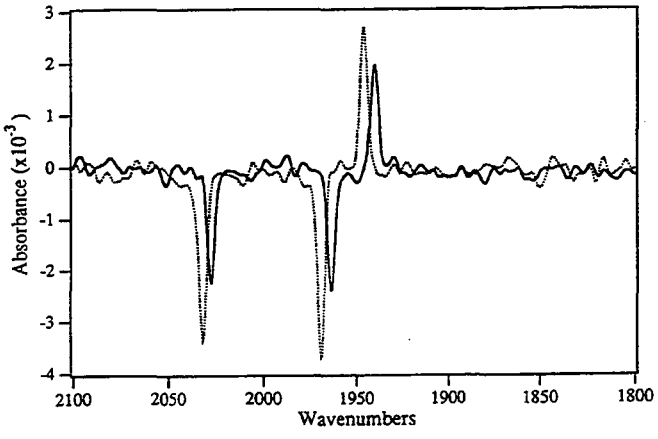

Figure 1-1. Rapid-scan FTIR spectra of Cp*Rh(CO)Xe in liquid Xe and Kr. Both are difference spectra resulting from photolysis of Cp*Rh$(CO)_2$ at 248 nm and 162.0 K. The solid line is for liquid Xe solvent, and the broken line is for a mixture of ~6 % Xe in Kr. The negative bands (2031 and 1969 cm^{-1} in Xe, 2027 and 1963 cm^{-1} in Kr) result from photolysis of Cp*Rh$(CO)_2$, and the positive bands (1946 and 1940 cm^{-1}) are assigned to Cp*Rh(CO)Xe. Each spectrum represents an average of 20 laser shots. (XBL 947-4156)

*This work was supported by the Director, Office of Energy Research, Office of Basic Energy Sciences, Chemical Sciences Division, of the U.S. Department of Energy under Contract No. DE-AC03-76SF00098.

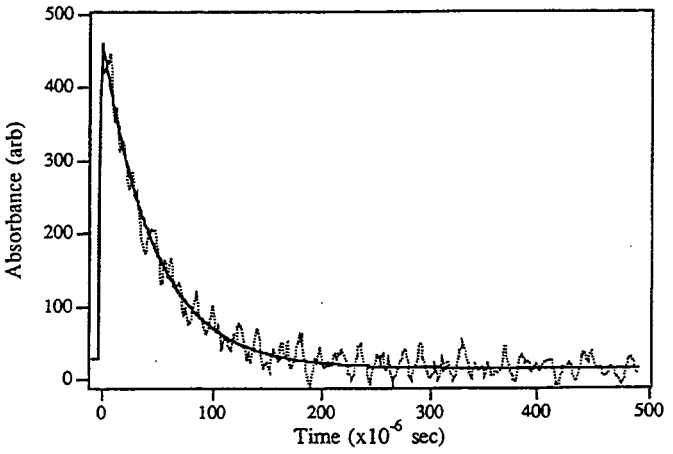

Figure 1-2. Kinetic trace of Cp*Rh(CO)Xe in liquid Xe. The CO concentration is 0.0124 M, and the temperature is 242 K. The solid line is the best fit to an exponential decay with decay constant k_{obs} = (2.11 ± 0.04) × 10^5 s^{-1}. The trace represents an average of 32 laser shots. (XBL 947-4157)

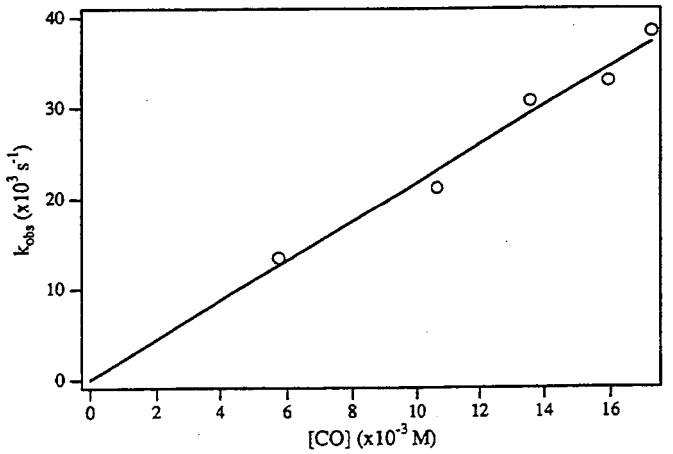

Figure 1-3. Dependence of k_{obs} on CO concentration. The temperature is 242 K, and the solid line is the linear least-squares fit with slope k_{co} = (2.1 ± 0.2) × 10^6 $M^{-1}s^{-1}$. (XBL 947-4158)

2. Reactions of $(MeC_5H_4)_3U(t\text{-Bu})$: Intermolecular Fluorine Atom Abstraction from Fluorocarbons Including Saturated Perfluorocarbons

M. Weydert, R.A. Andersen, and R.G. Bergman

Few examples of intermolecular C–F bond activation have been reported. The pronounced inertness of perfluorocarbons is undoubtedly caused by the high C–F bond dissociation energies and by the weakness of metal–fluorocarbon interactions. It has now been found that (η^5-$MeC_5H_4)_3U(t\text{-Bu})$ reacts with fluorocarbons, resulting in efficient fluorine abstraction under mild conditions in the presence of hydrocarbon solvents. For example, treatment of $(MeC_5H_4)_3U(t\text{-Bu})$ with 2 equivalents of hexafluorobenzene in toluene solution at room temperature for 24 hours gives the uranium(IV) fluoride $(MeC_5H_4)_3UF$. The organic products of this reaction are pentafluorobenzene, *t*-butylpentafluorobenzene, isobutane, and isobutene as well as small amounts of hexamethylethane, bibenzyl, and 2,3,4,5,6-pentafluoro-4′-methylbiphenyl. Reaction of $(MeC_5H_4)_3U(t\text{-Bu})$ in toluene solution at room temperature with C_6F_{12} gives a 1:1 mixture of $(MeC_5H_4)_3UF$ and $(MeC_5H_4)_3U(CH_2Ph)$ along with the organic products $C_6F_{11}H$, isobutane, and isobutene. We rationalize these observations by the radical mechanism outlined in Figure 2-1. Critical steps in this mechanism involve abstraction of a fluorine atom from C_6F_{12} by $(MeC_5H_4)_3U$ along with release of *t*-butyl radical and then reaction of the resulting C_6F_{11} radical with toluene to yield $C_6F_{11}H$ and benzyl radical. The benzyl radical then attacks another molecule of $(MeC_5H_4)_3U(t\text{-Bu})$ to yield $(MeC_5H_4)_3U(CH_2Ph)$ and a *t*-butyl radical. This study provides the first observation of the cleavage of a saturated secondary carbon–fluorine bond by a soluble metal complex.

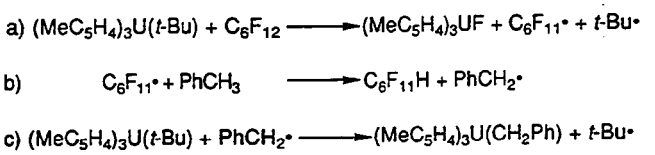

Figure 2-1. Proposed free-radical mechanism for the reaction of $(MeC_5H_4)_3U(t\text{-Bu})$ with perfluorocyclohexane. (XBL 947-4159)

3. Facile Intermolecular Activation of C–H Bonds in Methane and Other Hydrocarbons and Si–H Bonds in Silanes with the Ir(III) Complex $Cp^*(PMe_3)Ir(CH_3)(OTf)$

P. Burger and R.G. Bergman

Late transition metals typically react with hydrocarbons by oxidative addition of C–H bonds to low-valence, electron-rich metal centers. It has now been discovered that the more electron-deficient iridium(III) center in the trifluoromethanesulfonate (triflate) complex $Cp^*(PMe_3)Ir(CH_3)(OTf)$ (complex **1**, $Cp^* = \eta^5\text{-}C_5Me_5$, $OTf = OSO_2CF_3$) reacts under mild conditions (25–45 °C, CD_2Cl_2 solution) with several types of C–H bonds (Figure 3-1). For example, benzene reacts with complex **1** to give methane and $Cp^*(PMe_3)Ir(C_6H_5)OTf$ (complex **2**). Most strikingly, treatment of complex **1** with isotopically labeled $^{13}CH_4$ leads to attack on the methane C–H bond, leading to equilibration of complex **1** and $^{13}CH_4$ with $^{12}CH_4$ and $Cp^*(PMe_3)Ir(^{13}CH_3)(OTf)$, as established by

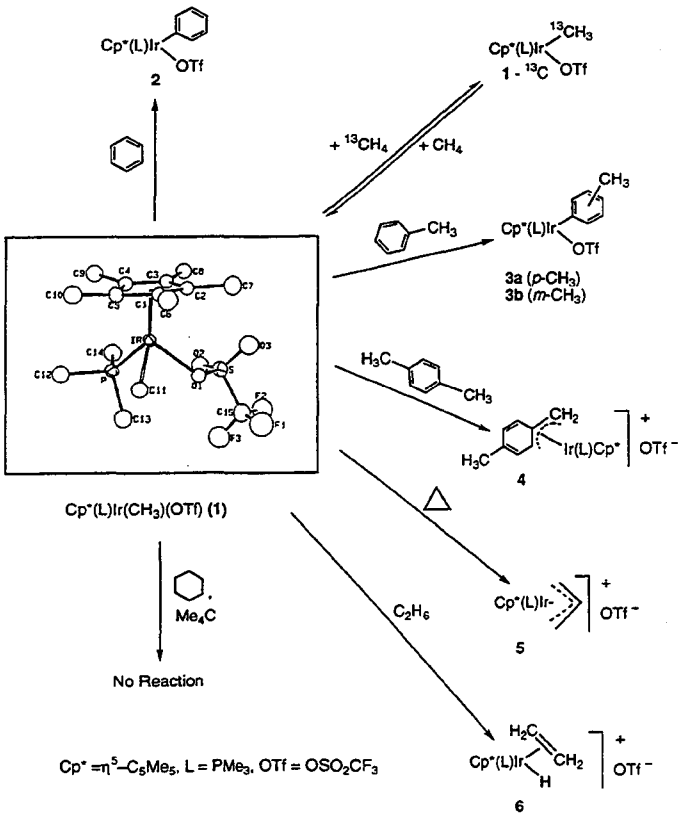

Figure 3-1. Products formed on reaction of $Cp^*(PMe_3)Ir(CH_3)(OTf)$ (complex **1**, $Cp^* = (\eta^5\text{-}C_5(CH_3)_5)$, $OTf = OSO_2CF_3$) with compounds containing various types of carbon–hydrogen bonds. An ORTEP diagram illustrating the results of the x-ray structure determination of complex **1** is shown in the inset. (XBL 947-4160)

^1H NMR analysis of the reaction mixture (Figure 3-2). Reaction with toluene leads to the $Cp^*(PMe_3)Ir(C_6H_4CH_3)OTf$ complexes (**3a** and **3b**) resulting from attack at the *p*- and *m*-C–H bonds in a 1.25:1 ratio (statistically corrected), and *p*-xylene gives only the product (complex **4**) resulting from attack at a benzylic C–H bond. Cyclohexane and neopentane do not react with complex **1**, and other alkanes react with rearrangement. For example, cyclopropane gives the cationic allyl complex $[Cp^*(PMe_3)Ir(C_3H_5)]OTf$ (complex **5**), and ethane leads to the ethylene hydride salt $[Cp^*(PMe_3)Ir(H)(C_2H_4)]OTf$ (complex **6**). Complex **1** also reacts with the Si–H bonds in silanes, again with rearrangement. For example, trimethylsilane gives $Cp^*(PMe_3)Ir(Me)(SiMe_2OTf)$, the product of methyl migration from Si to Ir, and triphenylsilane leads to $Cp^*(PMe_3)Ir(Ph)(SiPh_2OTf)$, the product of phenyl migration. Preliminary experiments with heterosubstituted silanes indicate that relative Si-to-Ir migratory aptitudes are H > Ph > CH_3. The structures of complexes **1** and **6** have been determined by x-ray diffraction.

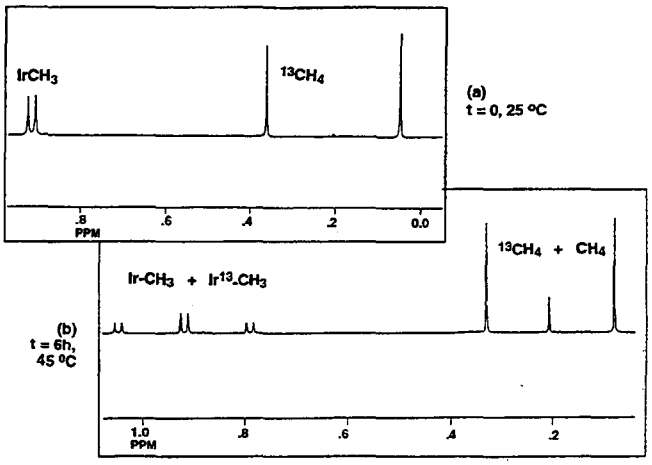

Figure 3-2. (a) High-field region of the ^1H NMR spectrum of a solution of complex **1** in CD_2Cl_2 under 2 atm of $^{13}CH_4$ immediately after mixing at 25 °C. (b) High-field region of the ^1H NMR spectrum of the same mixture after heating for 6h at 45 °C. (XBL 947-4175)

4. Work in Progress

The following research is in progress. Time-resolved infrared flash kinetic investigations are being carried out with a new diode laser system to achieve higher resolution so that metal–rare gas and metal–hydrocarbon complexes can be spectroscopically distinguished. The flash kinetic studies are also being extended from cyclohexane to a range of other saturated hydrocarbons to determine the effect of changing structure on the absolute rates of the Ir(I) C–H activation reaction. The flash kinetic technique is being utilized to understand selectivities and isotope effects in the Ir(I) C–H activation reaction. Studies on the new Ir(III) C–H activation will be expanded to determine the range of alkanes and other organic compounds that will react at the metal center and to elucidate the mechanism of the reaction.

FY 1993 PUBLICATIONS AND REPORTS

Refereed Journals

1. B.H. Weiller, E.P. Wasserman, C.B. Moore, and R.G. Bergman, "Organometallic CO Substitution Kinetics in Liquid Xe by Fast Time-Resolved IR Spectroscopy," J. Am. Chem. Soc. **115**, 4326 (1993); LBL-32834.
2. M. Weydert, R.A. Andersen, and R.G. Bergman, "Reactions of $(MeC_5H_4)_3U(t\text{-}Bu)$: Intermolecular Fluorine Atom Abstraction from Fluorocarbons Including Saturated

Perfluorocarbons," J. Am. Chem. Soc. **115**, 8837 (1993); LBL-35033.

3. P. Burger and R.G. Bergman, "Facile Intermolecular Activation of C–H Bonds in Methane and Other Hydrocarbons and Si–H Bonds in Silanes with the Ir(III) Complex $Cp^*(PMe_3)Ir(CH_3)(OTf)$," J. Am. Chem. Soc. **115**, 10462 (1993); LBL-34649.

Invited Talks

4. R.G. Bergman, "Activation of Carbon–Hydrogen Bonds in Alkanes and Other Organic Molecules Using Organotransition Metal Complexes," Mobil Chemical Company, Edison, NJ, November 10, 1992; Rhone–Poulenc, Collegeville, PA, November 11, 1992.
5. R.G. Bergman, "Synthesis and Chemistry of Carbon- and Heteroatom-Bridged Binuclear Complexes," University of California, San Diego, La Jolla, CA, January 29, 1993.
6. R.G. Bergman, "The Use of Organotransition Metal Complexes in the Formation and Cleavage of C–H, C–C, C–O and C–N Bonds," University of California, San Diego, La Jolla, CA, February 22, 1992.
7. R.G. Bergman, "The Use of Organotransition Metal Complexes in the Formation and Cleavage of Carbon–Hydrogen and Carbon–Heteroatom Bonds," Lectures in Modern Chemistry Series, University of British Columbia, Vancouver, BC, February 2, 1993; Simon Fraser University, Burnaby, BC, February 3, 1993; California Institute of Technology, Pasadena, CA, February 24, 1993; Gordon Conference on Physical Organic Chemistry, Holderness, NH, June 24, 1993.
8. R.G. Bergman, "The Use of Organotransition Metal Complexes in the Formation and Cleavage of Bonds to Carbon, Nitrogen and Oxygen," Organish-Chemisches Institut der Universität, Heidelberg, Germany, March 18, 1993.
9. R.G. Bergman, "The Use of Organotransition Metal Complexes in the Formation and Cleavage of C–N, C–H, and C–O Bonds," University of Delaware, Newark, DE, March 24, 1993.
10. R.G. Bergman, "Formation and Cleavage of Bonds to Carbon, Nitrogen, and Hydrogen Using Organozirconium Nitrene Complexes," American Chemical Society Meeting, Denver, CO, March 28, 1993.
11. R.G. Bergman, "The Use of Metal Trifluoromethanesulfonates in the Formation and Cleavage of Carbon–Hydrogen and Carbon–Oxygen Bonds," University of Pittsburgh, Pittsburgh, PA, April 22, 1993; University of Guelph, Ontario, Canada, April 24, 1993.
12. R.G. Bergman, "The Formation and Cleavage of Carbon–Hydrogen and Carbon–Heteroatom Bonds in Organic Molecules Mediated by Organotransition Metal Complexes," University of West Virginia, Morgantown, WV, April 23, 1993.
13. R.G. Bergman, "The Formation and Cleavage of Bonds to Carbon, Nitrogen, and Oxygen Using Organotransition Metal Complexes," Campaigne–Carmack Symposium, Indiana University, Bloomington, IN, May 27, 1993.
14. R.G. Bergman, "A New Intermolecular C–H Activation Reaction of Methane and Other Hydrocarbons with Ir(III) Complexes," Amoco Oil Company, Naperville, IL, August 20, 1993; Catalytica, Mountain View, CA, September 29, 1993.

Formation of Oxyacids of Sulfur from SO_2*

Robert E. Connick, Investigator

INTRODUCTION

The research is concerned with the basic chemistry of inorganic sulfur species in aqueous solution. Sulfur dioxide produced in coal-burning power plants is the major source of acid rain. Currently the primary method of removing it from flue gas is by absorption into aqueous scrubber solutions as bisulfite ion, which can undergo oxidation by oxygen in the water. The present research is focused on understanding the kinetics and mechanism of oxidation of bisulfite ion by oxygen, a reaction of importance not only in flue gas desulfurization but also in the formation of sulfuric acid from sulfur dioxide in atmospheric water droplets.

1. Work In Progress

Y.-X. Zhang and R.E. Connick

The oxidation of bisulfite ion by oxygen in aqueous solution,

$$2\,HSO_3^- + O_2 \rightarrow 2\,SO_4^{2-} + 2H^+ \quad , \qquad (a)$$

was found to have the following rate law in the absence of inhibitors and catalysts at pH 4.5:

$$\text{Rate} = k[HSO_3^-]^2 \qquad (b)$$

The reaction is a chain reaction, and the above rate law refers to the steady-state rate. If the reaction is perturbed from the steady state, e.g., by a change in bisulfite concentration or acidity, it returns to the steady state at a measurable rate. A study of the rate of return yields information about the mechanism of the reaction.

Previous research gave evidence that HSO_5^-, peroxymonosulfate, is formed as an intermediate in the reaction and that it reacts with bisulfite ion to initiate the chain. In addition, it is known that HSO_5^- reacts rapidly with bisulfite ion to form sulfate ions.[1] From the above information on HSO_5^- and the assumption that the chain is terminated by a bimolecular reaction of the chain carrier involved in the chain propagation step forming HSO_5^-, an expression was derived for the rate of return to steady state after a disturbance, with no assumptions having been made about bisulfite dependence. The equation was used to fit the data from experiments where a reaction at the steady state was perturbed by the sudden addition of more bisulfite ion and the return to the new steady state followed. Parameters were obtained for the new and original steady-state rates and the time constant for the rate of return to the steady state. From comparison of experiments at different bisulfite concentrations but the same pH, the dependence on bisulfite concentration of the propagation step and the initiation step could be deduced. The data are consistent with the following mechanism (where the acid dependence is not indicated):

Propagation:

$$SO_3^- + O_2 \rightarrow SO_5^- \qquad (c)$$

$$SO_5^- + HSO_3^- \rightarrow HSO_5^- + SO_3^- \qquad (d)$$

Initiation:

$$HSO_5^- + HSO_3^- \rightarrow SO_4^- + SO_3^- + H_2O \qquad (e)$$

$$SO_4^- + HSO_3^- \rightarrow SO_4^{2-} + SO_3^- + H^+ \text{ (rapid)} \qquad (f)$$

Termination:

$$SO_5^- + SO_5^- \rightarrow \text{unreactive products} \qquad (g)$$

Fate of HSO_5^-:

$$HSO_5^- + HSO_3^- \rightarrow S_2O_7^{2-} + H_2O \qquad (h)$$

$$S_2O_7^{2-} + H_2O \rightarrow 2\,SO_4^{2-} + 2H^+ \qquad (i)$$

The data at pH 4.5 gave a first-power dependence on bisulfite concentration for reactions (d) and (e) and an overall second-power bisulfite dependence for the steady state. All these results are consistent with the above mechanism. In addition, experimental lack of dependence on O_2 concentration for the overall rate and for steps (d), (e), and (g) is predicted by the mechanism.

From similar experiments where the pH was suddenly changed, the reaction (d) rate appeared to be inversely proportional to the hydrogen ion concentration, and reactions (e) and (g) appeared to be independent of $[H^+]$, all in the region of pH 4.5.

Reaction (d) is slightly more complex than indicated above, approximately half of it reacting as follows:

$$SO_5^- + HSO_3^- \rightarrow SO_4^- + SO_4^{2-} + H^+ \qquad (j)$$

$$SO_4^- + HSO_3^- \rightarrow SO_4^{2-} + SO_3^- + H^+ \text{ (rapid)} \qquad (k)$$

*This work was supported by the Director, Office of Energy Research, Office of Basic Energy Sciences, Chemical Sciences Division, of the U.S. Department of Energy under Contract No. DE-AC03-76SF00098.

The rate of reaction (j), like that of reaction (d), is inversely proportional to the hydrogen ion concentration. This branching has no effect on the prior conclusions about bisulfate dependence, except that both reactions (d) and (j) must have a first-power bisulfate dependence.

1. R.E. Connick, S. Lee, and R. Adamic, Inorg. Chem. 32, 565 (1993).

FY 1993 PUBLICATIONS AND REPORTS

Refereed Journals

1. R.E. Connick, S. Lee, and R. Adamic, "Kinetics and Mechanisms of the Oxidation of HSO_3^- by HSO_5^-," Inorg. Chem. **32**, 565 (1993).

Potentially Catalytic and Conducting Polyorganometallics*

K. Peter C. Vollhardt, Investigator

INTRODUCTION

Homogeneous organotransition metal clusters have great potential as catalysts for known or new organic transformations, and as building blocks for novel electronic materials. While much is known about how such clusters are assembled and disassembled, their chemistry is largely unpredictable and/or uncontrollable. This project constitutes an interdisciplinary approach to the designed construction of polymetallic arrays, anchored rigidly on novel π ligands that enforce hitherto unprecedented metallic topologies. For this purpose, new synthetic organic methodology has been developed that allows the stepwise chemo-, regio-, and loco- (i.e., identity of the metal sequence in heterometallic systems) specific building-up of strain and/or electronically activated π-systems and attached cluster chains. The physical and chemical properties of the resulting molecules are unparalleled and include: extreme ligand deformations, highly strained metal–metal bonds, intramolecular organic fragment migrations, new organic reactions, intrachain-electron transfers, and thermally reversible photochemical storage processes.

1. Two-Dimensional ^{1}H-NMR EXSY Study of the Fluxional Behavior of the Novel Carbenium Ion Complex $[FvMo_2(CO)_4(\mu,\eta^2,\eta^3\text{-}MeC{\equiv}CCH_2)][BF_4]$ (Fv = Fulvalene): Syntheses, Structures, and Reactivity (Publication 1)

H. El Amouri,† J. Vaissermann,‡ Y. Besace,† K.P.C. Vollhardt, and G.E. Ball

The catalytic transformation of hydrocarbons on metallic surfaces has often been related to the mode of coordination of these organic substrates on the metal centers at the molecular level.[1] As a homogeneous model for understanding bonding and reactivity of unsaturated hydrocarbons on metal surfaces, we chose to prepare the novel carbenium ion complex $[FvMo_2(CO)_4(\mu,\eta^2,\eta^3\text{-}MeCCCH_2)][BF_4]$ (**3**) in which a hydrocarbyl ligand is bonded to a dimetal framework.

Treatment of $FvMo_2(CO)_6$ (**1**) with an excess of $MeCCCH_2OMe$ in refluxing toluene gave $[FvMo_2(CO)_4(\mu,\eta^2,\eta^2\text{-}MeCCCH_2OMe)]$ (**2**) as the only product in an 80% yield (based on reacted $FvMo_2(CO)_6$). The title compound **3** was obtained quantitatively by protonation of **2** in ether. In solution, **3** was found to be fluxional. The mechanism of exchange was elucidated by 2-D ^{1}H-NMR EXSY (exchange spectroscopy), and the rate constants were determined with $k_{int} = 35 \pm 4\ s^{-1}$, $G^{\ddagger}_{70\,°C} = 17.7 \pm 0.4$ kcal mol^{-1} and $k_{rot} = 5 \pm 0.5\ s^{-1}$, $G^{\ddagger}_{70\,°C} = 19.1 \pm 0.4$ kcal mol^{-1} (int = interconversion; rot = rotation), equilibrating the various forms **3a-c** (see Figure 1-1).

Consistent with this fluxional behavior, the molecular structure of **3**, ascertained by x-ray analysis, showed a dynamic disorder in the solid state for the bridged hydrocarbyl ligand as well as for the carbonyl groups. The complex $[FvMo_2(CO)_4(\mu,\eta^2,\eta^3\text{-}MeC{\equiv}CCH_2)][BF_4]$ (**3**) crystallizes in the monoclinic space group $P2_1/n$ with $Z = 4$; cell dimensions a = 8.546, b = 26.4441, and c = 8.619 Å; and $\beta = 105.73°$ (see Figure 1-2). The reactivity of this carbenium ion complex with respect to various nucleophiles to give **4–6** is summarized in Figure 1-3. The x-ray molecular structure of the phosphonium derivative $[FvMo_2(CO)_4(\mu,\eta^2,\eta^2\text{-}MeC{\equiv}CCH_2PPh_3][BF_4]$ (**6**) obtained from phosphine addition to **3** is depicted in Figure 1-4.

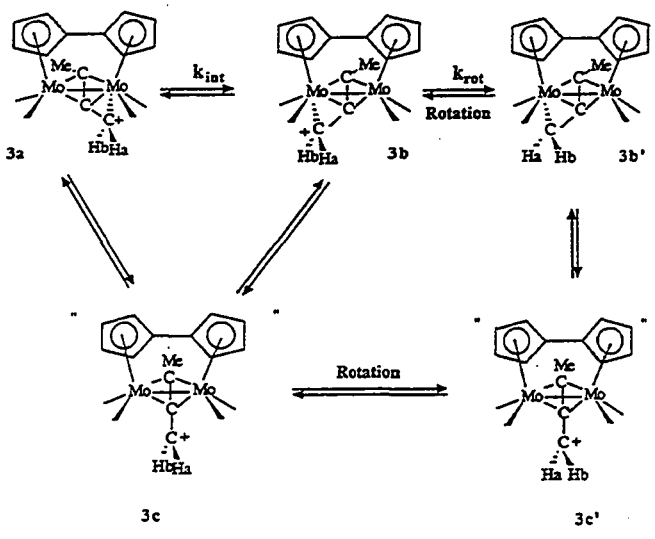

Figure 1-1. The fluxional behavior of 3. (XBL 947-4187)

*This work was supported by the Director, Office of Energy Research, Office of Basic Energy Sciences, Chemical Sciences Division, of the U.S. Department of Energy under Contact No. DE-AC03-76SF00098.

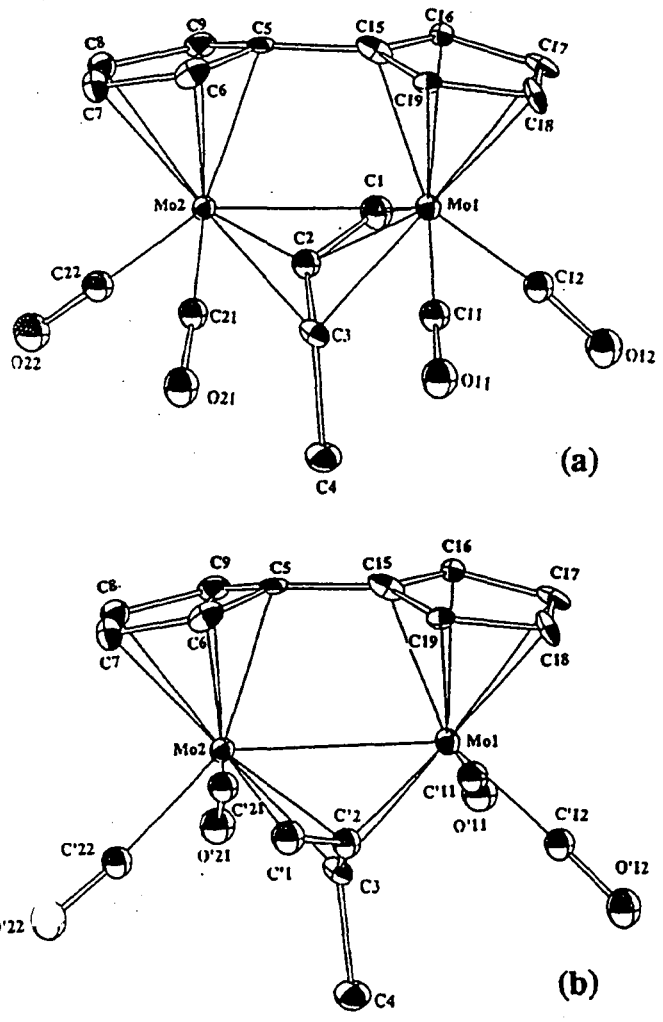

Figure 1-2. Molecular structure of the cationic part of molecule 3 (hydrogen atoms omitted). The two limiting structures, a and b, show different orientations for the carbenium ($-CH_2^+$) of the bridging hydrocarbyl ligand, either bound to Mo1 or to Mo2, their occupancy factor being one-half. The disorder is observed for the carbonyl groups and C1, C'1, C2, and C'2, while Mo1 and Mo2 have been identically placed in both forms a and b. (XBL 947-4188)

Compound **6** crystallizes in the monoclinic spacegroup $P2_1/c$ with $Z = 8$; cell dimensions $a = 13.243$, $b = 13.243$, and $c = 38.461$ Å; and $\beta = 93.92°$. The structure was refined to R and R_w values of 4.3% and 5.0%, respectively, using 6606 reflections.

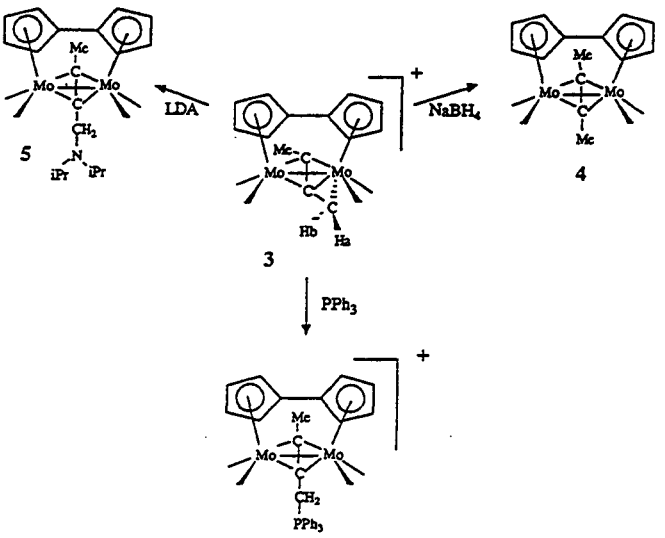

Figure 1-3. The results of nucleophilic attack on 3. (XBL 947-4189)

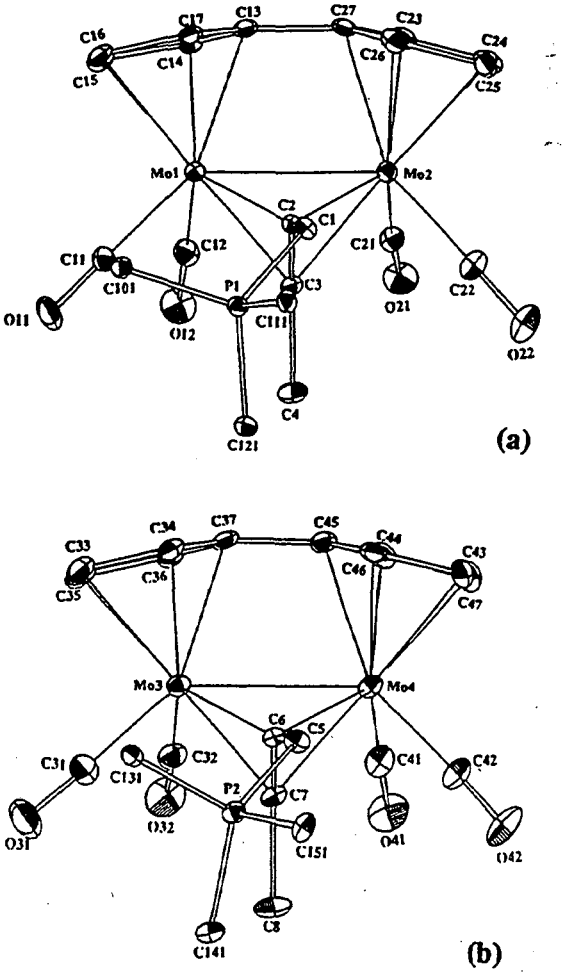

Figure 1-4. ORTEP plot of the cationic part of molecule 6, in its two independent molecular forms. The phenyl groups on the phosphorus atoms are omitted for clarity. (XBL 947-4190)

†Permanent address: URA 403, CNRS, ENSCP, 11 rue Pierre et Marie Curie, 75231 Paris Cedex 05, France.

‡Permanent address: URA 419, CNRS, Université Pierre et Marie Curie, Place Jussieu, 75252 Paris Cedex 05, France.

1. E.L. Muetterties *et al.*, Chem. Rev. **79**, 91 (1979); R.C. Brady and R. Petit, J. Am. Chem. Soc. **102**, 6181 (1980); V.C. Gibson, G. Parkin, and J.E. Bercaw, Organometallics **10**, 220 (1991).

2. The Thermally-induced Prototropic Isomerization of η^4–1,3–, η^4-1,4-, η^4-1,5-Dialkenes Complexed to (η^5-Cyclopentadienyl)cobalt (Publication 2)

J. A. King Jr.† and K.P.C. Vollhardt

Organometallic diene complexes have been known for more than sixty years. Research into the interaction of organometallic complexes with dienes has spawned a variety of commercially important processes. Catalytic olefin isomerization has been a central focus in much of this commercial chemistry.

In bound polyene systems, a variety of transition metals promote the thermal *cis* ↔ *trans* (*Z* ↔ *E*) isomerization, in addition to olefin migratory reactions. In the latter case, double-bond migrations generally proceed by either of two principal mechanisms: addition-eliminations or 1,3-hydrogen (prototropic) shifts. This study reports a series of facile, thermally induced, prototropic isomerizations of η^4-1,4- and η^4-1,5-dienes of (η^5-cyclopentadienyl)cobalt to their corresponding η^4-1,3-complexes. The data indicate the *E*-isomers to be thermodynamically favored over the *Z*-isomers. Furthermore, in the case of η^4-hexadiene complexes, the η^4-2,4-*EE*-isomer is observed to be thermodynamically preferred relative to either the η^4-2,4-*E,Z*- or η^4-1,3-*E*-isomer. Some representative reactions are summarized in Figure 2-1.

The facility with which the nonconjugated CpCo[diene] complexes rearrange to their conjugated analogs is consistent with a traditional prototropic isomerization mechanism.

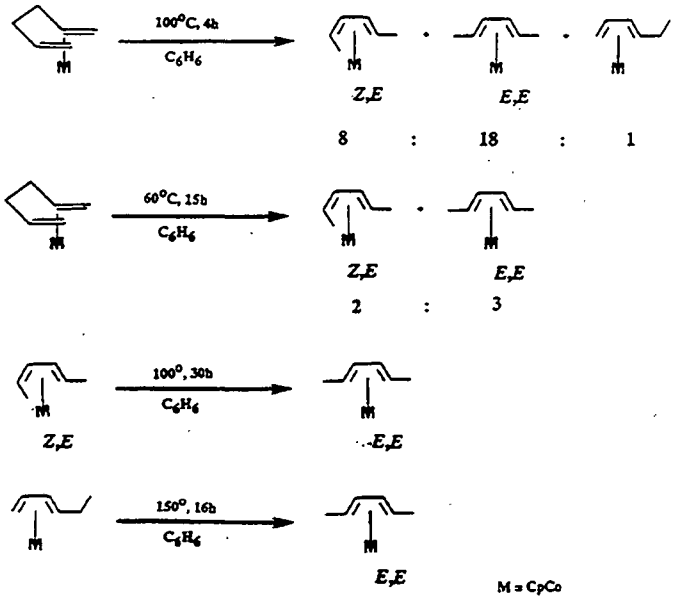

Figure 2-1. Isomerization cascade of η^4-1,5-hexadiene (η^5-cyclopentadienyl)cobalt. (XBL 947-4191)

†Permanent address: General Electric Corporate R&D, P.O. Box 8, Schenectady, NY 12301.

3. Semibuckminsterfullerene: MNDO Study of a Hemispherical Triindenotriphenylene (Publication 3)

R. Faust† and K.P.C. Vollhardt

Bowl-shaped polycyclic aromatic hydrocarbons (PAHs), whose carbon frameworks constitute cross sections of buckminsterfullerene, are attractive synthetic targets because of their potential as reference compounds for spherical carbon clusters and, more importantly, because their topology provides the opportunity to model the endohedral chemistry of the fullerenes. In this vein, a current target of synthesis in this laboratory is triindeno-[4.3,3a,2.1-*cdef*:4′,3′,3a′,2′,1′-*ijkl*:4″,3″,3a″,2″,1″-*opqr*]triphenylene (**1**), whose carbon skeleton was previously suggested as a possible intermediate in the formation of C_{60}. In order to aid the synthetic efforts, a computational investigation of the molecule and its lithium complex was performed. Geometry optimization (C_3 symmetry constraints imposed) using the MNDO parameter set clearly predicts the cup-shaped topology as a minimum on the $C_{30}H_{12}$ potential energy surface with deviation from planarity of 39° (see Figure 3-1). This clearly surpasses the degree of nonplanarity observed in corannulene (26.8°) and is somewhat closer to the value found in C_{60} (31°). The planar C_{3h} structure of **1** is estimated to be 77.3 kcal mol^{-1} higher in energy than the equilibrium C_3 geometry (Table 3-1), thereby essentially excluding a bowl inversion along this pathway.

The hemispherical geometry of **1** offers two topologically different coordination sites and thereby provides the opportunity to mimic exo- and endohedral metal complexes of C_{60}. Of the possible symmetry-unique locations for metal attachment, only those along the molecule's C_3 axis were examined computationally by coordinating Li^+ to **1** (Table 3-1). Surprisingly, it was found that complexation from the outside of the bowl, as

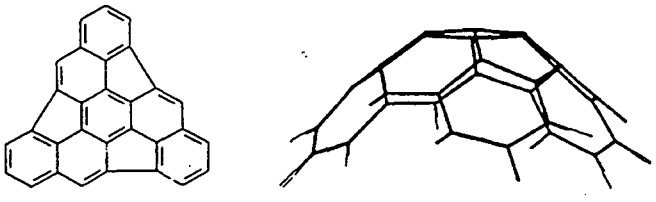

Figure 3-1. Structure and MNDO-optimized geometry of triindenotriphenylene **1**. (XBL 947-4192)

Table 3-1. Energies and selected bond lengths of triindenotriphenylenes **1** and **2**.[a]

	1	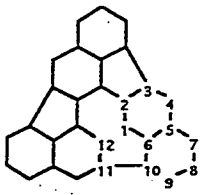	2_b
ΔH_f°	252.5[c]		344.6[d]
R(1–2)	1.385		1.411
R(1–6)	1.430		1.432
R(1–12)	1.452		1.478
R(2–3)	1.470		1.470
R(3–4)	1.395		1.400
R(4–5)	1.467		1.462
R(5–6)	1.414		1.417
R(5–7)	1.442		1.443
R(6–10)	1.466		1.464
R(7–8)	1.392		1.392
R(8–9)	1.442		1.443
R(9–10)	1.383		1.385
R(10–11)	1.505		1.502
R(Li–Bz)[e]			1.827[f]

[a]MNDO-values (C_3-symmetry constraints imposed). Heats of formation in kcal mol^{-1}, bond lengths *R* in Ångstroms. Cf. CC bond length in D_{6h}-benzene (MNDO): 1.470 Å. For reasons of clarity, the numbering scheme deviates from IUPAC recommendations.
[b]Convex coordination of Li^+ to **1**.
[c]ΔH_f° of planar C_{3h} geometry: 329.8 kcal mol^{-1}.
[d]ΔH_f° of concave isomer: 389.3 kcal mol^{-1}.
[e]Distance between Li and midpoint of the central benzene ring.
[f]Corresponding value of concave isomer: 2.048Å.

shown in Figure 3-2 for **2**, is favored by 44.7 kcal mol^{-1} over the alternative concave arrangement, in which the metal resides inside the hemisphere. Since the interaction between Li^+ and **1** is purely electrostatic, this result implies that the electron density is greater on the outside of the bowl than on the inside. Preferential convex coordination can thus be explained by pyramidalization (or rehybridization) of central ring carbons in a fashion that increases the spatial extensions of the p-type atomic orbitals on the outside of the bowl. Thus, synthesis of a metal fragment coordinated to cup-shaped PAHs in a concave fashion appears to be a formidable challenge.

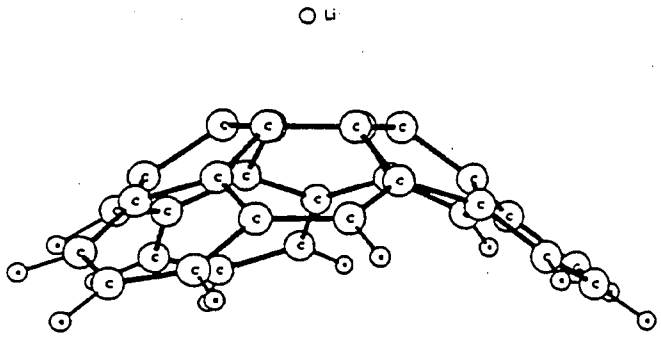

Figure 3-2. MNDO-optimized geometry of the convex Li-arene complex **2**. (XBL 947-4193)

4. The Role of Delocalizaton in Benzene (Publication 4)

E.D. Glendening,[†] R. Faust,[‡] A. Streitwieser, K.P.C. Vollhardt, and F. Weinhold[||]

One of the early successes and a cornerstone of modern molecular orbital (MO) theory is its ability to predict the stabilizing effect of π-electronic delocalization in benzene. Although this effect is generally accepted by the chemical community, the relationship between π delocalization and the geometry of benzene remains an issue of some debate. It has generally been argued, based on a valence bond picture, that resonance mixing of the Kekulé structures **1a,1b**

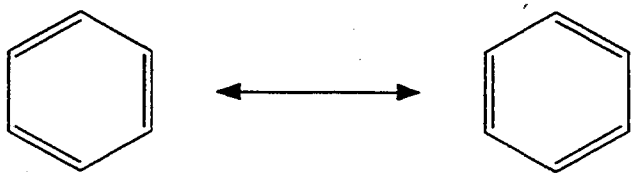

1a **1b**

leads to the symmetric (equilibrium) structure with C–C bond lengths (~1.40 Å) intermediate between those of idealized single and double bonds. Hence, the structure of benzene and the stabilizing effect of π delocalization appear to be directly related. Recent theoretical studies have, however, challenged this view, suggesting instead that the σ system, rather than the π, is responsible for the symmetric structure.

In this paper, the influence of π delocalization on the geometry of benzene is examined at the *ab initio* SCF level of theory. It is found that benzene favors a bond-alternating geometry when its canonical π MOs are

[†]Permanent address: Laboratorium für Organische Chemie, ETH Zentrum, Universitätsstrasse 16, CH-8092 Zürich, Switzerland.

replaced by three localized ethylenic orbitals, revealing that delocalization is in part responsible for the equilibrium symmetric structure. In apparent contrast, a σ–π energy partitioning analysis suggests that the benzene σ framework is responsible for the symmetric geometry, the π system preferring a distorted geometry. Shaik and others[1] have therefore concluded that delocalization is not an important symmetrizing force in this molecule. It is shown here, however, that the π-energy component contains a sizable and strongly geometry-dependent contribution from the localized (Kekulé) wave function. Thus, it appears to be misleading to judge the nature of delocalization based on a σ–π partition. We conclude that delocalization effects act to strongly stabilize symmetric benzene in essential accord with the concepts of classical resonance theory.

†Permanent address: Molecular Science Research Center, Pacific Northwest Laboratory, Battelle Blvd., MS K1-90, Richland, WA 99352.
‡Permanent address: Laboratorium für Organische Chemie, ETH Zentrum, Universitätsstrasse 16, CH-8092 Zürich, Switzerland.
||Permanent address: University of Wisconsin, Madison, WI 53706.

1. S.S. Shaik and R. Bar, Nouv. J. Chim. **8**, 411 (1984); S.S. Shaik *et al.*, Nouv. J. Chim. **9**, 585 (1985); P.C. Hiberty *et al.*, J. Org. Chem. **50**, 4657 (1985); S.S. Shaik and P.C. Hiberty, J. Am. Chem. Soc. **107**, 3089 (1985); S.S. Shaik *et al.*, J. Am. Chem. Soc. **109**, 363 (1987); S.S. Shaik *et al.*, J. Phys. Chem. **92**, 5086 (1988); G. Ohanessian *et al.*, Inorg. Chem. **27**, 2219 (1988); P.C. Hiberty, in *Topics on Current Chemistry*, edited by I. Gutman and S.J. Cyrin (Springer, NY, 1990), Vol. 153, p. 27.

FY 1993 PUBLICATIONS AND REPORTS

Refereed Journals

1. H. El Amouri, J. Vaissermann, Y. Besace, K.P.C. Vollhardt, and G.E. Ball, "Two-Dimensional ^{1}H-NMR EXSY Study of the Fluxional Behavior of the Novel Carbenium Ion Complex $[FvMo_2(CO)_4(\mu,\eta^2\eta,^3\text{-MeC}{\equiv}CCH_2)][BF_4]$(Fv = Fulvalene): Syntheses, Structures, and Reactivity," Organometallics **12**, 605 (1993); LBL-33507.
2. J.A. King, Jr. and K.P.C. Vollhardt, "The Thermally-induced Prototropic Isomerization of η^4-1,3-, η^4-1,4-, η^4-1,5-Dialkenes Complexed to (η^5-Cyclopentadienyl)cobalt," J. Organomet. Chem. **460**, 91 (1993); LBL-35123.
3. R. Faust and K.P.C. Vollhardt, "Semibuckminsterfullerene: MNDO Study of a Hemispherical Triindenotriphenylene," J. Chem. Soc., Chem. Commun. **1993**, 1471; LBL-35124.
4. E.D. Glendening, R. Faust, A. Streitwieser, K.P.C. Vollhardt, and F. Weinhold, "The Role of Delocalization in Benzene, J. Am. Chem. Soc. **115**, 10952 (1993); LBL-35125.
5. K.P.C. Vollhardt, "The Phenylenes," Pure and Appl. Chem. **65**, 151 (1993); LBL-33624.

LBL Reports

6. R. Faust, "On the Role of Delocalization in Benzene: Theoretical and Experimental Investigation of the Effects of Strained Ring Fusion," Ph.D. Thesis, University of California, Berkeley, CA, LBL-35126.
7. D.S. Brown, "I. Redox Chemistry of Bimetallic Fulvalene Complexes II. Oligocyclopentadienyl Complexes," Ph.D. Thesis, University of California, Berkeley, CA, LBL-35127.

Invited Talks

8. K.P.C. Vollhardt, "Cobalt-Mediated Total Synthesis of Natural and Unnatural Products," Plenary Lecture, 1st International Symposium on Selective Synthesis Mediated by Organometallic Compounds, Oviedo, Spain, July 14–16, 1993.
9. K.P.C. Vollhardt, "The Cobalt Way to Total Synthesis," Randolph T. Majors, Lecturer, University of Connecticut, Storrs, CN, October 25, 1993.
10. K.P.C. Vollhardt, "The Phenylenes. A Testing Ground for the Origin of Delocalization in Benzene," Randolph T. Majors Lecturer, University of Connecticut, Storrs, CN, October 26, 1993.
11. K.P.C. Vollhardt, "Oligocyclopentadienylmetals: Remarkable Organometallic Materials," Randolph T. Majors, Lecturer, University of Connecticut, Storrs, CN, October 27, 1993.
12. K.P.C. Vollhardt, "Recent Breakthroughs in Cobalt-Mediated Alkyne Cyclizations," Plenary Lecture, Finnish Chemical Congress, Symposium on Synthetic Chemistry, Helsinki, Finland, November 4, 1993.
13. K.P.C. Vollhardt, "Cobalt-Mediated Total Synthesis of Natural and Unnatural Products," University of Oslo, Norway, November 5, 1993.
14. K.P.C. Vollhardt, "Cobalt-Mediated Total Synthesis of Natural and Unnatural Products," University of Oregon, Eugene, OR, December 3, 1993.
15. K.P.C. Vollhardt, "The Phenylenes," Plenary Lecture, 3rd Tohwa International Symposium on Synthetic and Mechanistic Hydrocarbon Chemistry, Fukuoka, Japan, December 6–9, 1993.

HEAVY-ELEMENT CHEMISTRY

Actinide Chemistry*

Norman M. Edelstein, Richard A. Andersen, and Kenneth N. Raymond, Investigators

GENERAL INTRODUCTION

Development of new technological processes for the use, safe handling, storage, and disposal of actinide materials relies on the further understanding of basic actinide chemistry and the availability of a cadre of trained personnel. This research program is a comprehensive, multifaceted approach to the exploration of actinide chemistry and to the training of students. Research efforts include synthetic organic and inorganic chemistry for the development of new chemical agents and materials, chemical and physical elucidation through various characterization techniques, and thermodynamic and kinetic studies for the evaluation of complex formation.

The development and understanding of complexing agents that specifically and effectively sequester actinide ions form one program aspect. Such agents are intended for the decorporation of actinides in humans, in the environment, and in systems related to the nuclear fuel cycle. Extensive studies are underway to prepare organometallic and coordination compounds of the f-block elements and to show the differences and similarities among the f elements and between the f and d transition series elements. Optical and magnetic studies on actinides as isolated ions in ionic solids and in molecules provide information about electronic properties as a function of atomic number.

I. Specific Sequestering Agents for the Actinides

Kenneth N. Raymond, Investigator

INTRODUCTION

The coordination chemistry of the actinides and lanthanides is being studied in order to create agents that selectively and strongly bind f transition elements in their +4 and +3 oxidation states. Characterization of these compounds includes the use of NMR spectroscopy, x-ray crystallography, potentiometric and spectrophotometric titrations, and electrochemistry. Possible applications for these ligands include magnetic resonance imaging (MRI), plutonium decorporation, uranium extraction from sea water, and waste actinide extraction and long-term storage.

1. Pu(IV) Coordination

J. Xu, D.W. Whisenhunt, Jr., and K.N. Raymond

The polydentate 3-hydroxy-2-pyridones (3,2-HOPO's) have proved to be a promising class of Pu(IV) chelators, and several new ligands have been synthesized for study with Pu(IV). The crystal structure of the isoelectronic Gd(III)-[tren(3,2-HOPO)] complex has been determined, giving a model for the formation of similar stable octadentate actinide(III) complexes in the physiological pH range.

New tetradentate, hexadentate, and octadentate 3,2-HOPO ligands have been synthesized. The tetradentate ligands 5LI-O-(Me-3,2-HOPO) and 5LI-(Me-3,2-HOPO) (Figure 1-1) proved to be effective in removing Pu(IV) from contaminated mice, removing up to 85% and 84% Pu(IV), respectively. These ligands have also been shown to be nontoxic to mice.

2. Thermodynamic Stability of the Th(IV) Desferrioxamine B (DFO) Complex

W. Whisenhunt, Jr. and K.N. Raymond

The formation constants of the Th(IV) and Pu(IV) complexes of analogs of Desferrioxamine B (DFO) have been determined or estimated. The analogs used for this study were DFOCAMC, DFOMTA, and DFO-1,2-HOPO.

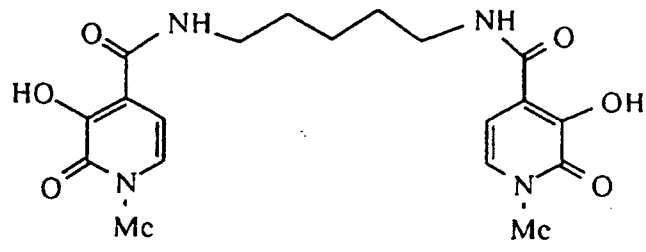

5LI-(Me-3,2-HOPO)

Figure 1-1. Chemical formula of 5LI-(Me-3,2-HOPO). (XBL 947-4163)

*This work was supported by the Director, Office of Energy Research, Office of Basic Energy Sciences, Chemical Sciences Division, of the U.S. Department of Energy under Contract No. DE-AC03-76SF00098.

These octadentate ligands have been found to bind Pu(IV) in preference to Fe(III) in the presence of EDTA (*N,N,N′,N′*-ethylenediaminetetraacetic acid) at pH 6. This has important implications for use of these materials in nuclear waste cleanup technologies, as Fe(III) is often an interfering agent in the extraction of Pu(IV).

Simple bidentate chelating groups (catechol, 1,2-hydroxypyridinone, and 3,4-hydroxypyridinone) have been attached to a polystyrene backbone and used to remove Th(IV) from organic solution. The synthesized materials displayed a high uptake capacity (0.7 mmol/g) for Th(IV). The acid/base properties of the synthesized materials parallel the known acid/base properties of the free chelating groups.

3. Solution Structure and Dynamics of the Lanthanide Complexes of the Macrocyclic Polyaminocarboxylate (DTPA-dien): An NMR Study and the Crystal Structures of the Lanthanum(III) and Europium(III) Complexes

S.J. Franklin and K.N. Raymond

The only lanthanide-containing MRI agent approved by the FDA is $[Gd(DTPA)(H_2O)]^{2-}$ (DTPA = diethylenetriaminepentaacetic acid). Neutral derivatives of this complex are of interest because they are nonionic, which reduces toxicity, and have been shown to be relatively more stable than $[Gd(DTPA)(H_2O)]^{2-}$ in the presence of physiological concentrations of Ca^{2+}, Cu^{2+}, Zn^{2+}, and H^+.[1] The x-ray crystal structure of [Gd(DTPA-bisethylamide)(H_2O)], studied in collaboration with a research group at Salutar, Inc.,[2] has revealed that both amide oxygens are bound to the metal. Several analogous bisamide macrocyclic chelators are being synthesized in order to fully encapsulate the metal, decreasing the ligands' degrees of freedom and limiting the number of possible complex isomers.

Nuclear magnetic resonance spectroscopy of the lanthanide complexes has been employed to study the dynamics of complex isomerization and the solution state structures of the complexes. Two isomers are present in solution for Ln(III) DTPA-dien, a diethylenetriamine-linked macrocyclic complex analogous to $Gd(DTPA)^{2-}$. Two-dimensional correlation spectroscopy has been used to determine the peak assignments, exchange kinetics, and exchange mechanisms of the Eu(III) complex. X-ray crystal structures of the La(III) and Eu(III) complexes have been determined and used as models for one aqueous isomer (Figure 3-1).

1. W.P. Cacheris, S.C. Quay, and S.M. Rocklage, Magn. Reson. Imag. **8**, 467 (1990).
2. M.S. Konings *et al.*, Inorg. Chem. **29**, 1488 (1990).

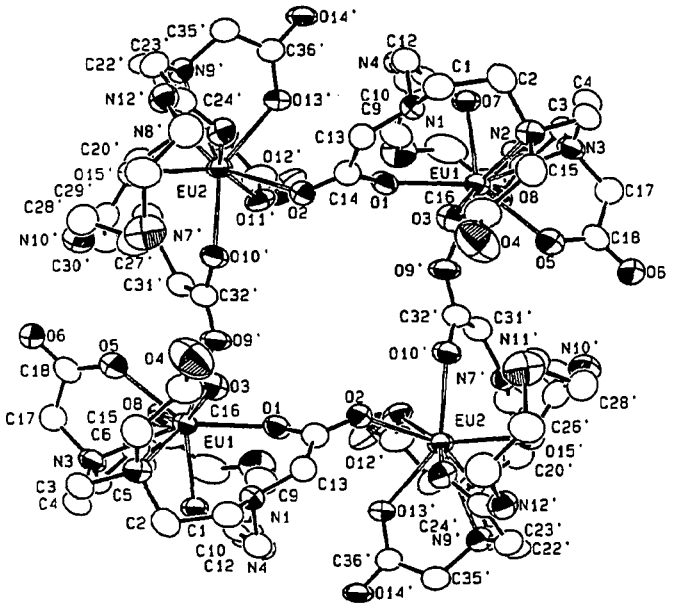

Figure 3-1. ORTEP view of the tetramer [Eu DTPA-dien $H^+]_4(CF_3SO_3)_4(NaCF_3SO_3)_6{\cdot}2OH_2$. The solvent and counterions have been omitted for clarity. (XBL 947-4164)

4. Work in Progress

Stereognostic Coordination Chemistry: The Design and Synthesis of Chelators for the Uranyl Ion

V. Freeman, P.H. Walton, and K.N. Raymond

Following the first paper in this series,[3] which described a new approach to ligand design for the sequestering of metal-oxo cations, a new generation of uranyl-chelating ligands is being studied. This "stereognostic" approach to ligand design incorporates conventional Lewis base coordination to the metal center and a hydrogen bond donor to interact with the oxo group(s).

The tripodal ligands tris-*N,N′,N″*-[2-(2-carboxyphenoxy)ethyl]-1,4,7-triazacyclononane bishydrochloride (ETAC·2HCl) and tris-*N,N′,N″*-[2-(2-carboxy-4-decylphenoxy)ethyl]-1,4,7-triazacyclononane tris hydrochloride (DETAC·3HCl) have been prepared. These ligands chelate the uranyl ion equatorially through three carboxylates and provide a hydrogen bond donor to interact with an oxo group through a protonated amine of the triazacyclononane backbone. CPK models predict that, upon uranyl binding, the hydrogen bond donor must point directly toward the oxo atom, enforcing a stereognostic interaction. Both ligands chelate the uranyl ion. The latter ligand is a powerful extractant and will quantitatively extract uranyl into an organic phase at pH 2.5 and above.

The predicted extraction coefficient is estimated to be approximately 10^{12} in neutral aqueous conditions. Oxygen-18 labeling of uranyl in conjunction with an infrared spectrum study of the labeled uranyl–ligand complex confirmed, for the first time, a stereognostic-type coordination to uranyl.

3. T.S. Franczyk, K.R. Czerwinski, and K.N. Raymond, J. Am. Chem. Soc. 114, 8138 (1992).

Pu(IV) Coordination

D.W. Whisenhunt, Jr. and K.N. Raymond

Efforts are currently under way to synthesize and test materials, similar to the catecholate and HOPO polystyrenes reported above, that will display a higher degree of hydrophilicity. The syntheses and study of these solid-support sequestering agents could lead to the development of materials useful for nuclear waste cleanup applications.

Lanthanide Coordination

C.O. Roth, C. Sunderland, and K.N. Raymond

In order to demonstrate the importance of the participation of amides as ligating groups for lanthanide complexes, a ligand with two noncoordinating arms that forms a water-soluble complex with Gd(III) has been designed. The synthesis and characterization of DTPA derivatives that contain two noncoordinating methyl groups and three acetic acid functional groups have been completed. This has been done to determine the strength of the amide oxygen–lanthanide bond and ultimately to evaluate the selectivity of the ligand for Gd^{3+} over other metal ions, such as Ca^{2+}, present under physiological conditions. The stability constants of these Gd(III) complexes in water have been measured and compared with those of the DTPA-bisamide complexes.

Cryptates are an elegant way to design a coordination environment in which one can form substitution-inert lanthanide–amine complexes. Such complexes[4] continue to be of interest and, in ideal situations, can lead to a unique and relatively well defined coordination environment. Progress is being made toward the synthesis of a cryptate formed by linking the amine nitrogens of two 1,4,7,10,13-pentaazacyclododecane ([15]aneN_5) macrocycles with methylene groups by a template synthesis approach.

Interest in further investigating the potential and significance of amide donors in ligands for lanthanide ions has involved exploring the utility of oxamide and oxamic acid groups. Initial results indicate that these functionalities are potentially good bidentate chelating ligands for lanthanide ions, and they will be studied as part of modified DTPA-based ligands as well as of other unique ligand structures.

4. P.H. Smith *et al.*, Inorg. Chem. 27, 4154 (1988).

II. Synthetic and Structural Studies of Actinides and Other Compounds

Richard A. Andersen, Investigator

5. Preparation and Synthetic Utility of $MCl_4(Me_2NCH_2CH_2NMe_2)_2$ Where M is Uranium or Thorium

P.G. Edwards, M. Weydert, M.A. Petrie, and R.A. Andersen

Uranium tetrachloride or thorium tetrachloride dissolves in a solution of $Me_2NCH_2CH_2NMe_2$ (tmed) in toluene to give green $UCl_4(tmed)_2$ or colorless $ThCl_4(tmed)_2$. These eight-coordinate compounds are soluble in aromatic or ethereal solvents, which makes them ideal synthons for further synthetic reactions. As an example, $ThCl_4$ is brick insoluble in solvents such as tetrahydrofuran (THF). Thus, refluxing a suspension of $ThCl_4$ with three molar equivalents of $NaMeC_5H_4$ in THF for 30 h gives $(MeC_5H_4)_3ThCl$ that is contaminated by $(MeC_5H_4)_4Th$. Separation of the latter from the former yields the former in about 30% isolated yield. In contrast, stirring a THF solution of $ThCl_4(tmed)_2$ with three molar equivalents of $NaMeC_5H_4$ at room temperature for 9 h yields $(MeC_5H_4)_3ThCl$ in 60% yield; no $(MeC_5H_4)_4Th$ is observed. Using four molar equivalents of $NaMeC_5H_4$ with $ThCl_4(tmed)_2$ in THF gives $(MeC_5H_4)_4Th$ in a yield of 85%. The uranium complex, $UCl_4(tmed)_2$, provides no such advantage, since base-free UCl_4 is soluble in THF. The chloride anions can be exchanged for bromide or iodide by refluxing $MCl_4(tmed)_2$, (M = Th or U) with neat Me_3SiX (X = Br, I). The resulting complexes are nonstoichiometric, having a composition of $MX_4(tmed)_x$ where M is Th or U, X is Br or I, and X lies between 1 and 2. The tmed ligands can be exchanged with phosphines such as $Me_2PCH_2CH_2PMe_2$(dmpe) to give $MX_4(dmpe)_2$. The synthetic utility of the tmed compounds is therefore demonstrated.

6. Preparation and Crystal Structure of the Eight-Coordinate Complexes Uranium Tetrachloridebis-[1,2-dimethylarsinobenzene], or $UCl_4(diars)_2$, and Uraniumtetrachloridebis[1,2-dimethylphosphinobenzene], or $UCl_4(diphos)_2$

J.S. Parry, P.G. Edwards, M.A. Petrie, R.A. Andersen, F.J. Hollander, and R.W. Gellert

The eight-coordinate phosphine and arsine compounds of the composition $UCl_4(diphos)_2$ and $UCl_4(diars)_2$ have been characterized by x-ray crystallography. The molecules are isostructural, and one ORTEP diagram is shown in Figure 6-1. The solid-state structures have I42m symmetry, the metal atom sitting on the $\bar{4}$ axis so that the molecules are described as a D_{2d}-dodecahedron. This geometry is maintained in solution. A solution of $UCl_4(diphos)_2$ in C_7D_8 does not exchange with added diphos at temperatures up to 110 °C, since the ^1H NMR spectrum shows the unperturbed resonances of both molecules and a plot of δ vs. $T^{-1}(K)$ is identical to that observed in C_7D_8 without added diphos. The $UCl_4(diars)_2$ behaves similarly, i.e., added diars does not exchange with coordinated diars up to 110 °C.

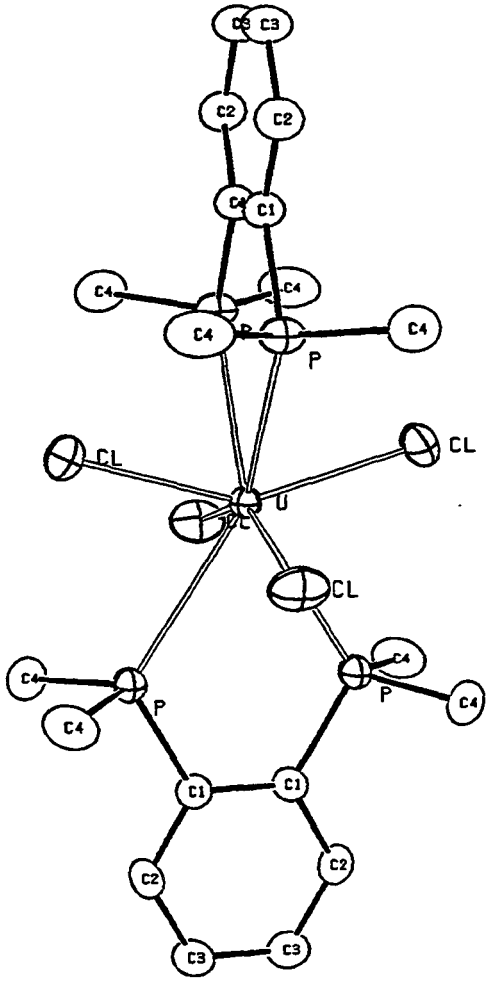

Figure 6-1. ORTEP view of $UCl_4(diphos)_2$. (XBL 947-4165)

7. Preparation of $(Me_3CC_5H_4)_4 M_2(\mu\text{-}Me)_2$ (M = Ce or U) and the Crystal Structure of the Cerium Derivative

S.D. Stults, R.A. Andersen, and A. Zalkin

The bridging methyl compound $(Me_3CC_5H_4)_4Ce_2(\mu\text{-}Me)_2$ is prepared from $(Me_3CC_5H_4)_3Ce$ or $(Me_3CC_5H_4)_4Ce_2(\mu\text{-}SCHMe_2)_2$ and MeLi in hydrocarbon solvents. The solid-state x-ray structure of the cerium methyl groups [orthorhombic, C_{mca}, a = 23.477(4) Å, b = 9.599(2) Å, c = 16.457(3) Å, V = 3708.7 Å^3, and Z = 4] shows that the methyl groups bridge the two $(Me_3CC_5H_4)_2Ce$ units such that the geometry at cerium is four-coordinate and pseudotetrahedral, in a symmetrical fashion. (See Figure 7-1.) The Ce–C(μ-Me) distance is 2.665(6) Å, and the Ce–C(μ-Me)–Ce angle is 89.9(3)°. All of the hydrogen atoms were located and refined isotropically; C–H (ave.) = 0.85 Å and H–C–H (ave.) = 108° for the bridging methyl group. The geometry of the bridging methyl group in $(Me_3CC_5H_4)_4Ce_2(\mu\text{-}Me)_2$ is similar to that in $(Me_4Al_2(\mu\text{-}Me)_2$. The uranium methyl group is prepared in the reaction of $(Me_3CC_5H_4)_3U$ and MeLi. The cerium and uranium methyl groups are unstable in the gas phase and in benzene solution, since they rearrange to $(Me_3CC_5H_4)_3M$ (M = Ce or U) and other materials.

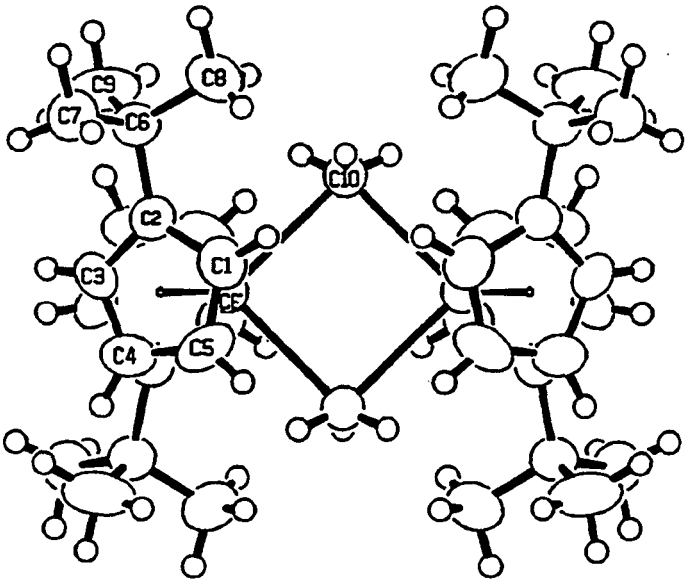

Figure 7-1. Structure of $(Me_3CC_5H_4)_4Ce_2(\mu\text{-}Me)_2$, showing the methyl groups bridging the two $(Me_3CC_5H_4)_2Ce$ units. (XBL 947-4166)

III. Physical and Spectroscopic Properties

Norman M. Edelstein, Investigator

8. Optical Spectroscopic Studies On Uranyl Chloride, UO_2Cl_2

J.C. Krupa, E. Simoni, J. Sytsma, and N. Edelstein

The absorption and emission spectra of single crystals of UO_2Cl_2 have been obtained at low temperature. Absorption spectra at 4.2 K are composed of progressions in the UO_2^{2+} symmetric vibrational mode separated by an interval of 748 cm^{-1}. Low-lying, weak, zero-phonon transitions arise from the excitation of a σ_u valence electron belonging to a molecular orbital constructed mainly from the oxygen 2p and uranium 5f and 6d atomic orbitals to the almost pure 5f empty orbitals of uranium(VI). These electronic transitions are accompanied by numerous vibronic side bands representing the density of states of the lattice phonons. Emission spectra (Figure 8-1), in which a higher energy progression mode (875 cm^{-1}) is also observed, show three prominent components. The first of these (1) is assigned to the pure electronic transition at 20549 cm^{-1}, and the other features (2 and 3) are attributed to vibronic transitions. A schematic orbital energy diagram proposed for UO_2Cl_2 is shown in Figure 8-2. The configuration coordinate model has been used to explain

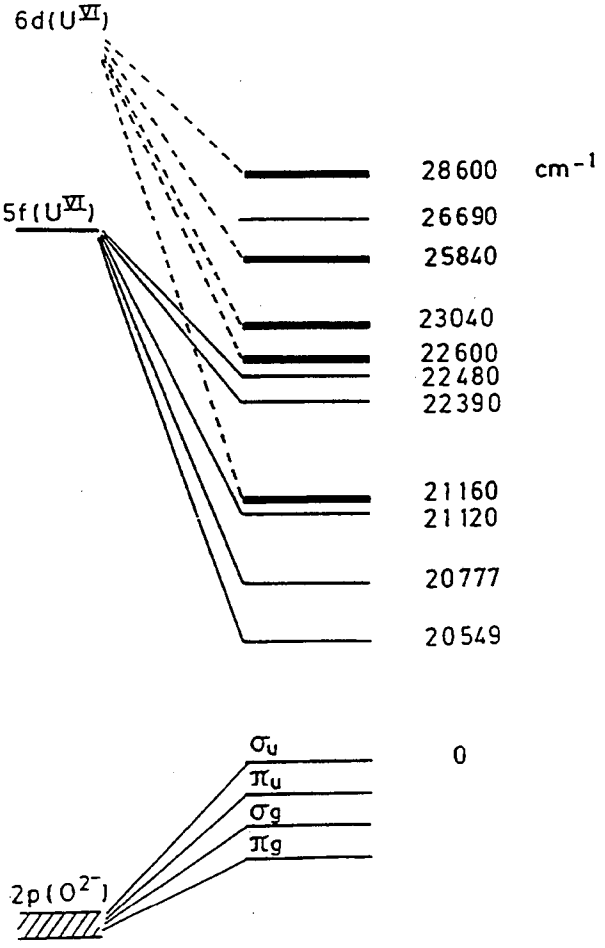

Figure 8-2. Schematic energy level diagram of UO_2Cl_2. (XBL 947-4168)

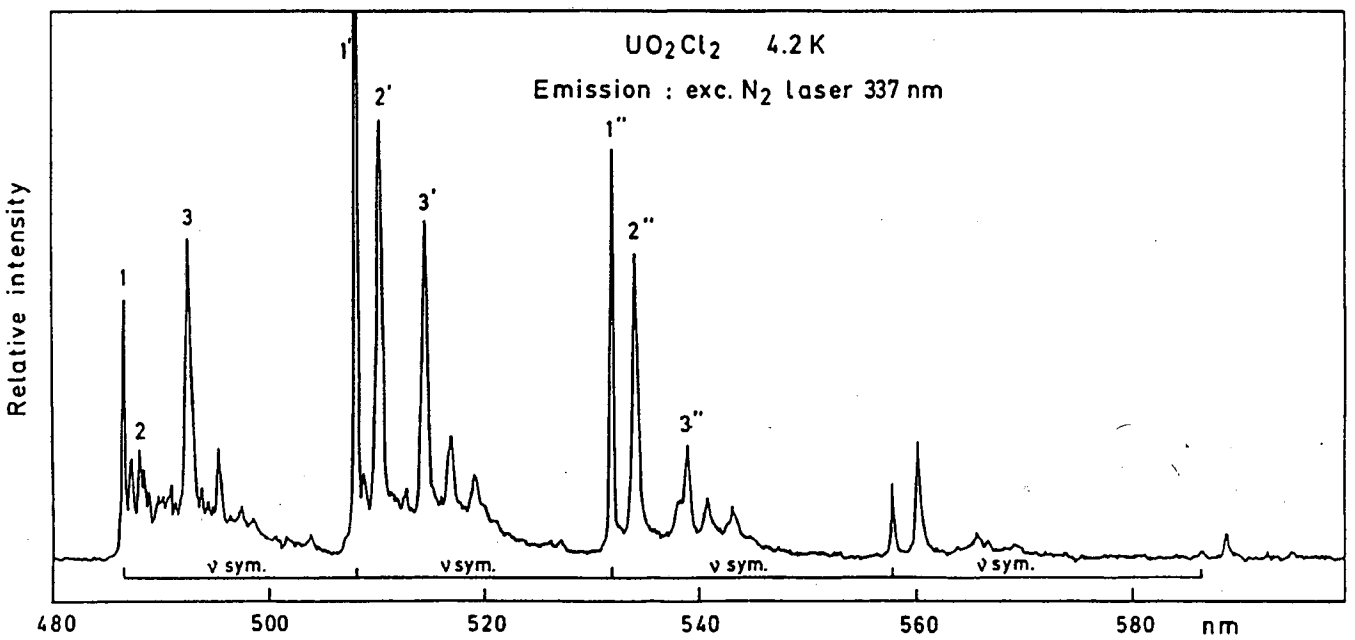

Figure 8-1. Emission spectrum of UO_2Cl_2 recorded at 4.2 K in the 480–600-nm region showing progressions separated by an interval of 875 cm^{-1}. (XBL 947-4167)

the shapes of broadband transitions that are attributed to electron transfer from the highest occupied orbital to unoccupied orbitals showing a large 6d character.

9. Electron Paramagnetic Resonance Spectrum of Pr^{4+} in $BaCeO_3$

Y. Hinatsu and N. Edelstein

The electron paramagnetic resonance (EPR) spectrum of a powder of Pr^{4+} in $BaCeO_3$ was measured at 8.5 K. (See Figure 9-1.) A very large hyperfine interaction with the ^{141}Pr nucleus was observed. In addition to the allowed hyperfine transitions, forbidden hyperfine transitions were observed. The results were analyzed based on the weak field approximation (i.e., the Breit–Rabi formula). The g value, $|g| = 0.745(1)$, and the hyperfine coupling constant, $|A| = 0.0606(2)$ cm^{-1}, were obtained. By using the measured g value and the $\Gamma_7 \rightarrow \Gamma_8$ crystal field transition for $BaPrO_3$ obtained from an earlier inelastic neutron scattering experiment and setting the spin–orbit coupling constant to its free-ion value, $\zeta = 865$ cm^{-1}, the energy levels of Pr^{4+} in $BaCeO_3$ were calculated. The measured magnetic susceptibility of $BaPrO_3$ was compared to the values calculated with the above model. The strength of the crystal field interaction relative to the spin–orbit coupling interaction is shown in Figure 9-2 for a number of $4f^1$ and $5f^1$ octahedral complexes.

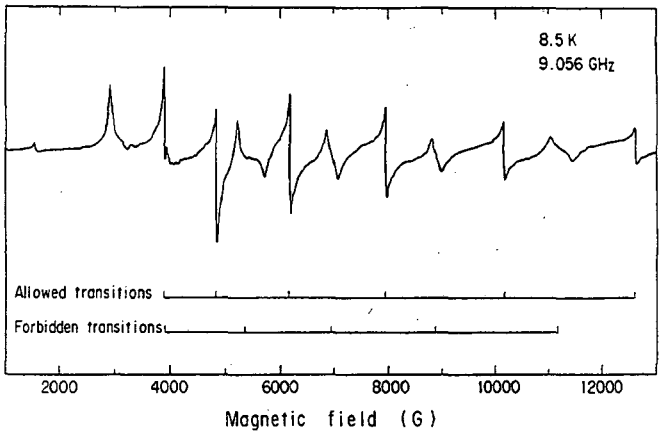

Figure 9-1. EPR spectrum of $BaPr_{0.02}Ce_{0.98}O_3$ at 8.5 K. Positions (resonance fields) calculated for allowed and forbidden transitions are also shown. (XBL 947-4169)

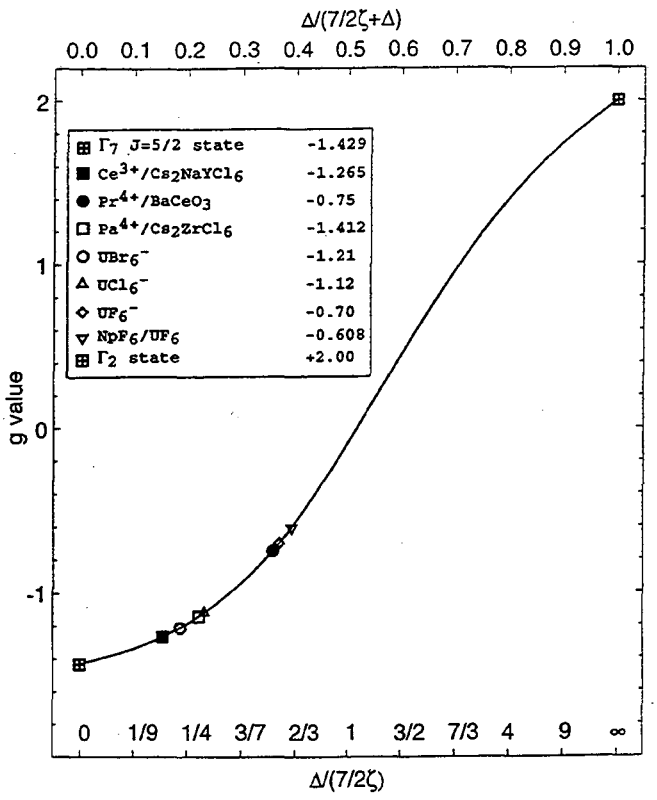

Figure 9-2. The g value vs. the ratio $\Delta/(7/2\zeta)$ for a number of f^1 compounds in octahedral symmetry. (XBL 947-4170)

10. The Electronic Structure of Organometallic Complexes of the f Elements XXXVI: Parameterization of the Crystal Field Splitting Pattern of $(CH_3OCH_2CH_2C_5H_4)_3Sm^{III}$

C. Qian, B. Wang, N. Edelstein, H. Reddmann, C. Hagen, and H.-D. Amberger

Bis base adducts of the moiety Cp_3U^+ ($Cp = \eta_5\text{-}C_5H_5$) have been known for more than four decades, but bis nitrile adducts derived from Cp_3Ln (Ln = La, Ce, Pr) were first described in 1985. Large single crystals of $Cp_3Nd(NCCH_3)_2$ can be grown; however, these crystals decompose within approximately one week when sealed in an inert atmosphere. Recently, it was found that $Cp_3Sm(NCCH_3)_2$ could be chemically stabilized by diluting a $Cp_3La(NCCH_3)_2$ matrix with about 20% of $Cp_3Sm(NCCH_3)_2$. Qian *et al.* have synthesized Cp'_3Ln

complexes (Cp′ = $CH_3OCH_2CH_2C_5H_4$; Ln = Ce–Yb), where two of the three Cp′ groups coordinate almost axially the pseudo-trigonal-plane Cp_3Ln moiety via the oxygen atoms. In contrast to the bis nitrile adducts, these complexes are stable in inert solvents such as glassy, freezing mixtures of methylcyclohexane and toluene in the ratio 1:1.

The low-temperature optical absorption and luminescence spectra of Cp'_3Sm dissolved in methylcyclohexane and toluene (ratio, 1:1) have been obtained. In addition, the magnetic susceptibility of Cp'_3Sm at low temperature has been measured. The optical spectra appear similar to those of $Cp_3La_{0.8}Sm_{0.2}(NCCH_3)_2$ and are assigned on that basis. Because the symmetry of Cp'_3Sm deviates from the D_{3h} symmetry of the nitrile compound, some of the weak lines are assigned to transitions that are forbidden under strict D_{3h} symmetry. On this basis, 42 levels have been assigned with an rms (root mean square) deviation of 42 cm^{-1}. The calculated magnetic susceptibility is in satisfactory agreement with the measured values.

11. The Hydrolysis Behavior of the Transuranium Elements

B. Jung, N.M. Edelstein, and G.T. Seaborg

In recent years, much of the research emphasis has shifted from the classical inorganic chemistry of the transuranium elements to topics that are more related to environmental aspects. These research projects are driven mainly by the need to evaluate initiatives for the safe disposal of nuclear waste in geologic repositories. One major concern is the possible leakage of nuclear waste containers, resulting in the contamination of the disposal site and surrounding environment and groundwater with radioactive material. Hence, the question arises of the identification of migrating species and the solubility-controlling phases under ambient conditions at a disposal site. In principle, this question can be answered only by a thorough description of the solution and heterogeneous equilibria under geochemical conditions, coupled with an accurate thermodynamic database for geochemical modeling and transport calculations. Despite efforts during the past five decades, definitive thermodynamic data are not available. The purpose of this review is to summarize recent work on the hydrolysis of transuranium ions for the oxidation states found in aqueous solution, An^{3+}, An^{4+}, AnO_2^+, and AnO_2^{2+}.

The data in the literature cover a wide range of ionic strengths and are usually obtained at ambient temperature or 25 °C. A number of solubility studies have been reported, approached both from undersaturation and oversaturation, but in most cases the solid materials that result from these studies are not well characterized. In solutions with high concentrations of salts, radiolysis effects play a major role in determining the oxidation states of the actinide ions under steady-state conditions. The times to reach steady-state conditions in some measurements reported in this survey varied from days to years, even with experiments run under similar conditions. New spectroscopic methods have now been utilized to determine the speciation in solution directly and to verify the species derived from potentiometric and solubility data.

In general, experimenters performing recent hydrolysis studies have recognized some of the problems in earlier work (such as the need to work in an inert atmosphere in order to avoid carbonate contamination), and these studies should be more reliable, especially when coupled with direct spectroscopic methods for species determination. The major problems associated with solubility studies remain the attainment of steady-state conditions, the identification of solid phases, and control of the redox conditions. Measurements of hydrolysis reactions and solubilities at temperatures other than 25 °C or ambient values are almost nonexistent.

IV. Actinide Synchrotron Radiation Program

David Shuh and Norman M. Edelstein, Investigators

INTRODUCTION

The proposed Environmental and Actinide Beamline (EAB) at the Advanced Light Source (ALS) will be a unique experimental facility used to investigate both fundamental and technological aspects of the chemistry and physics of environmentally relevant solid-state materials systems, many of which contain radioactive elements. The scientific and technological merits of the EAB facility have been critically addressed in the workshop held at LBL entitled "Synchrotron Radiation in Transactinium Research."

The entire EAB facility has been redesigned conceptually to achieve state-of-the-art photon energy resolution and throughput from ~10–1500 eV. The EAB safety concerns are being discussed with the appropriate personnel at the ALS. An interim solid-state synchrotron endstation without a safety enclosure has been fabricated, and the collaborative use of the system to investigate the surface chemistry of uranium is anticipated at SSRL in FY 1994.

Synchrotron radiation investigations in the x-ray regime continue to be pursued and exploited, since radioactive and hazardous materials may be safely contained for *in situ* investigations at these energies. X-ray Absorption Spectroscopy (XAS) techniques are useful, nondestructive probes employed to ascertain oxidation states of materials by X-ray Absorption Near Edge Structure (XANES) analysis and structural information from Extended X-ray Absorption Fine Structure (EXAFS) analysis. The XAS methodologies are compatible with low-concentration samples and are also highly amenable to studies of solutions, both of which are of the utmost importance for environmental purposes. Thus, these methodologies are well suited for detailed investigations of actinide materials, fission products, and other environmentally relevant systems.

Instrumentation development has been initiated to better utilize the available beamtime and to enable the study of systems that have an inherently low signal-to-background ratio. Remote sample handling and positioning, as well as sample packaging methods, have been addressed in order to ensure efficient data collection. Fabrication of a four-element germanium solid-state detector has been initiated specifically for use in a storage ring environment to improve the maximum attainable count rate from a fluorescence detector to approximately 5×10^5 counts/s.

12. X-ray Absorption Spectroscopy of the Rare Earth Orthophosphates†

D.K. Shuh, L.J. Terminello, L.A. Boatner, and M.M. Abraham

The electronic structures of the Rare Earth (RE) ions in the orthophosphates are of particular interest because RE orthophosphate materials are analogs of the corresponding actinide orthophosphates, which have been considered for nuclear waste disposal and are ideal host materials for optically active metal ions. Also, the lightly Ce-doped $LuPO_4$ has recently attracted interest as a new scintillator material. The XAS investigations of RE ions for characterizing electronic properties are ideal as a result of strong quasi-atomic $3d^{10}4f^n \rightarrow 3d^94f^{n+1}$ transitions. The XAS spectra of the RE ions in the orthophosphate matrix generally resemble the XAS spectra of the corresponding RE metals. This is not unexpected and emphasizes the major contribution of the trivalent state to the electronic transitions occurring at the RE metal 3d edges. These spectra unequivocally identify the transitions originating from well-characterized RE cores and correlate well with previous theoretical investigations.

†This work was performed in part at SSRL, which is operated by the Department of Energy, Division of Chemical Sciences.

13. Work in Progress‡

Characterization of Ce-Doped $LaPO_4$ by X-Ray Absorption Spectroscopy

D.K. Shuh, L.J. Terminello, L.A. Boatner, M.M. Abraham, and D. Perry

The XAS spectra of the Ce $M_{4,5}$ edges of $CePO_4$, CeO_2, and the range of Ce-doped lanthanum orthophosphates are shown in Figure 13-1. The spectrum from $CePO_4$ shown in Figure 13-1 is generally

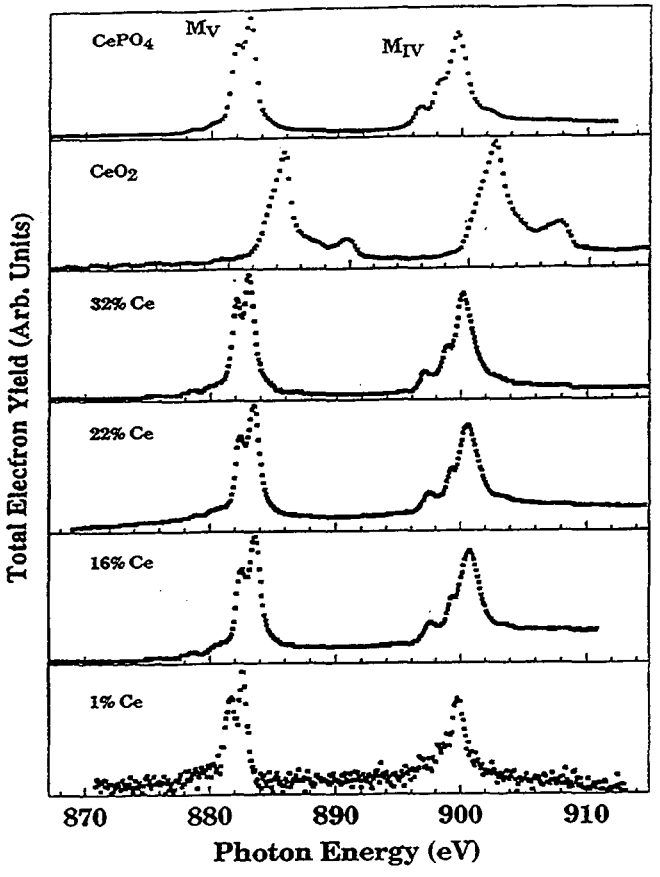

Figure 13-1. XAS spectra at the Ce $M_{4,5}$ edge of $CePO_4$, CeO_2, and the Ce-doped lanthanum orthophosphates collected with the monochromator diffraction grating satisfying the second-order Bragg condition to improve the spectral resolution. The spectra have been normalized to the largest respective feature. (XBL 947-4171)

representative of the total-yield spectra of the RE orthophosphates. The spin–orbit split Ce $3d_{5/2}$ and $3d_{3/2}$ peaks are the predominant features of the spectrum, whereas the exchange interaction provides the observed fine structure on each of the spin–orbit pairs. The XAS measurements confirm the Ce dopant concentrations in the $LaPO_4$ matrices to within ~1%. The Ce 3d spectra from the Ce-doped host materials show no appreciable energy shift or line-width difference compared to $CePO_4$. All of the Ce 3d orthophosphate spectra are chemically shifted to lower energy than the Ce 3d signal from CeO_2, indicating that the Ce ions occupy trivalent sites. The La $M_{4,5}$ edge spectra of $LaPO_4$ and of the corresponding range of Ce-doped lanthanum orthophosphates were also measured. The energy positions of the La absorption peaks from the Ce-doped samples are the same within experimental error. The full width half maximum (FWHM) of the La $3d_{5/2}$ decreases slightly with decreasing Ce content, but the experimental data are insufficient to firmly establish this relationship.

The results demonstrate that XAS techniques are capable of investigating and characterizing fundamental electronic properties of RE-containing optical materials that have RE concentrations at the 1% level. There is no appreciable energy shift of either the La or Ce 3d absorption peak positions from the Ce-doped $LaPO_4$ materials from those observed in well-characterized, undoped, single-crystal orthophosphate reference materials. Thus, the La and Ce spectra clearly indicate that the Ce doping of $LaPO_4$ is purely substitutional.

‡This work was performed in part at SSRL, which is operated by the Department of Energy, Division of Chemical Sciences.

X-Ray Absorption Near Edge Structure Investigations of Selenium Speciation After Bacterial Uptake

D.K. Shuh, N.M. Edelstein, J.J. Bucher, N. Kaltsoyannis, H. Nitsche, P. Torretto, K. Roberts, W. Lukens, I. Al Mahamid-Al Rifai, T. Leighton, and B. Buchanan

The concentration and stabilization of hazardous materials by microbial agents offers great potential for use in environmental remediation technologies. The *in situ* analysis of selenium following uptake by a common soil bacterium has been investigated by XANES in order to elucidate the speciation of the contaminant in the biomass. The aerobic soil bacterium, *Bacillus subtilus*, is known to incorporate Se somewhere within the vegetative bacterium (within the cell membrane), although the exact mechanism of uptake is not fully understood. The microbes were exposed to one of two Se solutions of different oxidation states, either selenite or selenate. The bacteria were prepared for the XAS investigations by centrifugation, washing, and resuspension.

The XANES measurements were performed at the SSRL on the wiggler branch beamline 4-1, utilizing Si(220) monochromator crystals that were detuned ~50% at the Se K edge (12.7 keV). The speciation of Se was determined by the charge state shifts at the Se K edge in comparison to respective standard materials. The Se XANES spectra of the two *B. subtilus* strains, B and K, after uptake of Se from a sodium selenite(IV) solution are shown in Figure 13-2. The bacteria did not, however, incorporate Se from the sodium selenate(VI) growth solution. Figure 13-2 includes the Se XANES spectra from the well-defined oxidation states of Se metal, a SeO_3^{2-} solution, and a SeO_4^{2-} solution for comparison to those from the microbes. The spectra in Figure 13-2 show that both *B. subtilus* strains take up Se(IV) and reduce the Se(IV) to Se metal.

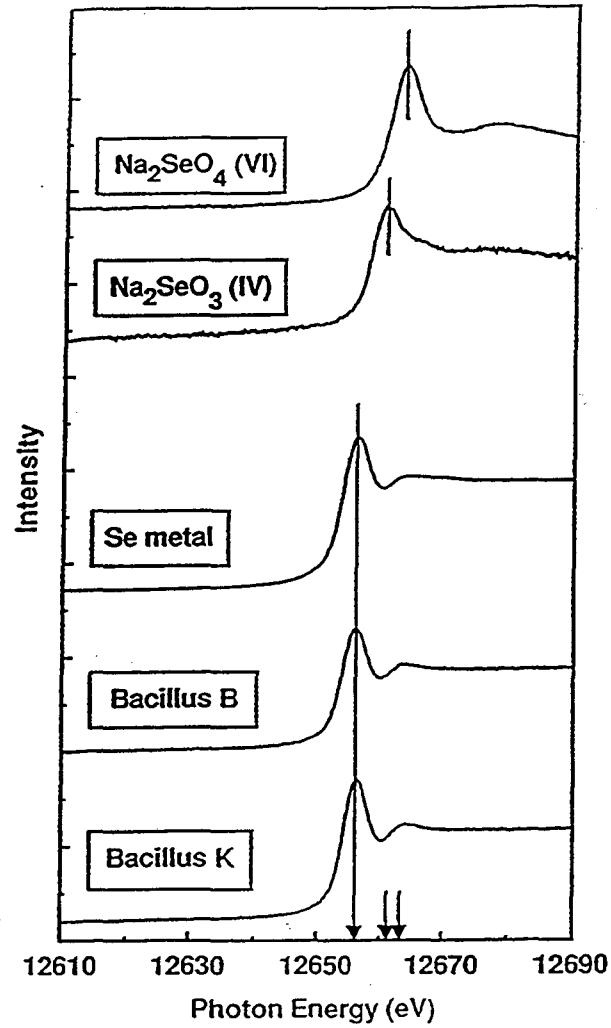

Figure 13-2. The Se K edge XANES spectra from *Bacillus subtilus*, strains B and K, after microbial uptake and the Se reference standards. (XBL 947-4172)

XANES Investigation of the Speciation of Tc in Cement After Chemical Treatment

D.K. Shuh, N.M. Edelstein, J.J. Bucher, N. Kaltsoyannis, H. Nitsche, S. Clark, I. Al Mahamid-Al Rifai, P. Torretto, W. Lukens, and K. Roberts

The immobilization of Tc in nuclear waste packaging materials, originally present as pertechnetate (TcO_4^-) in nuclear waste process streams, is a major concern. A proposed method to accomplish this task in cementitious wasteforms includes the addition of "slag" (a source of reduced Fe) to the primary cement formulation to reduce pertechnetate to insoluble TcO_2. The efficacy of the proposed process was determined by XANES measurements at SSRL with Si(220) monochromator crystals on the wiggler branch beamline 4-1.

Spectra were collected at the Tc K edge (~21.0 keV) for cements prepared with and without slag from a simulated waste stream spiked with pertechnetate. Technetium reference materials were collected simultaneously to establish Tc chemical shifts and for energy calibrations. The pertechnetate standard solutions were prepared from ammonium pertechnetate; TcO_2, by thermal decomposition of ammonium pertechnetate; and a slightly oxygen-deficient TcO_2, by controlled electrodeposition from a pertechnetate solution onto a gold-plated copper electrode.

The XANES spectra of the Tc-containing cements and the Tc standards [TcO_2(IV), electrodeposited TcO_2(IV), and TcO_4^-(VII)] are presented in Figure 13-3. There is a pre-edge feature present in the TcO_4^- spectra that arises from a second-order symmetry-allowed electronic transition that clearly fingerprints the Tc(VII) oxidation state. The spectra of TcO_2 have no pre-edge feature and exhibit edge positions significantly shifted from that of TcO_4^-. Comparison of the XANES spectrum of Tc in untreated cement to that of Tc in slag-treated cement shows that the oxidation state of Tc is the same in the both cements and that both display the pre-edge signature. Thus, the addition of slag to the cement formulation does not significantly reduce the TcO_4^- to TcO_2 in these samples. The same Tc samples were re-examined several months later, employing the same experimental techniques, and the results were identical. Additionally, the preliminary analysis of the EXAFS (Extended X-ray Absorption Fine Structure) results from both TcO_2 and Tc metal has been performed.

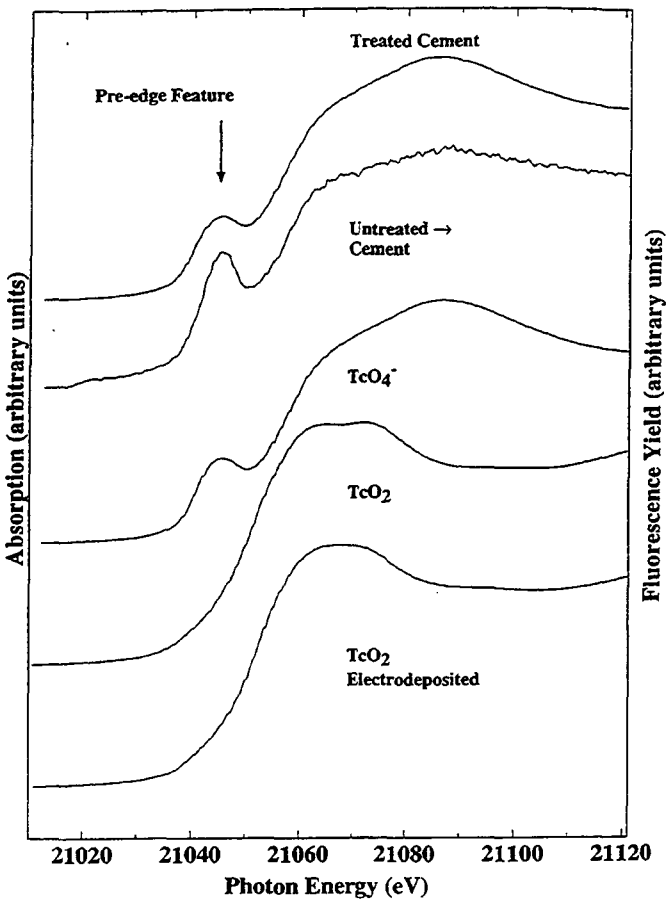

Figure 13-3. Technetium near edge spectra from cement samples and from Tc-containing materials used as reference standards. The pre-edge feature, indicative of tetrahedral coordination of the Tc species, is clearly evident. Spectra have been normalized to equivalent peak heights and aligned with respect to the experimental TcO_2 edge at 21,051 eV. (XBL 947-4173)

FY 1993 PUBLICATIONS AND REPORTS

Refereed Journals

1. G.N. Stradling, S.A. Gray, J.C. Moody, M.J. Pearce, I. Wilson, R. Burgada, T. Bailly, Y. Leroux, K.N. Raymond, and P.W. Durbin, Int. J. Rad. Biol. **64**, 133–140 (1993); LBL-35117.
2. J.L. Poncy, G. Rateau, R. Burgada, T. Bailly, Y. Leroux, K.N. Raymond, P.W. Durbin, and R. Masse, Int. J. Rad. Biol. **64**, 431-436 (1993); LBL-35118.
3. M.R. Smith, III, P.T. Matsunaga, and R.A. Andersen, "Preparation of Monomeric $(Me_5C_5)_2$ VO and $(Me_5C_5)_2$

Ti(O)(L) and their Decomposition to $(Me_5C_5)_4M_4(\mu\text{-}O)_6$," Am. Chem. Soc. **115**, 7049 (1993).

4. M. Weydert, R.A. Andersen, and R.G. Bergman, "Reactions of $(Me_5C_5H_4)_3U(t\text{-}Bu)$: Intermolecular Fluorine Atom Abstraction from Fluorocarbons Including Saturated Perfluorocarbons," J. Am. Chem. Soc. **115**, 8837 (1993).
5. W.K. Kot, N.M. Edelstein, M.M. Abraham, and L.A. Boatner, "Electron Paramagnetic Resonance of Pu^{3+} and Cf^{3+} in Single Crystals of $LuPO_4$," Phys. Rev. B **47**, 3412 (1993).
6. C.-K. Loong, L. Soderholm, M.M. Abraham, L.A. Boatner, and N.M. Edelstein, "Crystal-Field Excitations and Magnetic Properties of $TmPO_4$," J. Chem. Phys. **98**, 4214 (1993).
7. N.M. Edelstein and W.K. Kot, "Spectroscopic and Magnetic Studies of Tetravalent Pa and Trivalent Th Compounds," J. Alloys & Compounds **193**, 82 (1993).
8. K. Krämer, L. Keller, P. Fischer, B. Jung, N.M. Edelstein, H.-U. Güdel, and G. Meyer, "Magnetic and Crystal Structure Determination of K_2UBr_5," J. Solid State Chem. **103**, 152 (1993).
9. C.-K. Loong, L. Soderholm, J.P. Hammonds, M.M. Abraham, L.A. Boatner, and N.M. Edelstein, "Neutron Study of Crystal-Field Transitions in $ErPO_4$," J. Appl. Phys. **73**, 6069 (1993).
10. J. Sytsma, D. Piehler, N.M. Edelstein, L.A. Boatner, and M.M. Abraham, "Two-Photon Excitation of the $4f^1 \rightarrow 5d^1$ Transitions of Ce^{3+} in $LuPO_4$ and YPO_4," Phys. Rev. B **47**, 14786 (1993).
11. C.-K. Loong, L. Soderholm, J.P. Hammonds, M.M. Abraham, L.A. Boatner, and N.M. Edelstein, "Rare-Earth Energy Levels and Magnetic Properties of $HOPO_4$ and $ErPO_4$," J. Phys. Condens. Matter **5**, 5121 (1993).
12. S. Hubert, P. Thouvenot, and N. Edelstein, "Spectroscopic Studies and Crystal-Field Analyses of Am^{3+} and Eu^{3+} in the Cubic-Symmetry Site of ThO_2," Phys. Rev. B **48**, 5751 (1993).
13. W.K. Kot, N.M. Edelstein, M.M. Abraham, and L.A. Boatner, "Zero-Field Splitting of Cm^{3+} in $LuPO_4$ Single Crystals," Phys. Rev. B **48**, 12704 (1993).
14. D.K. Shuh, L.J. Terminello, L.A. Boatner, and M.M. Abraham, "X-ray Absorption Spectroscopy of the Rare Earth Orthophosphates," Mater. Res. Soc. Symp. Proc. **307**, 95–100 (1993).

LBL Reports

15. D.W. Whisenhunt, Jr. and K.N. Raymond, "Thermodynamic Stability of the Th(IV) Desferrioxamine B (DFO) Complex," LBL-35199.
16. S.J. Franklin and K.N. Raymond, "Solution Structure and Dynamics of the Lanthanide Complexes of the Macrocyclic Polyaminocarboxylate (DTPA-dien); An NMR Study and the Crystal Structures of the Lanthanum (III) and Europium (III) Complexes," LBL-35200.
17. P.G. Edwards, M. Weydert, M.A. Petrie, and R.A. Andersen, "Preparation and Synthetic Utility of $MCl_4(Me_2NCH_2CH_2NMe_2)_2$ Where M is Uranium or Thorium," LBL-34661.
18. J.S. Parry, P.G. Edwards, M.A. Petrie, R.A. Andersen, F.J. Hollander, and R.W. Gellert, "Preparation and Crystal Structure of the Eight-Coordinate Complexes, Uranium Tetrachloridebis [1,2-dimethylarsinobenzene], $UCl_4(diars)_2$, and Uraniumtetrachloridebis [1,2-dimethylphosphinobenzene], $UCl_4(diphos)_2$," LBL-29694.
19. S.D. Stults, R.A. Andersen, and A. Zalkin, "Preparation of $(Me_3CC_5H_4)_4M_2(\mu\text{-}Me)_2$ (M = Ce or U) and the Crystal Structure of the Cerium Derivative," LBL-30499.
20. J.C. Krupa, E. Simoni, J. Sytsma, and N. Edelstein, "Optical Spectroscopic Studies on Uranyl Chloride UO_2Cl_2," LBL-35181.
21. Y. Hinatsu and N. Edelstein, "Electron Paramagnetic Resonance Spectrum of Pr^{4+} in $BaCeO_3$," J. Solid State Chem. (in press); LBL-34178.
22. C. Qian, B. Wang, N. Edelstein, H. Reddmann, C. Hagen, and H.-D. Amberger, "The Electronic Structure of Organometallic Complexes of the f Elements XXXVI. Parameterization of the Crystal Field Splitting Pattern of $(CH_3OCH_2CH_2C_5H_4)_3Sm^{III}$," LBL-34315.
23. B. Jung, N.M. Edelstein, and G.T. Seaborg, "The Hydrolysis Behavior of the Transuranium Elements," LBL-35183.
24. W. Lukens, "Tris(trimethylsilylcyclopentadienyl) Zirconium Chloride," LBL-34891.
25. E. Brady, W. Lukens, J.R. Telford, and G. Mitchell, "Bis(pentamethyl cyclopentadienyl) titanium amide," LBL-34892.
26. M.E. Smith, "Synthesis, Characterization, and Reactivity of Pentamethylcyclopentadienyl Complexes of Divalent Cobalt and Nickel," Ph.D. Thesis; LBL-34753.

Invited Talks

27. K.N. Raymond, "Metal Ion Specific and Stereognostic Coordination Chemistry," The University of Michigan, Ann Arbor, MI, October 5, 1992.
28. K.N. Raymond, "Stereognostic Coordination Chemistry of Oxo Metal Cations," Symposium on Molecular Recognition, ACS Meeting, Denver, CO, March 29–April 4, 1993.
29. K.N. Raymond, "Metal-Ion-Specific and Stereognostic Coordination Chemistry," Plenary Speaker, Conference on Metal Ions in Solution, Melelane Game Lodge, South Africa, April 21–23, 1993.
30. K.N. Raymond, "Thermodynamic Stability of Iron Siderophore Complexes and Iron Mobilization," Plenary Speaker, 11th International Conference on Iron and Iron Proteins—IP 11, Jerusalem, Israel, May 2–7, 1993.
31. K.N. Raymond, "Metal-Ion-Specific and Stereognostic Coordination Chemistry," Humboldt Senior Scientist Lecture, Ruhr University, Bochum, Germany, May 19, 1993; College of Liberal Arts & Science, Okayama University, Japan, June 12, 1993.

CHEMICAL ENGINEERING SCIENCES

Molecular Thermodynamics for Phase Equilibria in Mixtures*

John M. Prausnitz, Investigator

INTRODUCTION

Phase equilibria are required for design of efficient separation processes and of new products in the chemical and related industries. In this context, "efficient" refers to optimum use of raw materials and conservation of energy.

Since the variety of technologically important fluid mixtures is extremely large, it is not possible to obtain all equilibria from experiment. Therefore, the objective of this project is the development of molecular thermodynamics to interpret and correlate reliable experimental data in order to confidently predict phase equilibria for engineering. The correlations are expressed through semitheoretical, physicochemical models in a form suitable for computer-aided design. Particular attention is given to those materials that may be useful for innovative low-energy-consuming separation processes, such as polymers and gels, and polyelectrolyte systems with possible applications in biotechnology. However, attention is also devoted to conventional materials for applications in fuel technology and for recovery of solutes from waste water.

Development of molecular thermodynamics calls for a combination of theoretical, computational, and experimental work. Further, it requires simultaneous awareness of progress in molecular science and of realistic requirements for engineering design.

1. Liquid–Liquid Phase Separations in Aqueous Solutions of Globular Proteins (Publication 1)

V. Vlachy, H.W. Blanch, and J.M. Prausnitz

A simple statistical-mechanical theory, known as the random-phase approximation, is applied to study liquid–liquid phase separations in solutions of globular proteins. Phase separation may be induced by the addition of nonionic polymers and/or ordinary electrolytes. In this analysis, the osmotic-attraction mechanism, whereby the depletion of "solvent" particles between two proteins causes an attractive force, is primarily responsible for phase separation. For one component model of protein solutions, the theory yields simple algebraic expressions for the equation of state and for the chemical potential of the protein. This analytical theory describes the observed solubility behavior of proteins, including the effect of protein and polymer size, protein charge, and concentration of simple electrolytes.

2. Liquid–Liquid Equilibria in Binary Systems: Monte Carlo Simulations for Calculating the Effect of Nonrandom Mixing (Publication 2)

S.M. Lambert, D.S. Soane, and J.M. Prausnitz

Monte Carlo simulations of a lattice model for incompressible monomer/r-mer mixtures are used to obtain accurate results for the configurational energy of mixing. Based on simulation results, the energy of mixing is correlated as a function of temperature and composition using an empirical expression. The configurational Helmholtz energy is obtained upon using the Gibbs–Helmholtz equation with Guggenheim's athermal entropy of mixing as the boundary condition. Since Monte Carlo simulations give essentially exact results for the lattice model, the effects of nonrandom mixing on the configurational thermodynamic properties of a binary mixture can be determined. The expression generated here produces coexistence curves that are more accurate than those from other models, especially near the critical region.

3. Structural and Catalytic Properties of Enzymes in Reverse Micelles (Publication 3)

A.L. Creagh, H.W. Blanch, and J.M. Prausnitz

Structural and catalytic properties of two enzymes, α-chymotrypsin and horse-liver alcohol dehydrogenase (LADH), are studied in bis(2-ethylhexyl) sodium sulfosuccinate (AOT)-isooctane reverse-micelle solutions. Circular dichroism (CD) and electron paramagnetic resonance spectroscopy (EPR) studies show little change in α-chymotrypsin structure upon incorporation into reverse micelles. These structural properties explain, in part, the observed activity of these two enzymes in reverse micelles. The α-chymotrypsin retains activity in reverse micelles and, in some cases, displays enhanced activity. A sixfold increase in the turnover number has been observed in w_0 = 10 reverse micelles. LADH has low activity in reverse

*This work was supported by the Director, Office of Energy Research, Office of Basic Energy Sciences, Chemical Sciences Division, of the U.S. Department of Energy under Contract No. DE-AC03-76F00098.

micelles compared to that in aqueous solution. At $w_0 = 70$, the turnover number for LADH is 18% of the aqueous value. Active-site titrations show a decrease in active enzyme concentration for both enzymes upon incorporation into reverse micelles. Little change in the structures of both LADH and α-chymotrypsin is observed with change of water content in the reverse-micelle system.

4. Lattice Thermodynamics for Binary Closed-Loop Equilibria: Ordinary and Polymer Systems (Publication 4)

T. Hino, S.M. Lambert, D.S. Soane, and J.M. Prausnitz

The incompressible lattice-gas model by Brinke and Karasz is adopted to introduce the effect of specific interactions into a recently-presented Monte-Carlo-based lattice expression for the Helmholz energy of nonrandom mixing. While the lattice remains incompressible, intermolecular forces consist of two types: London dispersion forces and specific (chemical) forces. The specific interactions between similar components, as well as those between dissimilar components, are incorporated in a systematic manner. Closed-loop, temperature-composition phase diagrams are obtained. The theory is compared with experimental data for several binary systems, including polymer solutions, that exhibit closed-loop coexistence curves. Theoretical and experimental results are in good agreement.

5. Application of Integral-Equation Theory to Aqueous Two-Phase Partitioning Systems (Publication 5)

C.A. Haynes, F.J. Benitez, H.W. Blanch, and J.M. Prausnitz

A molecular-thermodynamic model is developed for representing thermodynamic properties of aqueous two-phase systems containing polymers, electrolytes, and proteins. The model is based on the McMillan–Mayer solution theory and the generalized mean-spherical approximation to account for electrostatic forces between unlike ions. The Boublik–Mansoori equation of state for hard-sphere mixtures is coupled with the osmotic virial expansion truncated after the second-virial terms to account for short-range forces between molecules.

Osmotic second virial coefficients are reported from low-angle laser-light-scattering (LALLS) data for binary and ternary aqueous solutions containing polymers and proteins. Ion–polymer specific-interaction coefficients are determined from osmotic-pressure data for aqueous solutions containing a water-soluble polymer and an alkali chloride, phosphate, or sulfate salt.

When coupled with LALLS and osmotic-pressure data reported here, the model is used to predict liquid–liquid equilibria, protein-partition coefficients, and electrostatic potentials between phases for both polymer–polymer and polymer–salt aqueous two-phase systems. For bovine serum albumin, lysozyme, and α-chymotrypsin, predicted partition coefficients are in excellent agreement with the experiment.

6. Monte Carlo Simulations of a Hydrophobic Weak Polyelectrolyte. Charge Distribution as a Function of Conformation (Publication 6)

J.L.F. Abascal, A. Sassi, H. Blanch, and J.M. Prausnitz

The radial distribution of charges for a 40-segment, self-avoiding, lattice-model, hydrophobic, weak polyelectrolyte was examined using Monte Carlo simulations in the grand canonical ensemble. The fraction of ionizable segments was 0.325. Nonbonded nearest-neighbor segments interacted with a fixed potential, ε. Only cases where $\varepsilon < 0$ were considered so as to present polymer hydrophobicity. The interaction between ionized segments was described by a screened Debye–Huckel coulombic potential. If the polymer chain adopted a highly-collapsed configuration, changes were clustered predominantly on the surface, and the surface ionization was significantly greater than the average ionization. If, however, the charge density was sufficient to expand the chain into the extended conformation, the charge density was almost constant throughout the chain. For any combination of system variables, the average charge at a radial distance (from the center of mass) representing the mean extension of the chain was simply the mean ionization.

7. Miscibilities in Binary Copolymer Systems (Publication 7)

T. Hino, S.M. Lambert, D.S. Soane, and J.M. Prausnitz

A lattice theory is presented for liquid–liquid equilibria for binary systems containing random copolymers. This theory takes into account deviations from random mixing though a nonrandomness factor that follows from a generalization of Monte Carlo calculations for the three-dimensional Ising model. While the lattice remains incompressible, the effect of specific interactions (hydrogen

bonding) is introduced by superimposing on the nonrandom (Ising model) expression for the Helmholtz energy of mixing a correction based on the lattice-gas model by Brinke and Karasz. The resulting theory can predict immiscibility caused by lower critical solution temperatures. Several theoretical miscibility maps at a fixed temperature were computed. These are compared with those predicted by the random-mixing Flory–Huggins theory. Theoretical miscibility maps are also compared with experiments for a few systems with strong specific interactions.

FY 1993 PUBLICATIONS AND REPORTS

Refereed Journals

1. V. Vlachy, H.W. Blanch, and J.M. Prausnitz, "Liquid–Liquid Phase Separations in Aqueous Solutions of Globular Proteins," AIChE J. **39**(2), 215–223 (1993).
2. S.M. Lambert, D.S. Soane, and J.M. Prausnitz, "Liquid–Liquid Equilibria in Binary Systems: Monte Carlo Simulations for Calculating the Effect of Nonrandom Mixing," Fluid Phase Eq. **83**, 59–68 (1993).
3. A.L. Creagh, H.W. Blanch, and J.M. Prausnitz, "Structural and Catalytic Properties of Enzymes in Reverse Micelles," Enzyme Microb. Technol. **15**, 383–392 (1993).
4. T. Hino, S.M. Lambert, D.S. Soane, and J.M. Prausnitz, "Lattice Thermodynamics for Binary Closed-Loop Equilibria: Ordinary and Polymer Systems," AIChE J. **39**, 837–845 (1993).
5. C.A. Haynes, F.J. Benitez, H.W. Blanch, and J.M. Prausnitz, "Application of Integral-Equation Theory to Aqueous Two-Phase Partitioning Systems," AIChE J. **39**, 1539–1557 (1993); LBL-33927.
6. J.L.F. Abascal, A. Sassis, H. Blanch, and J.M. Prausnitz, "Monte Carlo Simulations of a Hydrophobic Weak Polyelectrolyte. Charge Distribution as a Function of Conformation," J. Chem. Phys. **99**(5), 4231 (1993); LBL-33763.
7. T. Hino, S.M. Lambert, D.S. Soane, and J.M. Prausnitz, "Miscibilities in Binary Copolymer Systems," Polymer **34**(22), 4756 (1993); LBL-33762.
8. A.L. Creagh, H.W. Blanch, and J.M. Prausnitz, "The Effect of Aqueous Surfactant Solutions on Alcohol Dehydrogenase (LADH)," Biotechnology and Bioengineering **41**, 156 (1993).
9. Y.C. Bae, J.J. Shim, D.S. Soane, and J.M. Prausnitz, "Representation of Vapor–Liquid and Liquid–Liquid Equilibria for Binary Systems Containing Polymers: Applicability of an Extended Flory–Huggins Equation," J. App. Polym. Sci. **47**,1193 (1993).
10. Y. Hu, X. Ying, D.T. Wu, and J.M. Prausnitz, "Molecular Thermodynamics of Polymer Solutions," Fluid Phase Eq. **83**, 289–300 (1993).
11. Y. Hu, X. Ying, D.T. Wu, and J. M. Prausnitz, "Liquid–Liquid Equilibria for Solutions of Polydisperse Polymers. Continuous Thermodynamics for the Close-Packed Lattice Model," Macrom. **26**(25), 6817–6823 (1993); LBL-33960.
12. Y. Hu, H. Liu, and J.M. Prausnitz, "A Model-Free Method for Calculating Vapor–Liquid Equilibria for Multicomponent Systems from Total-Pressure or Boiling-Point Data," Fluid Phase Eq. **95**, 73–92 (1994); LBL-34002.
13. A. Anderko and J.M. Prausnitz, "On the Relationship Between the Equilibrium Constants of Consecutive Association Reactions," Fluid Phase Eq. **95**, 59–71 (1994); LBL-34023.
14. J.P. Baker, I. Hong, H.W. Blanch, and J.M. Prausnitz, "Effect of Initial Total Monomer Concentration on the Swelling Behavior of Cationic Acrylamide-Based Hydrogels," Macrom. **27**(6), 1446–1454 (1994); LBL–34418.
15. J.P. Baker, H.W. Blanch, and J.M. Prausnitz, "Equilibrium Swelling Properties of Weakly Ionizable 2-Hydroxyethyl Methacrylate (HEMA)-Based Hydrogels," J. App. Polym. Sci. **52**(6), 783–788 (1994); LBL-34451.
16. Y. Song, S.M. Lambert, and J.M. Prausnitz, "Equation of State for Mixtures of Hard-Sphere Chains Including Copolymers," Macrom. **27**(2), 441–448 (1994); LBL-34464.
17. M. Kremer, E. Pothmann, T. Rossler, J. Baker, A. Yee, H.W. Blanch, and J.M. Prausnitz, "Pore-Size Distributions of Cationic Polyacrylamide Hydrogels Varying in Initial Monomer Concentration and Crosslinker/Monomer Ratio," Macrom. **27**(11), 2965–2973 (1994); LBL-34534.

Other Publication

18. M. Abbott and J.M. Prausnitz, "Modeling the Excess Gibbs Energy," in *Models for Thermodynamic and Phase Equilibria Calculations,* edited by Stanley I. Sandler (Marcel Dekker, Inc., New York, 1993).

LBL Reports

19 J.P. Baker, H.W. Blanch, and J.M. Prausnitz, "Swelling Equilibria for Acrylamide-Based Ampholytic Hydrogels, Progress Report: Theory and Experiment," LBL-33533.
20. H. Zerres and J.M. Prausnitz, "Thermodynamics of Vapor–Liquid and Liquid–Liquid Equilibria in Aqueous Systems Containing Organic Solvents and Salts," AIChE J. (in press); LBL-33928.
21. Y. Hu, X. Ying, D.T. Wu, and J.M. Prausnitz, "Liquid–Liquid Equilibria for Solutions of Polydisperse Polymers. Continuous Thermodynamics for the Lattice-Fluid Model," Fluid Phase Eq. (submitted); LBL-34003.
22. J.P. Baker, H.W. Blanch, and J.M. Prausnitz, "Popcorn-Polymer Formation During Hydrogel Synthesis," Polymer Gels & Networks (submitted); LBL-34449.
23. J.P. Baker, H.W. Blanch, and J.M. Prausnitz, "Swelling Equilibria for Cationic 2-Hydroxyethyl Methacrylate (HEMA)-Based Hydrogels," LBL-34450.

24. D. Walther, G. Sin, H.W. Blanch, and J.M. Prausnitz, "Pore-Size Distributions of Cationic Polyacrylamide Hydrogels of Different Compositions Maintained at the Same Swelling Capacity," J. Macrom. Sci. (Physics) (in press); LBL-34545.
25. Y. Song, S.M. Lambert, and J.M. Prausnitz, "Liquid–Liquid Phase Diagrams for Binary Polymer Solutions from a Perturbed Hard-Sphere-Chain Equation of State," Chem. Eng. Sci. (in press); LBL-34617.
26. Y. Song, S.M. Lambert, and J.M. Prausnitz, "A Perturbed Hard-Sphere-Chain Equation of State for Normal Fluids and Polymers," I&EC Res. (submitted); LBL-34658.
27. C. Lira-Galeana, A. Firoozabadi, and J.M. Prausnitz, "Computation of Compositional Grading in Hydrocarbon Reservoirs," Fluid Phase Eq. (submitted); LBL-34807.
28. D. Walther, G. Sin, H.W. Blanch, and J.M. Prausnitz, "Pore-Size Distributions of Cationic 2-Hydroxyethyl Methacrylate (HEMA) Hydrogels," Polymer Gels & Networks (submitted); LBL-34808.
29. D. Walther, H.W. Blanch, and J.M. Prausnitz, "Pore-Size Distributions of N-isopropylacrylamide (NIPA) Hydrogels," LBL-34875.
30. W.L. Jaecksch, "Liquid/Liquid/Solid Equilibria of Sodium Sulfate, Sodium Sulfite, and Sodium Carbonate; Water; and Acetone, 2-Propanol, and t-Butanol" (jointly with Prof. S. Lynn), M.S. Thesis, University of California, Berkeley, CA, October 1993.
31. J.P. Baker, "Equilibrium Swelling Properties of Ionized Hydrogels" (jointly with Prof. H.W. Blanch), Ph.D. Thesis, University of California, Berkeley, CA, August 1993.

Invited Talks

32. J.M. Prausnitz, "Molecular Thermodynamics: Some New Applications for Chemical Technology," Technische Hochschule, Darmstadt, Germany, October 1992.
33. J.M. Prausnitz, "Molecular Thermodynamics: Some New Applications for Chemical Technology," University of Karlsruhe, Germany, October 1992.
34. J.M. Prausnitz, "Molecular Thermodynamics: Some New Applications for Chemical Technology," University of Kaiserslautern, Germany, October 1992.
35. J.M. Prausnitz, "Molecular Thermodynamics for Chemical Process Design" and "Some New Frontiers in Molecular Thermodynamics," Bayer AG, Leverkusen, Germany, October 1992.
36. T. Hino, "Miscibilities of Binary Copolymer Systems," Annual Meeting of the American Institute of Chemical Engineers, Miami Beach, FL, November 1992.
37. T. Hauschild, "Monte Carlo Simulation of Simple Fluids Over a Wide Range of Density and Temperature. Application of a Field Term for Inclusion of Multibody Forces," Annual Meeting of the American Institute of Chemical Engineers, Miami Beach, FL, November 1992.
38. J.M. Prausnitz, "Against Babelism: Hermeneutics, Diversity and the Decline of Reductionism," University of Virginia, Charlottesville, VA, February 1993.
39. J.M. Prausnitz, "Molecular Thermodynamics: Some New Applications for Chemical Technology," Collaboratus III, Third Annual Merck Sponsored Distinguished Lectures, Rutgers University, NJ, March 1993.
40. J.M. Prausnitz, "New Dimensions for Berkeley's College of Chemistry. Rediscovering the Relevance of Chemical Engineering," Keynote Speech, Groundbreaking Ceremony for Tan Hall, University of California, Berkeley, CA, April 1993.
41. J.P. Baker, "Swelling Equilibria for Acrylamide-Based Ampholytic Hydrogels: Theory and Experiment," 205th ACS National Meeting, Division of Polymer Chemistry, Symposium on Polyelectrolytes, Denver, CO, March–April 1993.
42. J.M. Prausnitz, "Against Babelism: Diversity, Hermeneutics, and Legitimacy. Aspects of Engineering for the End of This Century," and "Molecular Thermodynamics for Chemical Process and Product Design," 1993 Warren K. Lewis Lectures, Massachusetts Institute of Technology, MA, May 1993.
43. P. Svejda, "Berechnung geschlossener flüssig-flüssig Phasengrenzkurven mittels einer dekorierten Gittertheorie," Hauptversammlung der Deutschen Bunsen-Gesellschaft für Physikalische Chemie e.V., Leipzig, Germany, May 1993.
44. J.M. Prausnitz, "Molecular Thermodynamics for Chemical Process and Product Design," 1993–94 Distinguished Lecturer Series, University of Toronto, Canada, September 1993.

LDRD

Exploration of the Interface Between Homogeneous and Heterogeneous Catalysis: Synthesis and Study of Organometallic Catalysts Supported on Novel Polysiloxane Materials with Controllable Solubility Properties*

Robert G. Bergman and Bruce M. Novak, Investigators

INTRODUCTION

Both homogeneous and heterogeneous catalysis are used by the chemical industry for conversion of feedstocks to commercial chemical products. Heterogeneous catalysts offer the practical advantage of catalyst stability and ease of processing; however, the structures of heterogeneous catalysts and the mechanisms of their reactions cannot be studied easily, and therefore it has historically been difficult to design or modify them in a rational way.

Homogeneous catalysts are more difficult to use but nevertheless are employed in several large-scale processes (e.g., hydroformylation, methanol carbonylation) because they provide selectivity or chemistry not available in heterogeneous systems. They are almost always more highly characterized than their heterogeneous counterparts, and the mechanisms of their reactions are better understood. As a result, homogeneous catalytic processes are typically more amenable to improvement by systematic structural modification.

In view of the complementary advantages of homogeneous and heterogeneous catalysts, for several years there has been intense interest in developing "hybrid" catalysts that combine the useful properties of both types of systems. An important approach to achieving this goal has been the development of systems in which well-characterized homogeneous catalysts are "heterogenized," i.e., they are covalently attached to robust solid supports.

Silica gel is one of the most important and widely used supports for organometallic catalysts. The goal of this project is the understanding of silica support–catalyst interactions through a continuum approach wherein the boundary between homogeneous and heterogeneous catalysis systems will be incrementally traversed.

*This work was supported by the Laboratory Directed Research and Development funds of the Lawrence Berkeley Laboratory under Department of Energy Contract No. DE-AC03-76SF00098.

1. Silica as a Ligand for Transition Metal Centers: Reversible Attachment and Displacement of Iridium(I) from a Silica Support

R.G. Berman, B.M. Novak, T.Y. Meyer, and S.J. Yu

During the first year of this project, soluble polysiloxane supports were prepared that consisted of polysilicic acid oligomers in which the free silanols were partially capped with trimethylsilyl groups. These polysiloxane supports have now been treated with both zirconium and iridium substrates to produce bound-metal complexes. Consistent with observations in analogous heterogeneous systems, the zirconium substrates, $Zr(CH_2CMe_3)_4$, $Zr(CH_2Ph)_4$, Cp^*ZrNp_3, and Cp_2ZrMe_2 [$Cp^* = \eta^5\text{-}C_5(CH_3)_5$; $Cp = \eta^5\text{-}C_5H_5$], bind to the polysiloxane supports by silanol protonation of one or more alkyl groups. The resulting polysiloxane-bound zirconium species are soluble in hydrocarbon and ethereal solvents. This solubility allows them to be characterized by NMR spectroscopy. Activation of these catalysts by treatment with hydrogen resulted in gelation in the cases of $Zr(CH_2CMe_3)_4$ and $Zr(CH_2Ph)_4$, but the use of the more sterically demanding and less labile Cp* ligand in the Cp^*ZrNp_3 substrate resolved this problem. Efforts are currently under way to characterize the resulting supported metal hydride complex and to investigate its catalytic activity.

Reaction of $Cp^*Ir(OH)(PMe_3)(Ph)$ with the soluble polysiloxane support produced the bound-metal complex $Cp^*Ir(Osiloxane)(PMe_3)(Ph)$. In this case, the metal complex binds by exchange of the hydroxide for a silanol group. This class of ligand exchange was further exploited to cleave the iridium complex from the support by reaction with phenol. The isolation of the cleavage product, $Cp^*Ir(OPh)(PMe_3)(Ph)$, confirmed that the complex had not undergone significant structural changes upon binding.

The ability to remove a metal complex from a support has direct application to the analogous heterogeneous systems. A complementary study of the chemistry of $Cp^*Ir(OR)(PMe_3)(Ph)$ [R = H, $OSiMe_2(t\text{-}Bu)$] on silica has thus been undertaken. As in the case of the soluble polysiloxane supports, the iridium complex can be bound and then removed by exchange with phenol. The supported complex also undergoes clean stoichiometric chemistry with organic reagents. For example, on treatment with acetylene dicarboxylate, the supported iridium complex reacts and then releases an organic product with a new metallocyclic ring. This chemistry is summarized in Figure 1-1. Thus, the starting iridium complexes can be (1) supported on silica; (2) removed in intact molecular form and fully characterized; and (3) converted to a new

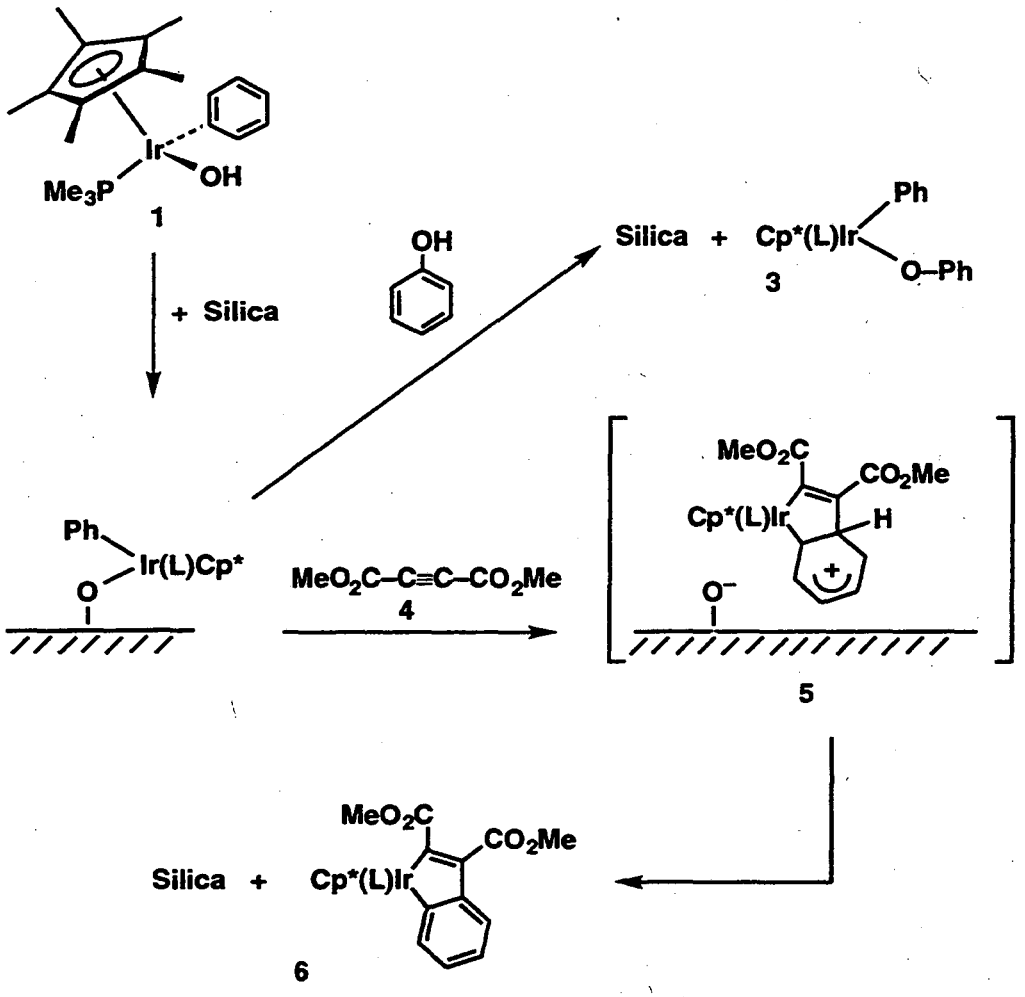

Figure 1-1. Observation of reversible and controllable chemisorption of an organometallic complex to a silica support. (XBL 947-4162)

supported complex, which also can be removed in intact molecular form and characterized. This is the first time that it has been possible to utilize the polymeric silica support as an apparently simple and detachable ligand in an organometallic transformation. In addition, in the phenol reaction it appears that substituted phenols with different acidities (pK_a's) remove different amounts of the supported iridium complex from the silica. This unique dependence of the extent of reaction on the pK_a of the substituted phenol is currently being investigated. Preliminary data suggest that this reaction may be useful for mapping silica sites with differing iridium affinities.

Ultrafast Dynamics of Electrons at Surfaces*

Charles B. Harris, Investigator

INTRODUCTION

We are developing techniques to examine the spectroscopy and dynamics of surface electronic excitations at interfaces with unprecedented precision. The electronic dynamics of surfaces are involved in many problems of fundamental interest, from two-dimensional magnetism to chemisorption. Directly related areas of technological significance include surface photochemistry, laser-surface interactions such as damage mechanisms in optics, surface recombination that can dominate carrier lifetimes at semiconductor interfaces, and magnetic data storage devices.

A complete understanding of excited-state dynamics at surfaces requires time, energy, and momentum resolution. Using angle-resolved two-photon photoemission (TPPE), one can study the band structure of electronically excited states at surfaces. We employ an unusual electron time-of-flight detection scheme that gives high sensitivity and extreme precision in energy measurements. Liquid helium cooling of the sample to 45 K enables the study of a wide variety of physisorbed and chemisorbed species. Our TPPE apparatus has an energy resolution that is an order-of-magnitude better than competing techniques and utilizes pico- and femtosecond laser pulses for time-resolved measurements.

1. Electron Localization at Interfaces in 2-D

C.B. Harris, R.L. Lingle, Jr., D. F. Padowitz, R. E. Jordan, and J.D. McNeill

A very significant discovery within the past year has been the observation of 2-D localization of electrons at metal–alkane interfaces as a nondispersive feature in angle-resolved TPPE. This represents the development of a new tool to study the spatial extent of interfacial electronic states. Our method is a unique and important tool for the study of Anderson localization because it measures the energy spectrum of the localized states and can be applied to atomically thin samples. Generally, we find that all aspherical alkanes support localized electronic states at the interface, while the spherical neopentane does not. We predict that similar localized states exist at metal–polymer interfaces and contribute to their electronic properties.

2. Dielectric Properties of Atomically Thin Metal–Insulator Interfaces

C.B. Harris, D. F. Padowitz, W. R. Merry, R. E. Jordan, J. D. McNeill, and R. L. Lingle, Jr.

We have completed a systematic study of physisorbed metal–alkane interfaces. First, we have extensively investigated the sensitivity of TPPE to various adsorption phenomena. We have shown that TPPE is extremely sensitive to layer thickness at the level of a few percent of a monolayer. We are able to distinguish between adlayer growth modes and map out surface phase diagrams. We have cataloged the distinct surface spectra characteristics of a 2-D gas layer, a 2-D solid layer, island formation, and clustering of a nonwetting adsorbate. Secondly, we have studied the dielectric properties of atomically thin slabs by measuring the effect of layer thickness on image-potential electron binding energy. These layer-by-layer shifts are due to dielectric screening of the image potential and show how the atomic polarizability develops into the bulk dielectric constant. Thirdly, dispersion measurements of the image-electron band structure have shown that the effect of the monolayer is to decouple the in-plane motion of the image-potential electron from the metal-bulk band structure, leaving it as a free electron in 2-D. However, the image-electron effective mass increases for alkane multilayers due to small polaron formation.

3. Theoretical Investigation of Alkali–Noble-Metal Interfaces

C.B. Harris J. D. McNeill

Alkali layers on noble metals have been investigated both experimentally and theoretically. A TPPE study of K/Ag(111) found that the effective mass of the image potential electron is in relatively good agreement with predictions of a density functional calculation. We have successfully modeled

* This work was supported by the Director, Office of Energy Research, Office of Basic Energy Sciences, Chemical Sciences Division, of the U.S. Department of Energy under Contract No. DE-AC03-76F00098.

the binding energy of image potential electrons on alkali layers using multiple reflection theory, contrary to results obtained by other workers. We conclude that multiple reflection theory is more robust than previously believed.

4. Layer-by-Layer Electronic Properties of the Xe/Ag(111) Interface

C.B. Harris, R. L. Lingle, Jr., D. F. Padowitz, J. D. McNeill, R. E. Jordan, and W. R. Merry

We have studied the electronic structure of the Xe/Ag(111) interface for thicknesses from zero to nine xenon layers. The first three members of the image potential Rydberg series for the bare surface evolve into states of the xenon slab as successive layers are added. The effective masses of the interfacial electrons have also been measured, making this the most complete characterization ever made of the conduction-band electronic structure of a nanometer scale interface.

FY 1993 PUBLICATIONS AND REPORTS

Refereed Journals

1. R.L. Lingle, Jr., D.F. Padowitz, R.E. Jordan, J.D. McNeill, and C.B. Harris, "Two-Dimensional Localization of Electrons at Interfaces," Phys. Rev. Lett. **72**, 2243 (1994).
2. D.F. Padowitz, W.R. Merry, R.E. Jordan, and C.B. Harris, "Two-Photon Photoemission as a Probe of Electron Interactions with Atomically Thin Dielectric Films on Metal Surfaces," Phys. Rev. Lett. **69**, 3583 (1992).
3. J.D. McNeill and C.B. Harris, "An Exact Phase Shift Model for Image States on Metal Surfaces with Alkali Metal Overlayers," Solid State Commun. **87** 1089 (1993).
4. W.R. Merry, R.E. Jordan, D.F. Padowitz, and C.B. Harris, "Electrons at Metal-Insulator Interfaces I. The Effect of Xe Monolayer on the Image Potential States of Ag(111)," Surf. Sci. **295**, 393 (1993).

Other Publications

5. R.L. Lingle, Jr., D.F. Padowitz, R.E. Jordan, J.D. McNeill, and C.B. Harris, "Localization of Electrons at Interfaces," *Proceedings of the 26th Jerusalem Symposium on Quantum Chemistry and Biochemistry*, edited by J. Jortner and B. Pullman (Kluwer Academic Press, The Netherlands, 1993).
6. R.L. Lingle, Jr., J.D. McNeill, R.E. Jordan, N.H. Ge, and C.B. Harris, "Simultaneous Monitoring of Adsorbate Effects on the Surface Barrier and Exterior Potential at a Metal Surface," J. Chem. Phys. (submitted).
7. R.E. Jordan, R.L. Lingle, Jr., J.D. McNeill, D.F. Padowitz, and C.B. Harris, "Electrons at Metal-Insulator Interfaces II: Adsorbate Morphology and Electronic Structure on Alkane Multilayers," (manuscript in preparation for Surf. Sci.).
8. R.L. Lingle, Jr., J.D. McNeill, D.F. Padowitz, R.E. Jordan, and C.B. Harris, "Layer-by-layer Development of the Electronic Structure of the Xe/Ag(111) Interface," (manuscript in preparation for Science).

Structure and Chemistry of Nonmetallic Adsorbates at Compound Semiconductor Interfaces Investigated by Synchrotron Radiation Techniques*

David K. Shuh, Investigator

INTRODUCTION

This project emphasizes the investigation of the surface structures and chemistries of simple, nonmetallic adsorbates on compound semiconductor surfaces utilizing two complementary synchrotron radiation (SR) techniques. The results provide insights into the fundamental chemisorption interaction on binary semiconductors that are important in semiconductor processing and growth technologies. A prime consideration is the application of SR approaches that will make extensive use of the Advanced Light Source (ALS).

The SR-based research relies on the emerging x-ray standing waves (XSW) technique for the determination of adsorbate-semiconductor surface structures, whereas synchrotron photoelectron spectroscopy (PES) has been utilized to characterize the chemical behavior of the systems under investigation. The XSW and PES experiments employ the existing endstations of the x-ray and vacuum ultraviolet electron storage rings of the Stanford Synchrotron Radiation Laboratory (SSRL) and the National Synchrotron Light Source prior to commencement of these activities at the ALS. Concomitant with the initial SR-based efforts, a surface science chamber with limited capabilities have been designed and constructed to support the initial SR-projects. This small surface science system permits testing of experimental apparatus under UHV and the preliminary research investigations on the selected adsorbate-semiconductor systems.

1. Prototype Iodine/GaAs(110) Interface Investigated by PES and XSW Techniques

D.K. Shuh

The iodine on GaAs(110) system at room temperature is a particularly interesting system since iodine may form an ideal termination of the bulk GaAs(110) structure, from both chemical and structural perspectives. The I/GaAs interface orders and forms a near monolayer coverage. The initial PES and XSW experiments were performed at SSRL Beamline 3-3. The iodine was dispersed by a solid-state electrochemical cell source that had been previously tested at LBL. The iodine coverage and a suitable iodine detection feature were characterized by PES at the photon energy required to perform the XSW measurements. The XSW results presented in Figure 1-1 were collected by sweeping photon energy through the GaAs (220) Bragg condition while simultaneously monitoring the photoelectron signals from both the I $3p_{3/2}$ peak and background region in the constant initial state (CIS) mode, then subtracting the background to extract the XSW signal from the iodine atoms.

The summed I XSW profiles are being fit to the dynamical x-ray theory of diffraction in order to extract the structural information from the I/GaAs(110) interface. In addition to the (220) back reflection that yields the vertical distance of the iodine in relation to the (110) of GaAs, the distinct (111) and $(11\bar{1})$ reflections that lie approximately ±35° from the (220) were also measured to triangulate the absolute position of the iodine atoms on GaAs(110). Preliminary interpretation of the I XSW response suggests that iodine chemisorption is coherent and that iodine atoms are located in sites 2.05 Å above the GaAs(110), which is similar to the distance in the Sb/GaAs(110) system.

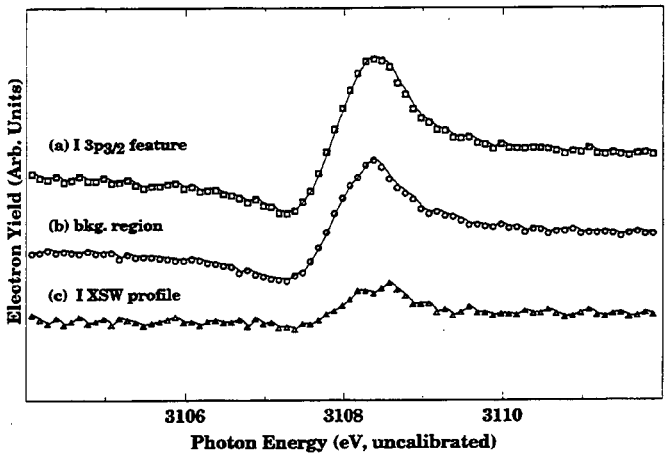

Figure 1-1. The XSW (220) GaAs back reflection component spectra from a single CIS measurement illustrating the signals from (a) the I $3p_{3/2}$ feature; (b) the background component taken 50 eV higher than in (a); and (c) the I XSW profile that results from the subtraction of (b) from (a).

*This work was supported by the Director, Office of Energy Research, Office of Basic Energy Sciences, Chemical Sciences Division, of the U.S. Department of Energy under Contract No. DE-AC03-76SF00098.

2. Design and Fabrication of a Simple Surface Science Chamber System

D.K. Shuh

To complement the SR program and to enhance the productivity of the SR-based efforts, a modest laboratory-based UHV system was designed and constructed. The system allows the testing of experimental apparatus, as well as the preliminary investigation of adsorbate-semiconductor experimental systems that are essential for successful experimentation at SR sources. The surface science chamber system provides the basic capabilities required to initiate and pursue a SR research program. The capabilities of the system can be increased, and the chamber could, with further enhancements, serve as a simple SR endstation.

FY 1993 PUBLICATIONS AND REPORTS

Other Publication

1. D.K. Shuh, T. Kendelewicz, and P. Pianetta, "Structure of Iodine on GaAs (100) by X-ray Standing Waves," (in preparation).

Work for Others

UNITED STATES OFFICE OF NAVAL RESEARCH

Normal and Superconducting Properties of High-T_c Systems*

Vladimir Z. Kresin, Investigator

INTRODUCTION

This research is concerned with various aspects of high-T_c superconductivity, such as the isotope effect, the symmetry of the superconducting state, charge transfer, pairing mechanisms, etc.

Nonadiabaticity of the nuclear motion and electronic term crossing at the apical oxygen lead to the appearance of a double-well structure and thus affect charge transfer. Since T_c depends strongly on the carrier concentration, an unusual isotope effect occurs in the high-T_c oxides.

Study of the oxygen stochiometry is crucial for determining the symmetry of the pairing state, and this is directly related to the problem of the origin of the high-T_c phenomenon.

1. Novel Isotope Effect (Publications 3, 4, and 6)

V.Z. Kresin and S.A. Wolf†

A new microscopic mechanism relating T_c with the isotope substitution for the doped superconductors such as the high-T_c oxides is proposed. Because it is impossible, strictly speaking, to fully separate the nuclear and electronic degrees of freedom, strong nonadiabaticity leads to a peculiar dependence of the carrier concentration n on the ionic mass M. For example, this case concerns the isotopic substitution of the axial oxygen YBCO. Because of the dependence of T_c on n, such substitution leads to the dependence of T_c on M, that is, to the isotope effect. The minimum value of the isotope coefficient corresponds to $T_c = T_{cmax}$.

†Permanent address: Naval Research Laboratory, Washington, DC.

2. Symmetry of the Pairing State. Microwave and Transport Properties (Publications 1, 2, and 6)

V.Z. Kresin, M.E. Reeves,† J.L. Cohn,‡ S.A. Wolf,† N. Klein,‖ N. Tellman,‖ M. Schulz,‖ and K. Urban‖

The concept based on an anisotropic s-wave state with gaplessness for a nonstochiometric compound provides a unified description of experimental data related to the problem of symmetry. In addition, one can perform a crucial microwave experiment using this concept.

Epitaxial thin films of $YBa_2Cu_3O_{7-x}$ with low cation and oxygen disorder exhibit two features in the temperature dependence of the microwave surface impedance that are consistent with a weak s-wave superconducting state associated with the CuO chains. First, both the microwave surface resistance and the magnetic field penetration depth exhibit a weak exponential temperature dependence below 30 K, corresponding to an energy gap of about 6 meV. Second, the penetration depth exhibits a small bump at about 60 K, which is consistent with a two-band BCS calculation using 6 meV for the smaller gap.

†Permanent address: Naval Research Laboratory, Washington, DC.
‡Permanent address: Department of Physics, University of Miami, Florida.
‖Permanent address: Institut für Festkörperforschung, Forschungszentrum Jülich GmbH, Jülich, Germany.

3. Gapless State (Publications 7, 8, and 9)

V.Z. Kresin, M.E. Reeves,† S.A. Wolf†

The removal of oxygen from $YBa_2Cu_3O_{7-x}$ has a profound impact on various properties of this compound. The model of induced two-gap superconductivity that we developed previously allows us to describe these properties. For example, for compositions between $0 < x < 0.1$, the energy gap on the chains changes drastically and vanishes. However, T_c remains relatively constant because it is determined mostly by the properties of the planes. The

* This work was supported by the U.S. Office of Naval Research under Contract No. N00014-92-F0002 through an agreement with the U.S. Department of Energy, under Contract No. AC03-76SF00098.

overdoped state is also gapless. This is caused by the mixed valence of Cu. The anisotropy of the order parameter leads to a broadening of the gapless region.

†Permanent address: Naval Research Laboratory, Washington, DC.

4. Order Parameter. Origin of High T_c (Publications 5, 7, and 8)

W. Fuller-Mora,† M.E. Reeves,† H. Morawitz,‡ S.A. Wolf,† and V.Z. Kresin

The general equation for the pairing function in the presence of electron–phonon interaction has been solved. When parameters of the high-T_c oxides are employed, the derived values of T_c and of the energy gaps are in good agreement with experimental data. In addition, we find from specific heat measurements that the electron–phonon coupling on the planes is sufficient to account for high-T_c in $YBa_2Cu_3O_{7-x}$.

†Permanent address: Naval Research Laboratory, Washington, DC.
‡Permanent address: IBM Almaden Center, San Jose, CA.

FY 1993 PUBLICATIONS AND REPORTS

Refereed Journals

1. J.L. Cohn, V.Z. Kresin, M.E. Reeves, and S.A. Wolf, "Superconducting-State Thermal Transport in $YBa_2Cu_3O_{7-\delta}$," Phys. Rev. Lett. **71**, 1657 (1993).
2. N. Klein, N. Tellman, H. Schulz, K. Urban, S.A. Wolf, and V.Z. Kresin, "Evidence of Two-Gap s-wave Superconductivity in $YBa_2Cu_3O_{7-x}$ from Microwave Surface Impedance Measurements," Phys. Rev. Lett. **71**, 3355 (1993).
3. V.Z. Kresin, M.E. Reeves, and S.A. Wolf, "Superconductivity, Gapless State and Isotope Effect in the Cuprates," Phys. C **209**, 319 (1993).
4. M.E. Reeves, D.A. Ditmars, S.A. Wolf, T.A. Vanderah, and V.Z. Kresin, "Evidence for Strong Electron–Phonon Coupling from the Specific Heat of $YBa_2Cu_3O_{7-\delta}$," Phys. Rev B **47**, 6065 (1993).

Other Publications

5. V.Z. Kresin and S.A. Wolf, "Microscopic Model for the Isotope Effect in the High T_c Oxides," Phys. Rev. B (in press).
6. V.Z. Kresin and S.A. Wolf, "Symmetry and Mechanism of the Pairing and the Isotope Effect in the Cuprates," J. Superconductivity, Special Issue, Proc. MOS (in press).
7. W. Fuller-Mora, S.A. Wolf, and V.Z. Kresin, "Solution of the Eliashberg Equation for Cuprates," *ibid* (in press).
8. V.Z. Kresin, H. Morawitz, and S.A. Wolf, *Mechanisms of Conventional and High T_c Superconductivity* (Oxford, NY), 1993.
9. V.Z. Kresin, M.E. Reeves, and S.A. Wolf, "Superconductivity and Gapless State in Cuprates," in *ICMAS-92, Technology Transfer Series*, edited by C. Chu and J. Fink (IITT Paris) 1993.

Invited Talks

10. V.Z. Kresin, "Spectroscopy and T_c of High T_c Oxides," Keynote Speaker, International Conference on Modern Aspects of Superconductivity, Paris, France, October 1992.
11. V.Z. Kresin, "Theoretical Aspects of High T_c Superconductivity," IBM, Zurich, Switzerland, October 1992.
12. V.Z. Kresin, "Oxygen Stochiometry and Properties of Cuprates," Center of Superconductivity, University of Caen, Caen, France, October 1992.
13. V.Z. Kresin, "Mechanisms of High T_c," Laboratoire de Phys. du Solide, ESPCI, Paris, France, October 1992.
14. V.Z. Kresin, "Gapless Superconducting State," MRS Meeting, Boston, MA, December 1992.
15. V.Z. Kresin, "United Approach in the Theory of High T_c," International SC Global Conference, San Jose, CA, January 1994.
16. V.Z. Kresin, "Theory of High T_c," University of California, La Jolla, San Diego, CA, April 1993.
17. V.Z. Kresin, "Symmetry, Mechanism of the Pairing, and the Isotope Effect in the Cuprates," International Conference on Molecular and Oxide Superconductors, Eugene, OR, June 1993.

Appendices

APPENDIX A

DIVISION PERSONNEL

1992 Scientific Staff

Investigators	Postdoctoral and Other Scientists	Graduate Students		Guests, Affiliates
Richard A. Andersen	M.A. Petrie	W.W. Lukens, Jr. M.E. Smith	C.D. Sofield M. Weydert	D.J. Schwartz M.R. Smith
Neil Bartlett	B.-C. Shen B. Zemva	J.C. Allman L.C. Chacon	G.M. Lucier B.-C. Shen	J. Munzenherg
Alexis T. Bell		J.N. Carstens D.B. Clarke C.S. Gittleman	R.M. Pittman M.J. Sandoval S.C. Su	H. Abe J. Fung T. Komaya D.-K. Lee S.S. Lee
Robert G. Bergman	T.Y. Meyer S.J. Yu	A.M. Baranger M.J. Burn M.D. Butts D.A. Dobbs	T.A. Hanna S.Y. Lee R.I. Michelman R.E. Minto	B.A. Arndtsen A.A. Bengali Y. Ma R.H. Schultz M.J. Tauber
Yongqin Chen	M.P. Blackwell			
Eugene D. Commins		B.C. Regan S.B. Ross		
Robert E. Connick	Y.-X. Zhang			
Norman M. Edelstein	J.J. Bucher B.G. Jung D.K. Shuh D.H. Templeton	A.-D.L. Nguyen		S. Hubert N. Kaltsoyannis K.P. Osborne D. Piehler A.R. Smith J. Sytsma L.K Templeton L.J. Terminello A. Zalkin
Harvey A. Gould	A. Belkacem			K. Momberger

Investigators	Postdoctoral and Other Scientists	Graduate Students		Guests, Affiliates
Charles B. Harris	R.L. Lingle D.R. Padowitz	S.E. Gadd R.E. Jordan	J.C. King J.D. McNeill	M.C. Asplund S.E. Bromberg J.K. Hane R.L. Lingle W.R. Merry, Jr. B.J. Schwartz C.T. Vala
Harold S. Johnston				
Vladimir Z. Kresin				K.T. Habte
Andrew H. Kung	J. Xie X. Yang			C.-Y. Ng A.M. Wodtke
Yuan T. Lee	L.F. Nahon A.G. Suits	C.L. Berrie D.A. Blank D.W. Boo A.S. Bracker J.D. Chesko H. Hou C.A. Longfellow	T.-T. Miau J.D. Myers S.W. North L.A. Smoliar M.J.J. Vrakking J. Zhang	S.-Y. Chiang G.-Y. Liu L.F. Nahon A.M. Soliva M. Stemmler D. Stranges M.J.J. Vrakking
William A. Lester, Jr.		W.R. Brown	M.M. Soto	W.A. Glauser J.A. Odutola Z. Sun J.Y. Yu
Richard Marrus		B.B. Birkett		
William H. Miller	D.T. Colbert	S.M. Auerbach L.F. Gaucher	J.D. Gezelter S. Keshavamurthy	J.D. Gezelter R. Hernandez J.J. Scherer G. Stock W.H. Thompson
C. Bradley Moore	S.K. Kim E.R. Lovejoy	R.A. Alvarez H.P. Beal	S.K. Kim E.A. Wade	H. Clauberg J. Petty
Daniel M. Neumark		C.C. Arnold D.W. Arnold	D.R. Cyr	D.J. Leahy D.L. Osborn
Kenneth S. Pitzer	A.M. Anderko C.S. Oakes T. Narayanan			J.P. Chan
John M. Prausnitz		J.P. Baker A.P. Sassi	A.L. Schiozer	E.G. Azevedo B.M. Boyd

Investigators	Postdoctoral and Other Scientists	Graduate Students		Guests, Affiliates
Michael H. Prior	J. Jin			F. Aumayr P. Beiersdorfer G.P. Borsoni M.A. Briere J.-P.L. Briand J.R. Crespo Lopez-Urrutia V. Decaux D.D. Dietrich R.A. Haar D.E. Ivie H. Khemliche J.W. McDonald J. Palinka V.L. Plano L.G. Sarkadi D.H. Schneider L.J. Westervelt S.-D. Yao P.A. Zavodszky
Kenneth N. Raymond		J.K. Cammack S.J. Franklin	C. Sunderland D.W. Whisenhunt, Jr.	B.A. Lulay-Bryan C.O. Roth J. Xu
Richard J. Saykally		R.S. Fellers	N. Pugliano	
David A. Shirley	Z. Hussain	Z. Huang E.A. Hudson W.R.A. Huff	S.A. KellarE.J. Moler B.L. Petersen	E.A. Hudson T. Reich P. Thalappil Y. Zheng
K. Peter C. Vollhardt		D.S. Brown J.K. Cammack R. Faust	D.L. Mohler B.A. Siesel	G.J. Braunlich H. Elamouri C.P. Lee D.W. Tien

SUPPORT STAFF

Division Administrative Staff

Division Administrator: Linda R. Maio

Administration	Personnel/Financial	Purchasing
L. Aubert	A. Winters	A. Winters
A. Winters	T. Lynem-Paynes	T. Lynem-Paynes
T. Lynem-Paynes	M. Graham	

Travel

S. Quarello*

Administrative/Secretarial Staff

I. Coble	E.A. Lawhead	F.J. Semwogerere
J. Denney	H. Manning	P. Southard
L. English	A. McClain	K. Steele
C. Fowler	B. Moriguchi-Iwai	P. Takahashi
C. Gliebe	V. Narasimhan	B.M. Thibadeau
J.M. Gotay	M.F. Noyd	
I. Katsumoto	T.C. Peoples	

APPENDIX B

INDEX OF INVESTIGATORS*

*Boldface numbers indicate investigators' main programs.

Lawrence Berkeley Laboratory
University of California
Technical and Electronic Information Department
Berkeley, California 94720